Analysis and Development of Power Quality Metrics for Railway Electric Networks

PhD Thesis

Yljon Seferi

Dynamic Power Systems Laboratory
Institute for Energy and Environment
Electronic and Electrical Engineering Department
University of Strathclyde, Glasgow

August 17, 2022

This thesis is the result of the author's original research. It has been composed by the author and has not been previously submitted for examination which has led to the award of a degree.

Acknowledgements

I would like to express my sincere gratitude to my supervisor Dr. Steven Blair and Prof. Graeme Burt for their invaluable advice, continuous support, and patience during my PhD study. I would like to extend my sincere thanks to the Department of Electronic and Electrical Engineering for the funding opportunity to undertake my studies at Strathclyde University.

I am immensely grateful and owe a lot to Prof. Brian Stewart for his continuous support, understanding, and suggestions throughout my PhD. I thank you for the trust you put in me.

I would also like to thank my colleagues in our research group: Renan Quijano, Richard Munro, Dr. Patrick Norman and Dr. Mazheruddin Syed who have assisted me in numerous ways over the past few years.

I am deeply grateful to colleagues at METAS, especially Dr. Christian Mester and Dr. Beat Jeckelmann, that have given me the opportunity to start my research career, and to Dr. Andrew Roscoe who believed in me and extended this journey.

I would like to thank my family: my mother Nexhmije and my sister Ledina for their great support, endless love, and believing in me during this journey; my Father Edmond – who, although no longer with us, continues to inspire me. This thesis is dedicated to them.

Last but not least, I would like to express my gratitude to my amazing wife Albana, for her decision to join me in this adventure, and for her support, sacrifices, and care for me, and to our lovely girls Ema and Mia. Without your help, this research would not have been possible. I love you! This thesis is also dedicated to them.

Abstract

Ensuring acceptable levels of power quality (PQ) in electrified railway networks has become crucial due to the increased utilisation of power electronics within locomotives and power grids. There is a lack of clear analysis and standardised procedures focusing on PQ measurement techniques explicitly for railway applications, and therefore a need to develop appropriate PQ measurement methods and indices.

This thesis addresses this gap through review and analysis of PQ phenomena and measurement methods applicable to AC railway signals. Recommendations of methods for rail PQ instruments are provided, including newly developed techniques to detect unique disturbances in AC and DC railway networks.

A new measurement technique to identify voltage interruptions at locomotive terminals resulting from network re-configuration has been developed. It allows distinguishing these disturbances from voltage interruptions caused by faults in the system or failure of equipment, thereby improving event identification and classification.

A half-cycle measurement interval, in contrast to the one-cycle approach proposed by the IEC 61000-4-30 standard for voltage dips and swells evaluation in grid applications, has been analysed and developed for improved detection and classification of short-time voltage events, allowing an enhanced correlation of their impact on rail assets, and supporting network planning and new standards for rail PQ instruments.

It is shown that a new aggregation time interval equal to 50 cycles for 50 Hz signals is required to improve the accuracy of voltage and current harmonics measurements by rail PQ instruments. Due to improved tracking of the time-varying frequency components, a better estimation of harmonic emission levels in 25 kV 50 Hz rail systems has been proven, leading to improved health condition monitoring of the network assets.

A novel and cost-effective method for detecting electric arcing phenomenon between

the pantograph and overhead contact line (OCL) of 3 kV DC railway networks has been developed. Information extracted about the geographical localisation of the arc enables predictive maintenance of the entire pantograph-catenary system, thereby reducing operational costs and improving the safety and reliability of DC rail networks.

In summary, this work has addressed the need for focused analysis of unique railway PQ phenomena, has developed and proven the effectiveness of new tools for rail PQ monitoring, and has established a new foundation for health and condition monitoring in rail electrical systems.

Contents

List of Figures

List of Tables

Glossary of Abbreviations

AC	Alternating Current
ADC	Analogue to Digital Converter
CT	Current Transformer
DAQ	Data Acquisition System
DC	Direct Current
DFT	Discrete Fourier Transform
EU	European Union
FIR	Finite Impulse Response
HV	High Voltage
HVDC	High Voltage Direct Current
IEC	International Electrotechnical Commission
NS	Neutral Section
OCL	Overhead Contact Line
PMU	Phasor Measurement Unit
PQ	Power Quality
PWM	Pulse-Width Modulation

RMS	Root Mean Square
ROCOF	Rate of Change of Frequency
ROCOP	Rate of Change of Phase
SNR	Signal to Noise Ratio
STFT	Short Time Fourier Transform
THD	Total Harmonic Distortion
TS	Traction Substation
VT	Voltage Transformer
WAMS	Wide Area Measurement Systems
4QC	Four-Quadrant-Converters
UTC	Coordinated Universal Time

Chapter 1

Introduction

1.1 Research Context

Railway networks are one of the main transportation systems throughout the world, and play a significant role in the economic and social development of societies and countries. These services are vital for a country's economic progress, and important for the quality of life of citizens [1]. In the European Union (EU), the railway transportation system has been the most utilised service in 2018, with 8 billion passengers, compared to maritime and aviation sectors, with 0.4 billion and 1 billion respectively [2]. Rail passenger transport use in the EU has increased to 416 billion passenger-kilometres, in 2019 – 14% more than 2013 data [3].

The rail transportation system consists of trains and network infrastructure. The latter comprises railway tracks formed by metallic rails fixed on sleepers at ground level, signaling systems, the electric lines for the electrified railways, and the train stations. Trains are usually composed of one or two locomotives and several passenger coaches or freight wagons coupled together. The locomotive is responsible for providing the traction power that is produced either by diesel engines using combustible fuels or drawn by a dedicated electric system. In electrified railways, the electric energy is collected from an electric line through a particular mechanical system installed on the train roof or beside the track at ground level. This system allows the train to draw the electric energy continuously as it runs between stations, but also to return a portion

of the energy produced by the train during the braking process. Electric trains have several advantages – they do not pollute the environment and usually are more efficient, comfortable, and reliable [4]. They also contribute to a more sustainable transportation system as there is no direct oil dependence [1].

Since the 19th century, rail transportation systems have undergone many technological changes [4], from the earliest steam locomotives which have evolved to the present high-speed electric locomotives. Although diesel locomotives are still operating in railways of many countries, electrified railway transportation is rapidly growing and expected to replace more traditional fuel types by 2050 [1]. This is because the electrification of the railway networks is seen as an important step towards environmental decarbonisation and for better management of natural fuel resources. Therefore, to achieve a reduction of greenhouse gas emissions at a level below 80-95% compared to 1990 levels, by 2050 [1], significant changes and development in the infrastructure of the transportation system also are required. These changes will substantially impact the railway service to achieve some objectives set by the EU, such as to expand high-speed railway lines by 2030; to shift more than 50% of medium distance road freight transport and the majority of passenger transport to rail services by 2050; and to enlarge the railway network and interconnect it with more airports and seaports by 2050 [1]. Therefore, railway services will take an even more important role in the transportation system of EU countries. This change has already started, and countries like Latvia, Lithuania, and Estonia have become pioneers, reporting rail transport as the main inland transport undertaking respectively 75.8%, 67.9%, and 46.2% of all transport in 2018 [2].

Electrified railways are considered large power consumers of the main electric grid. It is estimated that 1.3% of the total electric energy generated in the EU in 2018 has been consumed by the railway networks, considering the net annual energy generation of about 2806 TWh [5], and the European railway system annual energy consumption of about 36.5 TWh [6]. AC and DC railway systems usually have dedicated electric networks, comprising high voltage (HV) distribution lines, power substations, traction substations (TS), converter systems, and electric lines that continuously supply AC or

DC locomotives. Trains actively interact with the main power grid through the railway grid by exchanging energy flows in both directions during all possible modes of operation including acceleration, coasting, braking, when standing at railway stations, or even between each other by exchanging surplus of energy flows. This interaction can cause many power quality (PQ) problems both inside the railway grid and on the supplying AC grid. This is due to the unique operational dynamics of trains, interaction between trains, and the non-linear characteristics of the rolling stock equipment such as traction converters and auxiliary converters used for lighting, heating, and other services [7–10]. Although many PQ monitoring and mitigation techniques have been developed, it is difficult to limit all the disturbances due to several factors such as the presence of mixed-type traction loads operating under the same network [11]; interaction of the loads with the power supply system and other loads [11, 12]; the unpredictable occurrence of the short-time PQ events; and the time-varying nature of the signals [9, 13]. The PQ disturbances of the railway signals, having peculiar characteristics [9] present challenges to the standardised PQ measurement methods used to evaluate them. The reason is related to the fact that measurement methods described in standards IEC 61000-4-30 [14] and IEC 61000-4-7 [15] are not specifically developed and optimised for railway applications. Also, they do not cover specific disturbances such as the voltage interruptions caused by network topology and the electric arcing phenomenon occurring between OCL and pantograph – an important short-time PQ event in railway networks. Presently, no standard or measurement procedure exists that defines acceptable metrics for both AC and DC electrified railway networks [16, 17].

The main challenges associated with PQ measurement methods which are investigated in this thesis are:

- Periodic voltage interruptions due to the specific design of the traction network are common at the locomotive input terminals in 25 kV 50 Hz traction systems. These voltage interruptions are not properly evaluated by the standardised method [14] because it is not able to identify which voltage interruptions are caused as a result of failure of equipment and/or tripping of protection devices installed in the network, and which voltage interruptions are caused due to the phase separation

sections, as part of the power supply network of the train. New technique for detection of voltage interruptions is needed in AC traction systems of 25 kV 50 Hz to provide a better event identification and classification, enhanced locomotive monitoring over time, and support standardisation with a new advanced PQ metric typical for railway networks.

- Because the electric signals of railway networks are characterised by short variations in voltage magnitude due to the traction load variability, voltage dip and voltage swell events lasting shorter than one cycle are common. These events are not accurately characterised by the standardised measurement methods [14] that require the event evaluations to be performed over a one-cycle measurement interval. In such a context, shorter calculation intervals are needed for more accurate evaluation, and closer tracking of voltage dips and voltage swells events, thereby enhancing the sensitivity to voltage variability, improving event classification, providing a more accurate statistical analysis for network plannings, providing useful guidance for PQ monitoring instruments designed for railway applications, and enhancing the correlation of voltage events impact on rail network assets.

- Harmonic voltages and currents in AC traction systems are present in significant levels and are time-varying in nature [9,11]. Due to the variability resulting from the changing operational modes of the train [9,10,12], harmonic levels are, however, underestimated because of the smoothing effect the aggregation algorithms have on the measurement results [14,15]. Therefore, to have more accurate harmonic emission levels estimated by PQ instruments, better tracking of the time-varying frequency components in 25 kV 50 Hz traction systems, and to support network planning and network condition monitoring strategies, the accuracy and correctness of the application of standardised harmonic measurement algorithms to AC traction systems must be carefully reviewed.

- Although the electric arcing phenomenon causes unwanted PQ phenomena and damages the current collection system in electrified railway networks [18–22], a standardised method to detect these short-time PQ events does not exist yet.

Several methods have been proposed to detect electric arcing phenomenon in DC railway networks by the research community. However, some of the proposed methods are costly and employ extensive signal processing techniques, hence are inappropriate for real-time operation, and others cannot be applied successfully to DC railway networks because they are conceived for AC railways and require accurate knowledge of the network infrastructure. Furthermore, they rarely provide the geographical localisation of the arc occurrence [23] – a feature that can be very useful to lower the maintenance cost and improve the reliability of the transportation service.

Therefore, a new cost-effective arc detection method is required, to provide information about the kilometric arc position along the line, to support pantograph-catenary condition monitoring, and to reduce the expensive costs related to OCL inspections.

1.2 Thesis Aim and Objectives

This thesis initially aims to verify whether standardized PQ measurement methods defined in IEC 61000-4-30 [14], and used in the monitoring of PQ indices of 50 Hz electrical grids, are sufficient for accurate evaluation and classification of the PQ phenomena in 25 kV AC traction systems, and secondly to recommend modifications to the current methods and propose new techniques for enhanced conditioning monitoring of electrified railway systems. The objectives of this thesis are as follows:

- To review and analyse the differences between PQ disturbances encountered in the railway system and PQ disturbances present in traditional electric grids, and to evaluate the application accuracy and correctness of standardised methods to railway acquired waveforms.
- To understand the voltage interruption mechanism resulting from the configuration of AC traction network through carefully observing and analysing the behaviour of voltage and current waveforms recorded in 25 kV 50 Hz railway sys-

tems, to allow the development of an improved technique for detection of voltage interruptions in AC traction systems.

- To quantitatively evaluate the effect that one cycle and half-cycle measurement intervals have on the voltage dip and voltage swell measurement results to propose recommendations for PQ monitoring instruments that better reflect the characteristics of the phenomena.

- To assess the current and voltage harmonics emission levels present in 25 kV 50 Hz traction systems, and through a comparative analysis to quantitatively evaluate the effect that different aggregation time intervals have on harmonics measurements. The analysis will allow new recommendations to be provided for PQ rail instruments that better track the time-varying frequency components and produce more accurate harmonics emission levels.

- To quantify the level of harmonics active powers resulting from significant distortion of current and voltage waveforms, to estimate its impact on the energy meters of the train, and understand whether the need for improved energy meter strategies that reflect better the relevant and correct cost of power usage exists.

- To develop, test, and propose a new pantograph-catenary arc detection method that can also identify their geographic kilometric position along the railway track to enhance the safety, reliability, and support better maintenance and condition-monitoring of DC electrified railway systems.

1.3 Research Contributions

This thesis provides the following contributions to knowledge:

- Investigation and evaluation of the challenges involved with the application of IEC 61000-4-30 standardised PQ measurement algorithms to 25 kV 50 Hz electric railway waveforms.

- Development of an improved estimation technique able to identify voltage interruptions caused by phase separation sections of the 25 kV 50 Hz network and differentiate those from other voltage interruption causes, thereby improving event classification.

- Recommendations are provided for PQ measurement algorithms to use half-cycle integration intervals in contrast to the one-cycle measurement window size proposed by IEC 61000-4-30 standard when measuring the voltage dips and voltage swells in 25 kV 50 Hz railway networks. The use of shorter integration intervals has shown an improved accuracy and a better classification of the events for statistical analysis.

- A new time interval to aggregate the results of harmonic measurements for 50 Hz signals is proposed for railway power quality measurement instruments. It offers a more accurate estimation of harmonic emission levels in railway systems compared to the standardised IEC 61000-4-30 method hence, a better understanding of the negative effects of harmonics on the network components, and improved tracking of harmonic variability.

- Development and testing of a novel pantograph-OCL arc detection method for 3 kV DC electrified railways, able to determine and localise in time electric arcs occurring during coasting and regenerative braking phases of a running train. The detected number of arcs can be used to calculate the current collection quality index of the locomotive and can assist the maintenance service in better scheduling of OCL inspections. This method provides a new cost-effective solution for accurate condition monitoring of DC rail infrastructures.

- Extension of the capabilities of the new arc detection method to allow even the kilometric localisation of electric arcs along the railway line. The new feature has the potential to enable predictive maintenance at specific track positions, thereby avoiding lengthy stoppage of transportation service, reducing the operational costs, and improve the reliability of a DC rail network.

In summary, this thesis analyses the accuracy of standardised PQ measurement methods when applied to 25 kV 50 Hz railway waveforms; proposes modifications of the PQ methods to better represent the levels of disturbances in traction systems; proposes new techniques to detect specific PQ disturbances that are characteristic in railway networks; and provides recommendations for future PQ measurement rail instruments.

1.4 Thesis Overview

Chapter 2 introduces the definitions of PQ disturbances and categorizes the phenomena based on their respective characteristics. Standardised measurement methods are also presented. A review of PQ in electrified railway systems is presented in Chapter 3, including disturbance sources, mitigation techniques, and emphasising the challenges of the present measurement methods.

Chapter 4 builds on this discussion and investigates the application of the measurement methods to evaluate voltage interruptions, voltage dips, and voltage swells in a 25 kV 50 Hz railway network. In Chapter 5 the effect of several time-aggregation intervals on the measurement results of harmonic voltages and harmonic currents is analysed.

In Chapter 6 a new method for detecting electric arcs occurring between the pantograph and the OCL in DC railway systems is developed and presented. The results of this method are used in Chapter 7 to propose a solution for the kilometric localisation of the electric arcs needed to support the real-time condition monitoring of DC railway networks.

Chapter 8 summarises the main conclusions of this thesis and suggests future work resulting from this research.

1.5 Publications

The work undertaken during this PhD process has contributed to the following publications:

1.5.1 Journal Articles

- Fan, F., Wank, A., Seferi, Y., and Stewart, B.G., "Pantograph Arc Location Estimation using Resonant Frequencies in DC Railway Power Systems," in *IEEE Transactions on Transportation Electrification*, doi: 10.1109/TTE.2021.3062229.

- Seferi, Y., Blair, S.M., Mester, C. and Stewart, B.G., 2021. A Novel Arc Detection Method for DC Railway Systems. *Energies, 14*(2), p.444.

- Seferi, Y., Blair, S.M., Mester, C. and Stewart, B.G., 2020. Power Quality Measurement and Active Harmonic Power in 25 kV 50 Hz AC Railway Systems. *Energies, 13*(21), p.5698.

- Quijano Cetina, R., Seferi, Y., Blair, S.M. and Wright, P.S., 2021. Energy Metering Integrated Circuit Behavior beyond Standards Requirements. *Energies, 14*(2), p.390.

- Psaras, V., Seferi, Y., Syed, M.H., Munro, R., Norman, P., Burt, G., Compton, C., Grover, K., and Collins, J., 2022. Review of DC Series Arc Fault Testing Methods and Capability Assessment of Test Platforms for More and All Electric Aircraft *IEEE Transactions on Transportation Electrification* (accepted).

1.5.2 Conference Papers

- Seferi, Y., Quijano Cetina R., and Blair, S.M., 2021, September. Review of PMU Algorithms Suitable for Real-Time Operation with Digital Sampled Value Data. In *2021 IEEE 11th International Workshop on Applied Measurements for Power Systems (AMPS)* (pp. 1-6). IEEE.

- van den Brom, H., Giordano, D., Gallo, D., Wank, A. and Seferi, Y., 2020, August. Accurate Measurement of Energy Dissipated in Braking Rheostats in DC Railway Systems. In *2020 Conference on Precision Electromagnetic Measurements (CPEM)* (pp. 1-2). IEEE.

- Seferi, Y., Clarkson, P., Blair, S.M., Mariscotti, A. and Stewart, B.G., 2019, September. Power Quality Event Analysis in 25 kV 50 Hz AC Railway System Networks. In *2019 IEEE 10th International Workshop on Applied Measurements for Power Systems (AMPS)* (pp. 1-6). IEEE.

- Quijano Cetina R., Seferi, Y., Blair, S.M. and Wright, P.S., 2019, April. Analysis and Selection of Appropriate Components for Power System Metrology Instruments. In *2019 2nd International Colloquium on Smart Grid Metrology (SMAGRIMET)* (pp. 1-6). IEEE.

- Cipolletta, G., Delle Femine, A., Gallo, D., Seferi, Y., Fan, F., and Stewart, B.G. Detection of Dips, Swells and Interruptions in DC Power Network. In *2022 IEEE 20th International Conference on Harmonics and Quality of Power (ICHQP)* (accepted).

- Seferi, Y., Arshad, A., Syed, M.H., Burt, G., and Stewart, B.G. Effect of Sampling Rate and Sensor Bandwidth on Measured Transient signals in LV AC and DC Power Systems. In *2022 IEEE 12th International Workshop on Applied Measurements for Power Systems (AMPS)* (accepted).

Chapter 2

Metrics and Power Quality Indices in Power Systems

2.1 Introduction

This chapter provides a literature review of metrics, PQ indices, and recent developments in estimating electrical power system signal properties. The chapter begins by introducing the importance of measurements in power systems and then continues with the formal definition of the PQ parameters and the associated standardised methods required to calculate them.

2.2 Measurements in Electric Power Systems

Electrical measurements are the basis of the successful and stable operation of every electric power system. Measurements are performed to determine the behaviour of electric signals and the resulting operational conditions of transmission grids, distribution grids, high voltage direct current (HVDC) grids, railway grids, and microgrids.
All of these grids require accurate measurements for a variety of applications such as control, protection, monitoring, and energy consumption. Measurements are made available by the measurement chain, which usually consists of interfacing transducers such as voltage transformers (VT) or resistive/capacitive voltage dividers, for the

voltage inputs; and current transformers (CT), current shunt resistors, Rogowski coils, or Hall effect clamps for the current inputs; and measurement instruments like power and energy meters; PQ analysers; data acquisition (DAQ) devices for waveform recording, and phasor measurement units (PMUs). All of these instruments are designed to provide accurate information of the respective estimated network indices, and should be said that they are continuously evolving to reflect the needs of electric grids for enhanced monitoring of the AC and DC signal properties and to contribute towards optimization of real-time control tasks. In turn, enhanced monitoring can contribute to a more stable and reliable power supply. However, it is important to note that it is the measurement purpose itself that guides the kind of instrumentation to be used [24].

In general, power and energy meter instruments are conventionally used in transmission and distribution grids to measure active and reactive power, and energy flow in all four quadrants for billing purposes [25, 26]. High-grade electric energy meters are usually deployed at large power capacity consumers, transmission lines, and substations. Due to the importance of the transactions, they measure the electrical energy with relatively high accuracy (relative error 0.1% to 0.5%), and can also implement some functionalities that allow the calculation of several PQ indices.

Recently, energy meters of a different type [27] are required to be installed in all trains to quantify the real energy consumption. While electric energy meters used in transmission and distribution grids are responsible for calculating the electrical energy provided to their terminals by external voltage and current transformers, the energy meters for rail applications are more complex devices. Voltage and current sensors are an integral part of these meters, and specifications comprise the complete system, not just the energy meter itself like in utility energy meters. Usually, they can accommodate different external sensors to allow transition from one energy system to another energy system characterised by different voltages and frequencies. They continuously transmit data on ground-based data collection systems for rail energy billing applications and are required to comply with different standards than the utility energy meters.

PQ analysers for online disturbance characterisation and waveform recorders using for example DAQ devices are employed relatively in a smaller number than energy

meters. However, their utilisation is directly related to the need of investigating local PQ disturbances on the network, usually caused by various interactions and modes of operation of devices and components connected within the same network. In such a context, on-site measurements of PQ can be used for the following purposes:

- For statistical surveys of voltage characteristics [28] provided by public networks.
- To define harmonic emission levels injected into the grid, for example, by an industrial plant.
- To measure network disturbance levels affecting a particular equipment or installation (immunity of equipment/installation) [29].
- To locate the PQ disturbance sources in the network and propose their mitigation.
- To resolve contractual issues between the suppliers and customers regarding agreed predefined conditions of the quality of voltage supply [24].
- To evaluate the PQ disturbances through measurement campaigns and propose new PQ metrics, for example, in special kinds of electric networks, such as railway networks [30, 31].
- To define waveform datasets for testing purposes.

One interesting approach is to use several PQ analysers on the grid [32], or GPS synchronised DAQs to form a wide-area measurement system (WAMS), and use it synchronously acquire PQ measurements for PQ propagation studies across the network [33], power flow analysis, PQ disturbance source identification, or for example to validate network models.

Recently, synchronised measurement systems are becoming increasingly utilised in electrical grids because of the ability to compare network signal characteristics acquired at geographically distant locations, and to support the stable operation of smart grids [33]. Phasor measurement units (PMUs) are the instruments that can provide measurements of voltage and current phasors, synchronised to a common time reference, usually to Coordinated Universal Time (UTC) [34].

PMUs are widely deployed in electricity grids of transmission systems [35] because of their capability to provide accurate, reliable, fast, and comparable measurements of synchrophasors, frequency, and rate of change of frequency (ROCOF). Thanks to accurate compensation of the internal influential factors, and the appropriate selection of the measurement algorithm, these instruments can provide real-time information about the parametric measurements of the signals. These advanced features have enabled PMUs to be utilised in measurement-based control and protection schemes [36]; to support state estimation algorithms [35, 37]; and to monitor network disturbances such as harmonics, voltage stability indicators, inter-area oscillations, and power system dynamic phenomena of the transmission system through WAMS [35, 38].

PMU instruments also are installed in distribution electric grids for voltage, current, and power flows monitoring [39]; to estimate the line parameters [40], and for protection such as loss of main and load shedding [41]. They are expected to have a larger utilisation to enhance the monitoring and real-time control capability of these grids, considering the increasing integration of renewable energy generation.

2.3 Definition and Classification of Power Quality Phenomena

Power quality is a principal issue in electric power systems because it has a direct impact on the smooth and stable operation of electric grids [24, 42]. However, PQ is not seen only from the power system security point of view but also from the customer and equipment immunity point of view.

In many cases, the customers themselves are responsible for deteriorating the PQ of the grid [24, 43]. For example, in a distribution grid where several linear and nonlinear loads are connected at the same bus, nonlinear loads typically draw distorted currents and are responsible for distorting the voltage that also supplies other loads of the grid in the local area. In this situation, the nonlinear loads are causing poor PQ, whereas the electric network is responsible for propagating the disturbances to other loads. This situation creates many concerns for customers as their equipment can

experience a malfunction, or in most severe cases, failure of operation. For example, computers, microprocessor-based devices, and other electronic devices do not tolerate voltage reduction of more than 10 % to 20 % from the nominal voltage for a few cycles; transformers and cables experience increased heating due to harmonic current presence; harmonic voltage can reduce converter efficiency; voltage unbalance can lead to negative sequence components and reduce three-phase motor efficiency. The affected customers usually do not have the legal and ethical rights to blame other customers but can complain to the utility supplier, which is responsible to resolve the issue, about the poor PQ supplied at their premises and the problems experienced by their equipment.

In such a context, the power quality concept is defined either as a combination of a loading-quality with the supply-quality [43], or as voltage and current quality where their values deviate from the ideal conditions [42, 44].

The interest in studying and understanding this topics of PQ, its sources, and the effects on the network components, in more depth has increased in the previous decades from both the research community and utility suppliers because of the following reasons [29, 42, 43, 45]:

- PQ disturbances are increasing due to the proliferation of nonlinear loads and distributed generation, which is typically interfaced to the grid using power electronic converters which can introduce PQ issues.
- Electronic equipment are typically composed of circuits that do not tolerate poor PQ, such as voltage dips.
- Stoppage of industrial processes due to PQ disturbances has a large cost, therefore, equipment failure is unwanted.
- In an open electricity market, customers can choose the supplier who offers the best supply quality.
- To identify the sources of the disturbances and propose effective mitigation actions.

Power quality is estimated by several indices that in turn evaluate the wide range of electromagnetic phenomena that characterize both the voltage and current signals of the grid. The following sub-sections will describe each of the PQ phenomena, and will provide illustrative examples. According to their attributes, disturbances also are categorised.

2.3.1 Transients

Transients are electromagnetic events occurring in a very short time period and are characterised by a significant change in voltage or current magnitude. Depending on the shape the waveform takes during a transient, they are classified into two types, impulsive (voltage or current waveform becomes unidirectional in polarity) and oscillatory (voltage or current signal oscillates with respect to the time axis) [29]. However, this classical distinction cannot be taken as absolute, as transient may contain both waveform shapes combined during their propagation on the network [44].

- Impulsive transients

An impulsive transient as per the IEEE 1159 [29] standard definition is: "*a sudden, non-power frequency change from the nominal condition of voltage, current, or both, that is unidirectional in polarity (primarily either positive or negative)*".
The main cause of these transients is due to lightning strikes. These disturbances occur at random and are unwanted because the large overvoltages they create can affect the device insulation and, usually, these disturbances lead to other undesired phenomena such as resonances and voltage interruptions. Figure 2.1, presents an example of a current impulsive transient caused by lightning.

- Oscillatory transients

An oscillatory transient as per IEEE 1159 standard definition is "*a sudden, non-power frequency change in the steady-state condition of voltage, current, or both, that includes both positive and negative polarity values*". These transients are usually caused by switching events in electric circuits. As a distinguishing feature from the impulsive

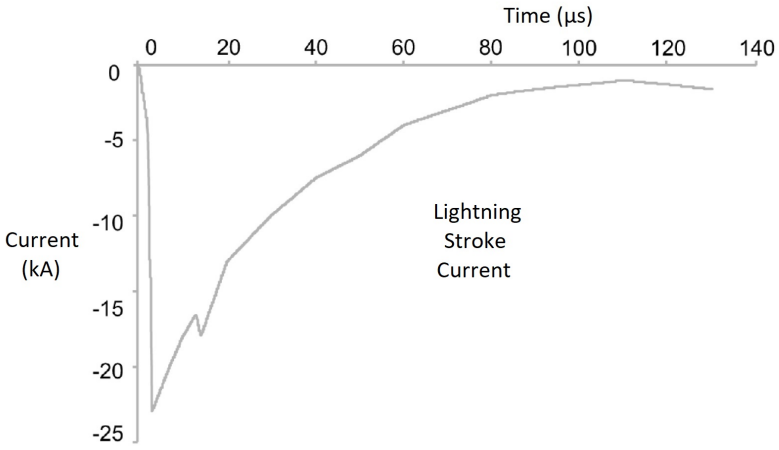

Figure 2.1: Impulsive current caused by lightning as per IEEE 1159-2019 standard.

transients, these transients experience an oscillatory decaying behavior. This behavior is shown in Figure 2.2, where a voltage transient is experienced during a capacitor energization. The voltage transient is a consequence of capacitor inrush transient current.

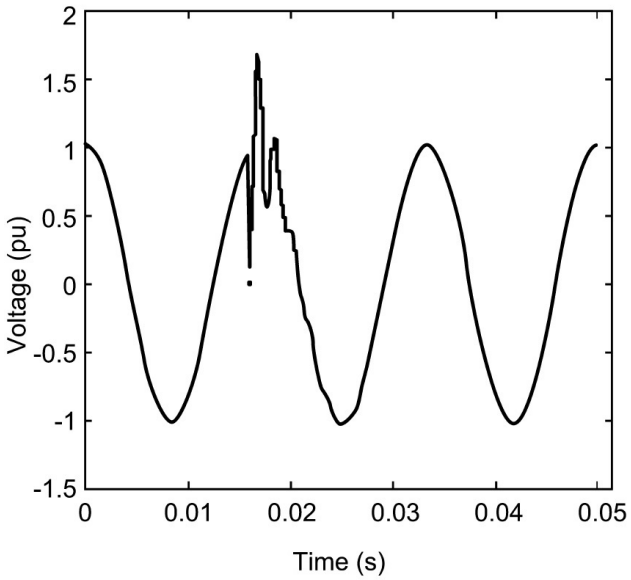

Figure 2.2: Oscillatory transient caused by capacitor switching as per IEEE 1159-2019.

Depending on the main frequency component and time duration, these transients are further categorised into low, medium, and high frequency transients.

2.3.2 Voltage Interruptions

Voltage interruption as per the IEEE 1159 standard, is defined as "*a condition where the supply voltage decreases below the 10% of the nominal voltage for different time periods*". These periods can range between 0.5 cycles to 3 s; over 3 s to 1 minute; and longer than 1 minute, respectively for momentary, temporary, and sustained interruptions.

Voltage interruptions in power systems are mainly caused by short circuits and earth faults in the system, equipment failure, and false operation of switching devices. Figure 2.3 presents the time domain instantaneous voltage behavior during an artificial voltage interruption lasting for two cycles.

2.3.3 Voltage Sags (Dips)

A voltage sag (also known as a voltage dip as per IEC definition) as per the IEEE 1159 standard is defined as "*a decrease in rms voltage to between 0.1 pu and 0.9 pu for durations from 0.5 cycles to 1 min*". Depending on the time duration, voltage sags can be further classified as instantaneous sags, momentary sags, and temporary sags, lasting respectively between 0.5 cycles to 30 cycles; 30 cycles to 3 s; and 3 s to 1 minute. Voltage dips are caused by faults in the system, transformer energization, abrupt load changes, and when switching on large loads requiring high starting currents, such as starting large motors. An example of an artificially created voltage dip, lasting for two cycles is presented in Figure 2.4.

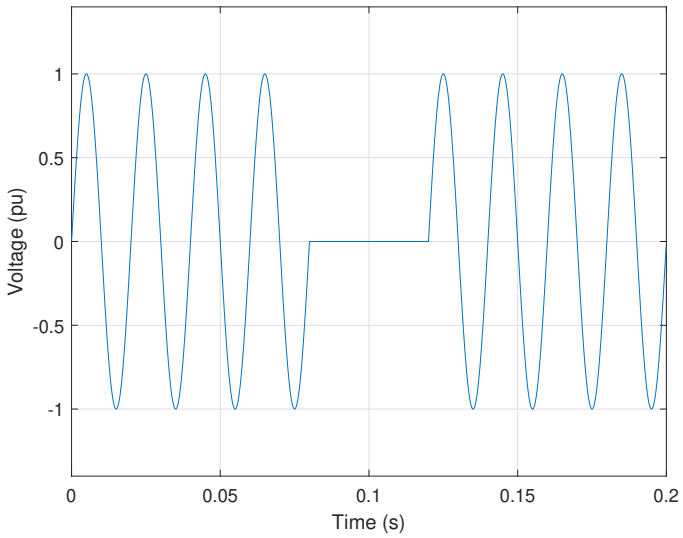

Figure 2.3: Time domain representation of a voltage interruption event.

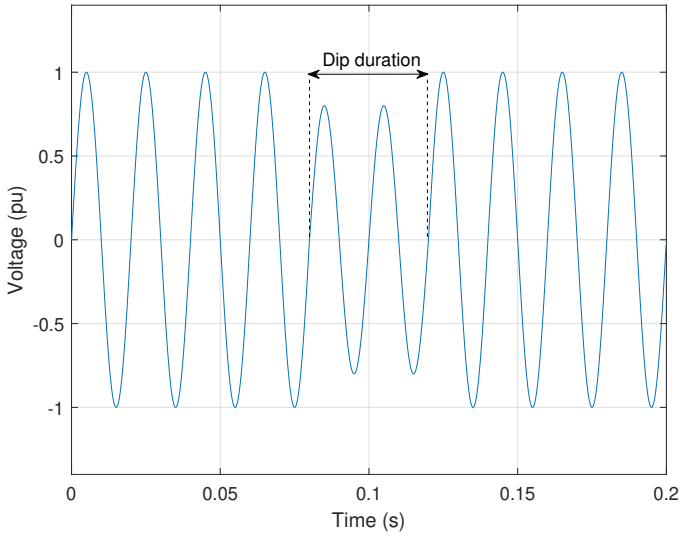

Figure 2.4: Time domain representation of a voltage dip event.

2.3.4 Voltage Swells

Voltage swells are the opposite of voltage dips. As per the IEEE 1159 standard, a swell is defined as "*an increase in rms voltage above 1.1 pu for durations from 0.5 cycles to 1 min*". Similar to voltage dips, voltage swells are classified as instantaneous, momentary,

and temporary swells, depending on the same time duration intervals. Typically longer duration voltage swells have a lower increase in voltage magnitude in relation to the nominal system voltage.

Voltage swells are caused by switching off large loads, abrupt load changes, and when switching on large capacitors for example when injecting reactive power to compensate for the voltage drop along the line using a static VAR compensator [46]. Figure 2.5, illustrates the time domain instantaneous voltage during a voltage swell of four cycles.

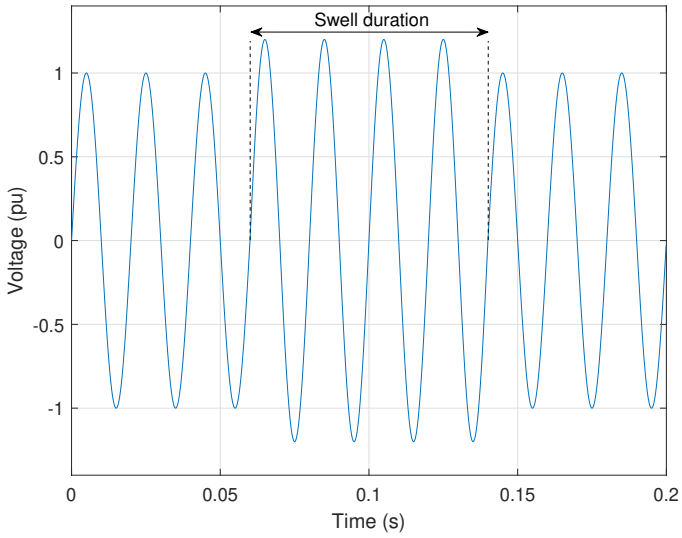

Figure 2.5: Time domain representation of a voltage swell event.

2.3.5 Overvoltage

Overvoltage as per the IEEE 1159 standard is defined as "*an rms increase in ac voltage greater than 1.1 pu for a duration longer than 1 min*". Overvoltage is caused by load disconnections, switching on capacitor banks, and by the incorrect operation of the mechanisms designated to regulate the voltage level of the network. Additionally, in railway system, overvoltage can also occur during regenerative braking of the train where the produced energy is delivered back to the OCL [47].

2.3.6 Undervoltage

Undervoltage is the opposite event of overvoltage. It is defined as "*a decrease in rms voltage less than 0.9 pu for a duration longer than 1 min*" by the IEEE 1159 standard. Undervoltage is caused when large loads are switched on, during overloaded network conditions, and when a capacitor bank is switched off.

2.3.7 Unbalance

Unbalance (or imbalance as per IEEE 1459) is the condition in the three-phase power supply system where the voltage (or current) magnitudes of every phase are not equal, and/or the respective phase angle differences differ from 120 degrees.

Unbalance in three-phase systems is caused due to the presence of single-phase loads unequally distributed among the phases. In Figure 2.6 the unbalanced voltage waveforms (representing the unbalance in magnitudes only) of a three-phase power supply system are presented. As indicated, the voltage magnitudes of every phase are not equal, creating a non-symmetric voltage supply system.

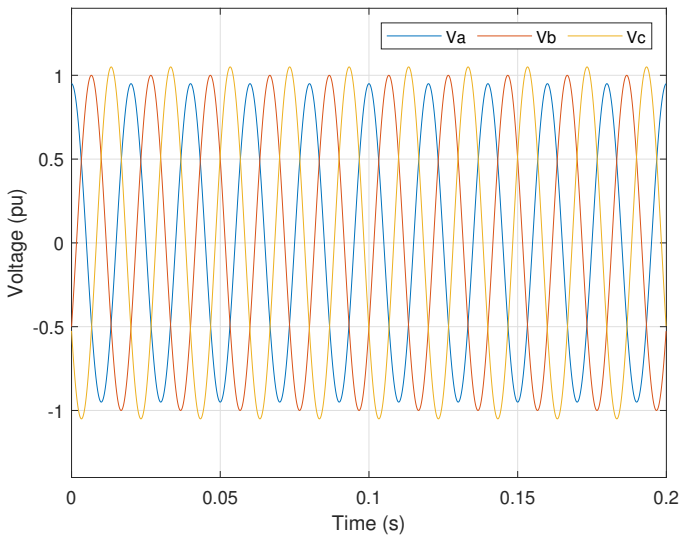

Figure 2.6: Voltage unbalance in three-phase system.

2.3.8 Harmonics

Harmonics as per the IEEE 1159 standard are defined as "*sinusoidal voltages or currents having frequencies that are integer multiples of the fundamental frequency (50 Hz or 60 Hz)*". If the harmonic frequency has an an odd relationship with the fundamental frequency, these harmonics are called odd harmonics, for example the 3^{rd}, 5^{th}, 7^{th}, 9^{th},.., etc., are odd harmonics. Similarly, harmonics having an even relationship with the fundamental frequency are named even harmonics, for example the 2^{nd}, 4^{th}, 6^{th}, 8^{th},..., etc.

Harmonic components are normally superimposed to the fundamental frequency component, producing waveform distortion. An illustrative waveform distortion containing the fundamental frequency component and some odd harmonics (3^{rd}, 5^{th}, and 7^{th}) is presented in Figure 2.7.

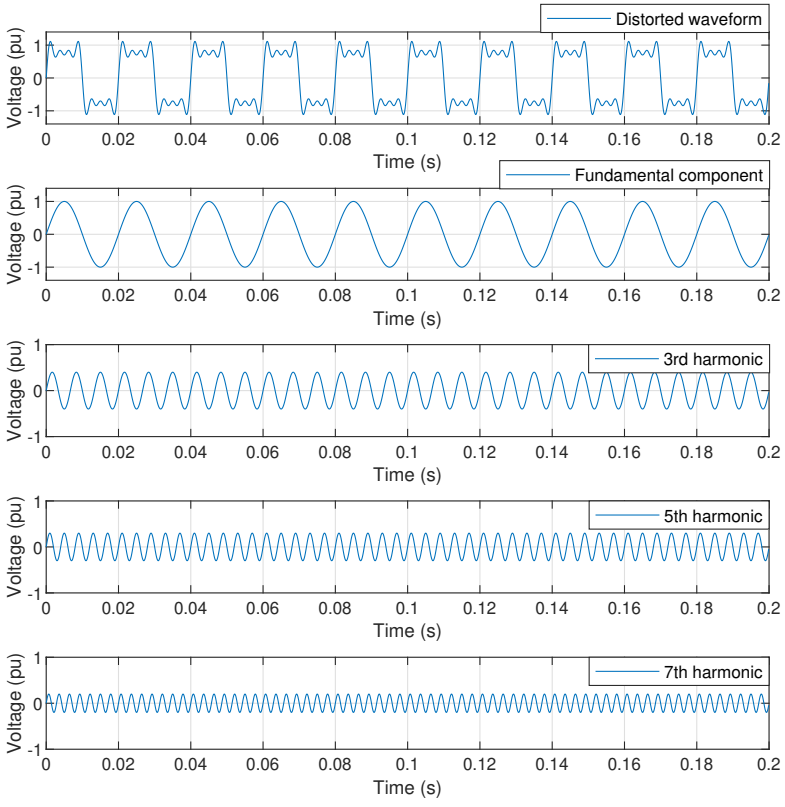

Figure 2.7: Waveform distortion due to the presence of odd harmonics.

The figure shows how the superposition of the harmonic components make up the distorted waveform and simultaneously how a non-sinusoidal periodic signal is decomposed into sinusoidal components of frequencies at integer multiples of the fundamental.

Harmonics in power systems are mainly caused by loads having non-linear characteristics, such as AC/DC converters, adjustable-speed drives, arc furnaces, computers, and household electronic devices [42, 48].

2.3.9 Interharmonics

Interharmonics as per the IEEE 1159 standard are defined as "*voltage or current having frequency components that are not integer multiples of the frequency at which the supply system is designed to operate (e.g., 50 Hz or 60 Hz)*". The main cause of interharmonics are static frequency converters, cycloconverters, arc welding, and induction furnaces [29, 48].

2.3.10 Notching

Notching as per the IEEE 1159 standard "*is a periodic voltage disturbance caused by the normal operation of power electronics devices when current is commutated from one phase to another*". Figure 2.8, illustrates the voltage notching phenomenon, occurring periodically (denoted by the sharp changes) on the voltage signal.

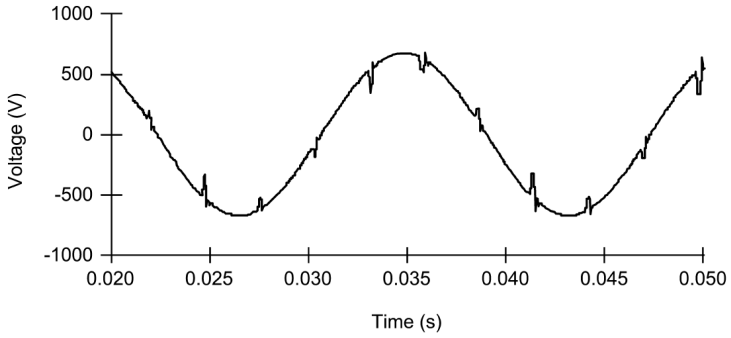

Figure 2.8: Example of voltage notching phenomenon as per IEEE 1159-2019 standard.

2.3.11 DC offset

DC offset is defined as the presence of DC voltage or current in AC signals. DC offset in power systems is caused by the operation of rectifiers and transformer saturation [29,49]. A decaying DC offset is also often present during short circuit faults. Additionally, DC offset can be caused by geomagnetic disturbances resulting from the interaction of the earth's magnetic field with the charged magnetic clouds produced by solar storms. This phenomenon can cause geomagnetic induced currents of magnitudes between 1 A to 10 A [50–53] and in some cases above 25 A [54, 55].

2.3.12 Noise

Noise is an electrical signal superimposed on the voltage or current signal of the power systems. The spectral content of noise is limited to less than 200 kHz, whereas its magnitude usually stays below 1% of the voltage magnitude [29].

The main causes of electric noise are arc furnaces, welding equipment, power electronic devices, control circuits, etc., [29, 49].

2.3.13 Voltage Fluctuations

Voltage fluctuations as per the IEEE 1159 standard are defined "*as systematic variations of the voltage envelope*". The variations in voltage magnitude normally stay within the 0.95 pu to 1.05 pu voltage range. Such variations create a change in light intensity of lamps, known as the flicker phenomenon. An example of a voltage waveform, created to represent the voltage fluctuations phenomenon, is presented in Figure 2.9.

Voltage fluctuations are caused by loads experiencing rapid variations, such as arc furnaces, arc welding devices, and traction loads [29, 44].

2.3.14 Power Frequency Variations

Power frequency variation is the phenomenon where the system frequency deviates from the nominal fundamental frequency, defined as either 50 Hz or 60 Hz. This phenomenon

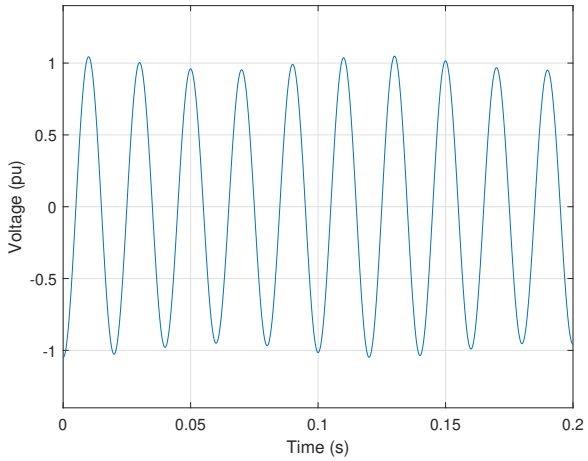

Figure 2.9: Time domain representation of a voltage fluctuation phenomenon.

is caused due to the unbalance between the active power demand and the generated active power.

The above described and illustrated PQ phenomena are classified into different categories by standard IEEE 1159 [29]. These phenomena are summarised in Table 2.1.

Table 2.1: Categorisation of electromagnetic phenomena as per IEEE 1159-2019.

Categories	Spectral content	Time duration	Variation magnitude
1.0 Transients			
1.1 Impulsive			
1.1.1 Nanosecond	5 ns rise	<50 ns	
1.1.2 Microsecond	1 μs rise	50 ns – 1 ms	
1.1.3 Millisecond	0.1 ms rise	>1 ms	
1.2 Oscillatory			
1.2.1 Low frequency	<5 kHz	0.3–50 ms	0–4 pu*
1.2.2 Medium frequency	5–500 kHz	20 us	0–8 pu
1.2.3 High frequency	0.5–5 MHz	5 us	0–4 pu
2.0 Short-duration root-mean-square (rms) variations			
2.1 Instantaneous			
2.1.1 Sag		0.5–30 cycles	0.1–0.9 pu
2.1.2 Swell		0.5–30 cycles	1.1–1.8 pu
2.2 Momentary			
2.2.1 Interruption		0.5 cycles – 3s	<0.1 pu
2.2.2 Sag		30 cycles – 3 s	0.1–0.9 pu
2.2.3 Swell		30 cycles – 3 s	1.1–1.4 pu
2.2.4 Voltage Imbalance		30 cycles – 3 s	2%–15%
2.3 Temporary			
2.3.1 Interruption		>3 s – 1 min	<0.1 pu
2.3.2 Sag		>3 s – 1 min	0.1–0.9 pu
2.3.3 Swell		>3 s – 1 min	1.1–1.2 pu
2.3.4 Voltage Imbalance		>3 s – 1 min	2%–15%
3.0 Long duration rms variations			
3.1 Interruption, sustained		>1 min	0.0 pu
3.2 Undervoltages		>1 min	0.8–0.9 pu
3.3 Overvoltages		>1 min	1.1–1.2 pu
3.4 Current overload		>1 min	
4.0 Imbalance			
4.1 Voltage		steady state	0.5-5%
4.2 Current		steady state	1.0-3.0%
5.0 Waveform distortion			
5.1 DC offset		steady state	0–0.1%
5.2 Harmonics	0–9 kHz	steady state	0–20%
5.3 Interharmonics	0–9 kHz	steady state	0–2%
5.4 Notching		steady state	
5.5 Noise	broadband	steady state	0–1%
6.0 Voltage fluctuations	<25 Hz	intermittent	0.1–7% 0.2–2 Pst**
7.0 Power frequency variations		<10 s	± 0.10 Hz

* pu refers to per unit.

** Flicker severity index P_{st}

2.4 Evaluation of Power Quality Disturbances

In the previous section, the power quality indices have been defined and classified into various categories depending on their characteristics, such as spectral content, time duration, and magnitude variation. Based on how these characteristics are measured, the phenomena can also be classified into two main groups [42, 44]:

- Variations – including all the disturbances that are characterised by slow and small variations from their nominal values, for example, voltage variations, frequency variations, harmonics, unbalance.
- Events – encompassing all the phenomena that experience large variations from their steady-state conditions, for example, voltage interruptions, voltage dips, voltage swells, and voltage transients.

The focus of this section will be on the description of the measurement methods used to measure and interpret the power quality indices. These measurement methods are defined in standards IEC 61000-4-30 and IEC 61000-4-7 [14, 15], and because of their relevance to the contribution of this thesis, some of them will be briefly described here.

- Power frequency – according to standard IEC 61000-4-30 [14], is required to be estimated over 10 s time intervals. The method counts the number of integer cycles within 10 s and estimates the total duration of these cycles. The fundamental frequency is calculated by dividing the number of integer cycles by the total duration.

  Using the same approach, it is obvious that average frequency can be estimated over shorter intervals, for example, every 1 s. However, in applications such as control, protection, enhanced monitoring, etc., the frequency estimation is required much faster, for example, after every cycle.

  It is worth noting that the zero-crossing method required by standard IEC 61000-4-30 is not the only method to measure the frequency. Other methods are avail-

able such as: phase-locked loops [44, 56]; methods based on the Discrete Fourier Transform (DFT) [57]; methods based on time-domain signal analysis [58]; and methods based on demodulation and filtering [34, 59].

- Voltage magnitude – as per IEC 61000-4-30 standard is defined by the rms value estimated over 10 or 12 cycle time intervals, respectively for 50 Hz and 60 Hz power supply systems. Because the system frequency varies, the length of the interval usually is not precisely 200 ms. As a result, the time-interval has to be determined by the fundamental frequency using, for example, the previously estimated frequency or by using adaptive sampling in real-time [44, 56].

  Similarly, the voltage magnitude can be estimated with other techniques too, for example, by considering the amplitude value of the waveform, or by extracting the fundamental component from the frequency spectrum of the considered voltage signal.

- Voltage dips and swells – are based on the rms voltage measurements calculated over one cycle and updated every half-cycle $U_{rms(1/2)}$, or every cycle $U_{rms(1)}$ depending on the class A or S type of the PQ measurements [14]. Classes A and S are assigned to PQ measurement instruments. They indicate what measurement method is used to measure and calculate a PQ parameter and what measurement uncertainty is associated with the particular PQ parameter. Higher accuracy and lower measurement uncertainty are associated with class A. Therefore, class A certified PQ instruments are used where precision is required, whereas class S for measurement campaigns to support statistical PQ surveys. Both phenomena are characterised by two attributes: residual voltage and time duration for voltage dips, and swell voltage and time duration for voltage swells. Such characteristics allow a further phenomena understanding and classification as presented in Table 2.1.

- Voltage interruptions – are based on the rms voltage measurements (as for voltage dips and swells).

- Voltage transients – are detected differently compared to the rms approach used

for the measurement of dips, swell, and interruptions. Standard IEC 61000-4-30 does not define any method, but only gives recommendations. Different methods are proposed in literature, including Fourier transform-based; wavelet transform; dv/dt method with an appropriate threshold; the cycle-by-cycle difference method; comparison with the fundamental waveform method; and using high-pass digital filters. [14, 44, 60].

- Voltage unbalance – is evaluated by using the method of symmetrical components.
- Voltage and Current harmonics – are extracted by the DFT algorithm after processing the digital samples acquired from the analog to digital converter (ADC). Harmonics measurements are estimated over 10/12 cycles intervals respectively for 50/60 Hz supply systems, in order to achieve a 5 Hz frequency resolution after applying the DFT algorithm. To consider the spread of spectral energy from harmonic bins to adjacent bins during voltage fluctuations, the concept of harmonic (and interharmonics) grouping is introduced in standard IEC 61000-4-7 [15]. Harmonics are required to be estimated up to the 50^{th} order for class A and up to the 40^{th} order for class S of measurements.

2.5 Chapter Summary

In this chapter, an overview of electrical measurements performed in electrical power systems has been presented, where the importance of accurate, reliable, and fast measurements for different applications has been emphasised. Some basic and advanced measurement instruments and their utilisation for various problem-solving approaches in electric power systems also have been shown. Because of the relevance of PQ phenomena to the contributions of this thesis, detailed definitions and classifications of the disturbances in various categories based on spectral content, time duration, and magnitude variation characteristics have been provided. Measurement techniques used to detect and measure the PQ phenomena also have been briefly presented. It has been shown that besides the standardised measurement methods, other alternative techniques exist to measure the effect of these disturbances in electric power systems.

Chapter 3

Power Quality in Electrified Railway Systems

3.1 Introduction

This chapter provides a literature review of the recent developments in the electrified railway networks. It begins by introducing the different traction power supply systems in use and then focuses on the sources of PQ disturbances, discusses some mitigation techniques, and emphasises the need of having improved PQ measurement methods.

3.2 Railway Traction Power Supply Systems

Different power supply system configurations have been employed to feed railway electric networks, depending on the train service (tramway, metro, commuter rail, freight rail), predicted load, and the available train technology in use [61]. The main power supply electrification schemes widely adopted around the world are:

- DC power supply electrification system.
- AC power supply system at 50 Hz frequency.
- AC power supply system with autotransformers at 50 Hz frequency.
- AC power supply system at 16.7 Hz frequency.

3.2.1 DC Railway Electrification System

DC power supply systems are commonly used to supply light rails such as metros and tramways, and commuter rails operating in urban, suburban, and regional areas [4, 61, 62]. A typical power supply network used to feed a DC railway traction system is depicted in Figure 3.1. The system consists of traction substations (TS), evenly spaced within 20 km, that transform and convert the three-phase high voltage AC power supply into a DC voltage level, appropriate to supply the DC locomotive with energy through either an overhead contact line (OCL) or a third rail mounted beside the track.

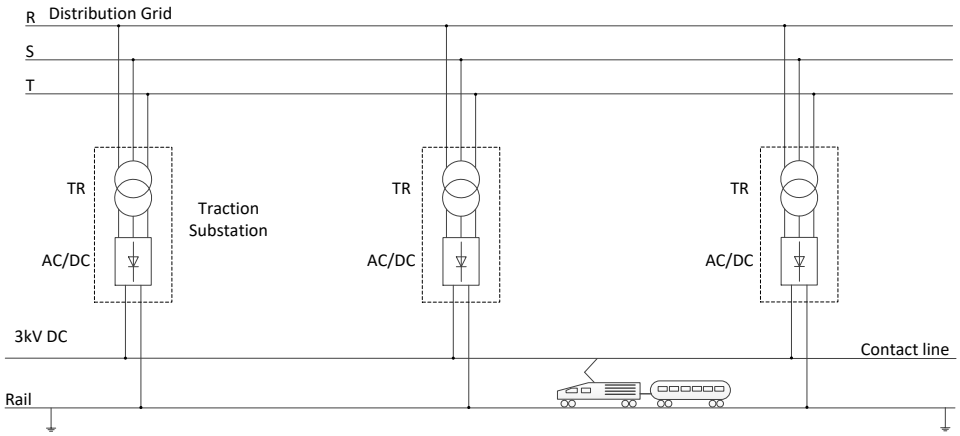

Figure 3.1: DC Power supply system.

Each TS has a power transformer, typically with one or two secondary windings, that feeds either a 6-pulse or a 12-pulse rectifier, and normally filters to attenuate characteristic harmonics resulting from the conversion groups. The most commonly used voltage in the DC railway networks of European countries is 3000 V. However, voltage levels of 750 V DC and 1500 V DC are still in use in some parts of the UK, France and the Netherlands. Other voltage levels such as 600 V DC, 750 V DC, and 1500 V DC are normally used to feed tramways, metros, and trolleybuses.

This configuration allows the TS to work in parallel and therefore providing redundancy in the case that one TS is out of service. In addition, sections supplied by each TS do not need to be isolated from other adjacent sections, minimizing the complexity of the network, and ensuring service continuity.

3.2.2 AC Railway Electrification System at Mains Frequency

AC power supply systems of 25 kV 50 Hz are the most widespread electrified railways networks. This is because the electrified scheme is simple and uses only power transformers to convert the energy from the high voltage (HV) feeding lines to a voltage level acceptable for AC traction units. In addition, higher voltage levels achieved in AC systems reduce the flowing current in the OCL, and consequently, the size of network components [4].

Figure 3.2 represents a typical power supply configuration, widely used to feed AC traction systems of 25 kV 50 Hz. Several TSs are equally spaced along the railway line and are fed by dedicated HV distribution lines. In each TS, two power transformers are used to supply defined sections of the OCL. Considering that the locomotives are large single-phase loads, power has to be distributed equally among the three-phases of the utility grid. To achieve this, and reduce the negative sequence current resulting from the system unbalance as much as possible [4,17,61,62], transformers at TS are connected to different pairs of the utility phases. Consequently, this requires the electrical isolation of the various supply sections by means of phase separation sections or neutral sections (NS) as depicted in Figure 3.2 to avoid short-circuiting the two different phases of the adjacent OCL sections by the train passing under them.

In this configuration, the train collects the power from the OCL through a pantograph structure that continuously slides on the OCL.

Another distinct characteristic of AC traction systems of 25 kV 50 Hz compared to 3 kV DC traction systems is the narrower variation of the line voltage distribution and the negligible effect the loading has on the system voltage. Such voltage variations for the two railway systems are presented in Figure 3.3, where it can be observed that the maximal difference in the voltage level in 25 kV 50 Hz system [63] is approximately

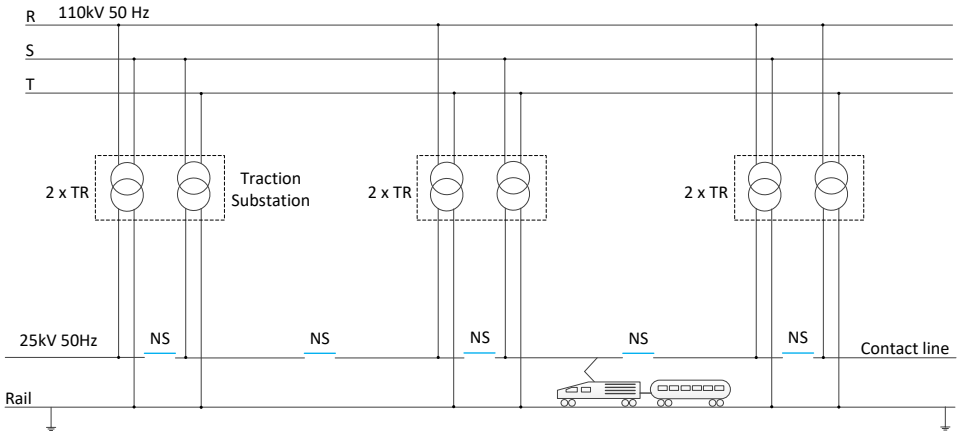

Figure 3.2: AC Power supply system at 25 kV 50 Hz frequency.

300 V or 1.2% of the standardised nominal voltage. Whereas, in the DC system [64], voltage varies up to 1200 V or 40% of the nominal voltage. Smaller voltage variations allow more trains to run safely under the same power supply section in high traffic conditions.

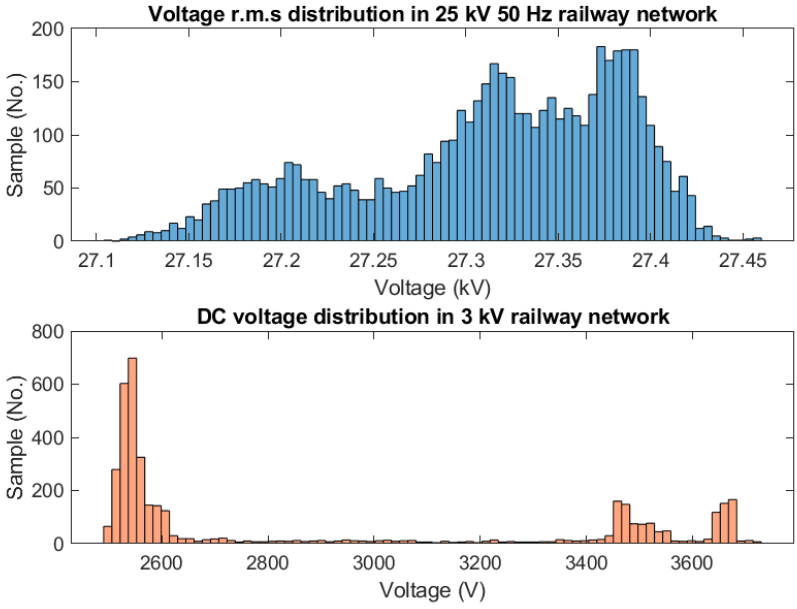

Figure 3.3: Statistical analysis of voltage variation in 25 kV 50 Hz and 3 kV DC railway networks.

3.2.3 AC Autotransformer Electrification System

Another commonly adopted AC power supply system for electrified railway networks is the 2 × 25 kV 50 Hz system [4, 65, 66], presented in Figure 3.4. The system is realized with a power transformer installed at the TS, and three autotransformers units evenly spaced at approximately 12.5 km between each other. The secondary nominal voltage of the transformer is 50 kV, and it has three output terminals. The center terminal of the secondary winding is connected to the rail, at earth potential, whereas the other terminals are connected respectively at the OCL, at +25 kV, and at the feeder line, at -25 kV. Both the voltages have the same potential with respect to the ground, but they are in opposite phase.

When the train is between two autotransformer units, the traction current is partially supplied by the transformer located at the TS, and partially by the two adjacent autotransformers. By transmitting the power at 50 kV, the losses in the traction circuit are reduced. Also, the system provides reduced voltage drops for the same traffic, compared to the 1× 25 kV 50 Hz solution, and therefore a reduced number of TSs [4, 67], that are spaced at 50 km among each other.

These advantages have made this power supply system configuration the system of choice for high speed and high capacity electrified railway networks [68], that is currently in use in many countries such as in France and Italy.

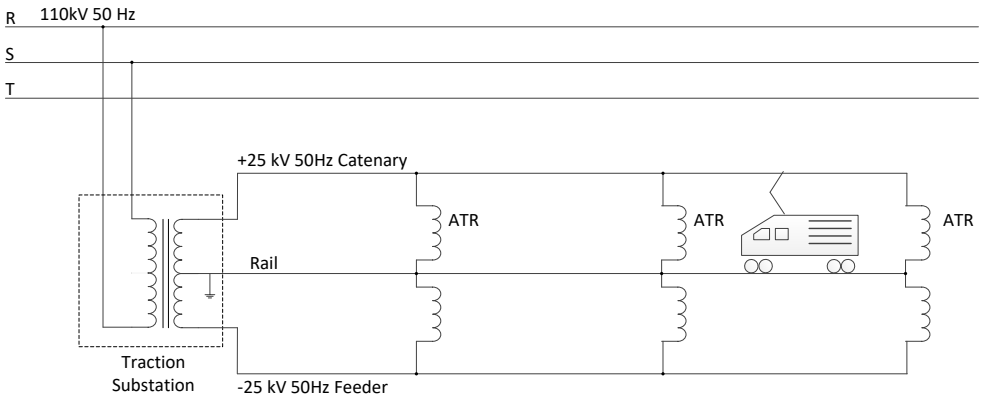

Figure 3.4: AC Power supply system at 2 × 25 kV 50 Hz frequency.

3.2.4 AC Railway Electrification Systems at Special Frequencies

Single-phase networks at special frequencies of 16.7 Hz (one-third of the industrial 50 Hz frequency), used in Europe, or at 25 Hz, used in the U.S, have been in operation since the beginning of railway electrification [4].

The use of these special frequencies was motivated by the fact that a lower frequency in the OCL can produce lower reactive voltage drops and therefore the distance between substations can be potentially increased.

A typical power supply system schematic used to supply a 16.7 Hz railway network at 15 kV is presented in Figure 3.5. This system is currently in use in Germany, Austria, Sweden, and Norway.

Frequency conversion from the industrial 50 Hz to the special 16.7 Hz can be achieved at TSs either by rotating frequency converters or by static converters as represented in Figure 3.5.

In the first case, the energy from the three-phase distribution line, powers a three-phase motor through a three-phase power transformer. The motor shaft is connected to a single-phase generator that creates the desired frequency to feed the railway network by exploiting different combinations of the number of poles of the motors with the number of poles of the generator [69,70]. In the second case, a power electronic converter

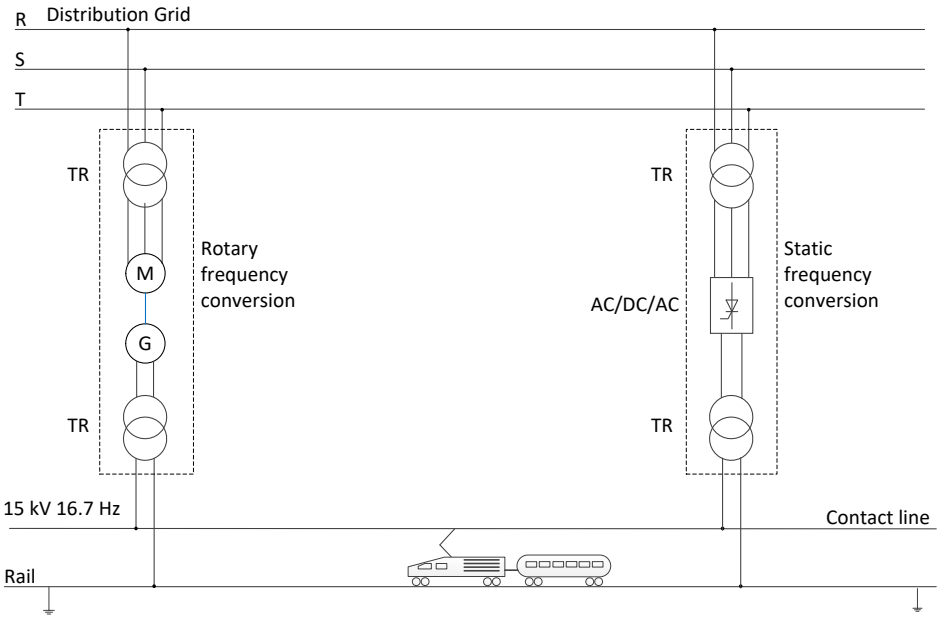

Figure 3.5: AC Power supply system at 15 kV 16.7 Hz special frequency.

is used to convert the frequency.

3.2.5 Facts and Figures of Railway Electrification Systems in Europe

Various railway traction power supply schemes, characterised by different AC and DC voltage levels have been adopted in different countries. Table 3.1 summarizes the voltage levels implemented to feed railway networks in European counties.

It can be seen that the majority of the countries have implemented the 2 × 25 kV 50 Hz power supply system solution. Railway electrification schemes supplied by 1.5 kV DC and 3 kV DC voltage levels and the 15 kV at the special frequency of 16.7 Hz solutions are also widely used. A non-standardised voltage level of 1650 V DC is used in Denmark to supply the urban and suburban railway service. The 750 V DC power supply system is used in some parts of England to supply the railway service through a third-rail system, and it is the only location in Europe to use this system voltage to supply a railway network.

In Table 3.2, the total length of the railway network per country is presented, together with the electrified and non-electrified lengths respectively. It can be concluded, that only a few countries like Albania and Kosovo do not have an electrified rail network, and a few countries such as Liechtenstein and Switzerland have the entire railway network electrified. For convenience, percentages of the electrified networks relative to the total railway network are presented in Figure 3.6 for the European countries having a railway system in place. In total, 59.4 % by distance of the railway network in Europe is electrified.

The majority of the data presented in Table 3.2 is made available from the European Union statistical database, Eurostat [71], whereas the data of the countries highlighted in blue color are taken from Wikipedia [72].

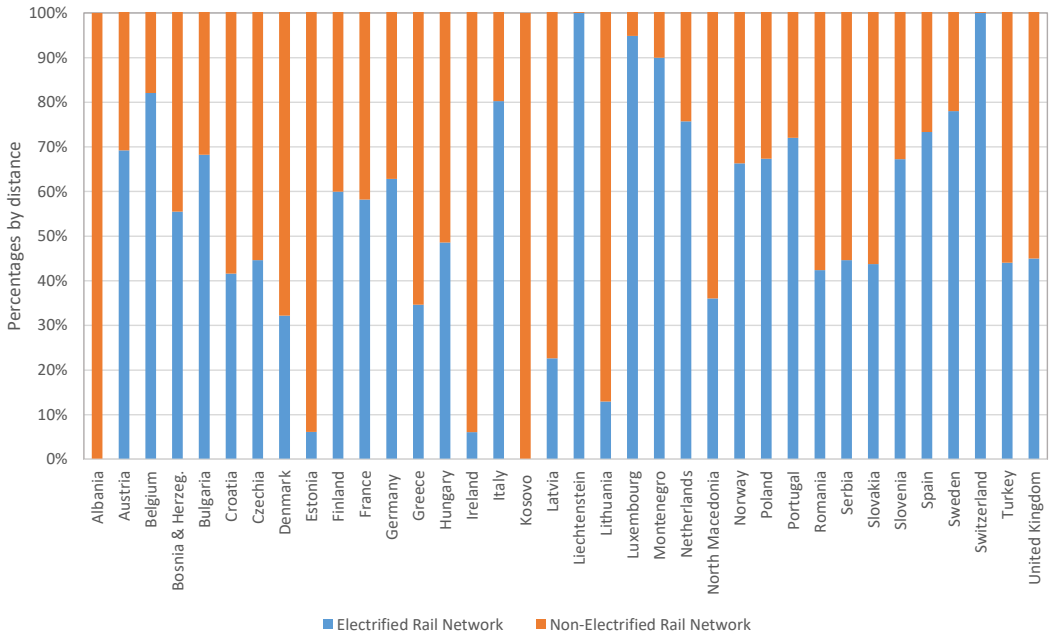

Figure 3.6: Percentages by distance of the electrified rail networks to the total railway networks in European countries.

Table 3.1: Power supply system implemented in European railway networks.

Country	**750 V DC**	**1.5 kV DC**	**1650 V DC**	**3 kV DC**	**15 kV 16.7 Hz**	**25 kV 50 Hz**
Albania						
Austria					x	
Belgium				x		x
Bosnia & Herzeg.						x
Bulgaria						x
Croatia						x
Czechia				x		x
Denmark			x			x
Estonia				x		
Finland						x
France		x				x
Germany					x	
Greece						x
Hungary						x
Ireland						
Italy				x		x
Kosovo						
Latvia				x		
Liechtenstein					x	
Lithuania						x
Luxembourg				x		x
Montenegro						x
Netherlands		x				x
North Macedonia						x
Norway					x	
Poland				x		
Portugal						x
Romania						x
Serbia						x
Slovakia				x		x
Slovenia				x		
Spain				x		x
Sweden					x	
Switzerland					x	
Turkey						x
United Kingdom	x					x

Table 3.2: Electrified, non-electrified and total length of railway networks in European countries.

Country	Non-electrified rail network length (km)	Electrified rail network length (km)	Total length in (km)
Albania	334	-	334
Austria	1,701	3,826	5,527
Belgium	647	2,960	3,607
Bosnia & Herzeg.	453	565	1,018
Bulgaria	1,736	3,734	5,470
Croatia	2,300	1,640	3,940
Czechia	8,580	6,908	15,488
Denmark	1,347	640	1,987
Estonia	2,008	132	2,140
Finland	3,411	5,114	8,525
France	11,540	16,053	27,593
Germany	25,067	42,333	67,400
Greece	1,807	957	2,764
Hungary	5,827	5,509	11,336
Ireland	2,319	150	2,469
Italy	4,840	19,663	24,503
Kosovo	440	-	440
Latvia	1,715	502	2,217
Liechtenstein	-	9.5	9.5
Lithuania	2,032	303	2,335
Luxembourg	32	590	622
Montenegro	25	225	250
Netherlands	741	2,314	3,055
North Macedonia	580	327	907
Norway	1,407	2,770	4,177
Poland	12,117	24,970	37,087
Portugal	907	2,337	3,244
Romania	11,582	8,522	20,104
Serbia	2,976	2,398	5,374
Slovakia	2,040	1,587	3,627
Slovenia	713	1,465	2,178
Spain	5,831	16,050	21,881
Sweden	3,425	12,146	15,571
Switzerland	-	5,196	5,196
Turkey	6,942	5,467	12,409
United Kingdom	17,486	14,292	31,778

3.3 Voltages and frequencies in electrified rail networks - Standard requirements

Railway electrification grids are designed to operate with large varying loads, and often at full capacity characterised by the lowest minimal distance between trains, allowed by the signaling systems. These conditions cause significant variation of the voltage level on the OCL, and usually, this voltage level is different from the nominal voltages set out in EN 50163 [47].

In Table 3.3, the nominal voltages of the standardised power supply electrification systems are provided, together with their allowed variations boundaries for European railway networks [47]. During normal operation conditions, the OCL voltage normally ranges between U_{min1} and U_{max1}, and may be as low as U_{min2} or as high as U_{max2} for limited periods of time (e.g. 2 and 5 minutes, respectively).

Table 3.3: Nominal voltage and their permissible limits in traction system.

Electrification system	Lowest non-permanent voltage U_{min2} (V)	Lowest permanent voltage U_{min1} (V)	Nominal Voltage U_{n} (V)	Highest permanent voltage U_{max1} (V)	Highest nonpermanent voltage U_{max2} (V)
DC (mean values)	400	400	600	720	800
	500	500	750	900	1000
	1000	1000	1500	1800	1950
	2000	2000	3000	3600	3900
AC (r.m.s value)	11000	12000	15000	17250	18000
	17500	19000	25000	27500	29000

During no load conditions, the voltage level at AC traction substations is allowed to be less than or equal to U_{max1}, whereas in DC traction substations, the voltage can be acceptable up to U_{max2} level.

Under higher traffic load conditions, the OCL voltage level ranging between U_{min2} and U_{min1} shall not cause any damages on system components and rolling stock. Whereas, voltage levels between U_{max1} and U_{max2} can only occur during regenerative braking or as a result of the substation voltage regulation mechanism.

As a result, traction units and network components are designed and sized to tolerate wide variations of system voltage. This fact makes the electrified transportation service viable and efficient.

Frequency variation limits in AC traction systems are presented in Table 3.4.

Table 3.4: Limits of frequency variation in AC traction systems.

Electrification system	For systems with synchronous connection to an interconnected system	For systems with no synchronous connection to an interconnected system	For system connected to the railway 16.7 Hz interconnected grid
Power supply systems at 50 Hz	50 Hz ± 1% * 50 Hz +4% / -6%	50 Hz ±2 % ** 50 Hz ± 15 %	-
Power supply systems at 16.7 Hz	16.7 Hz ±1 % * 16.7 Hz +4% / -6%	16.7 Hz ± 2% ** 16.7 Hz ± 15 %	16.7 Hz +2% / -3%

* During 99.5 % of a year.

** During 99.5 % of a week.

It can be noted that larger deviations of frequencies are allowed in isolated networks. The third column of Table 3.4 refers to 16.7 Hz traction systems supplied by dedicated power plants and distribution grids.

3.4 Sources of Power Quality Disturbances in Railway Network

Railway electric networks are characterized by peculiar PQ phenomena, because trains continuously interact with traction substations, overhead contact lines and other trains within the same power supply section. They exchange power during acceleration, coasting and regenerative braking. This producer-consumer behaviour of the locomotive with the rest of the system components gives rise to short time-varying PQ disturbances which further deteriorate the power quality of the railway grid. Sources of the following PQ phenomena are described in this section:

- Voltage dips and swells.

- Voltage interruptions.
- Voltage and current harmonics.
- Electric arcs.
- Resonances.

3.4.1 Voltage Dips and Swells

Dips and swells are voltage disturbances that affect the quality of the voltage in the railway networks. In AC traction systems, voltage dips are mainly caused by switching on large loads simultaneously, such as when several locomotives are starting to run at the same time or when passing under a phase separation section and connecting to the same supply section. The latter may also cause voltage swells, depending on the position along the line, as demonstrated in [68], due to resonance phenomena.

With a behaviour similar to MV distribution networks, a voltage dip may be also caused by faults in other sections of the network, where a sudden voltage reduction before the fault is cleared is coupled through the high voltage feeding network (often arranged as a HV bus feeding some TSs in parallel).

In general, voltage swells and slower voltage rises are mainly associated with regenerative braking and switching off of locomotive onboard loads.

3.4.2 Voltage Interruptions

Supply voltage interruption in AC railway networks is a phenomenon caused by faults in the system, failure of equipment and tripping of protection devices installed in the feeding substations (similar to transmission and distribution grids).

In AC traction systems of 25 kV 50 Hz, in addition to the factors stated above, the supply interruption of the locomotive is periodically caused by the network configuration characteristics employing phase separation sections (neutral sections) [13, 73].

These voltage interruptions are frequent and periodic. Figure 3.7 represents two consecutive voltage interruptions caused by phase separation section, recorded on-board train during a measurement campaign within European countries.

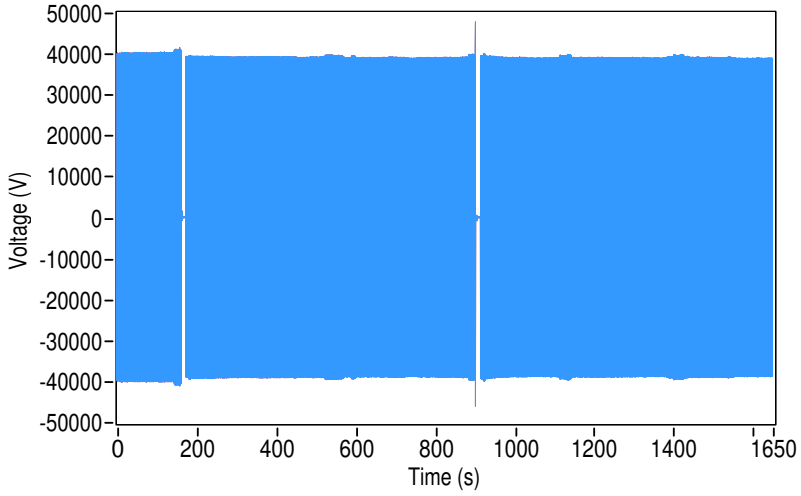

Figure 3.7: A typical voltage waveform in 25 kV 50 Hz rail networks.

To reduce the unbalance on the three-phase power supply system, caused by single phase loads, each TS is connected to different pairs of the utility phases and this requires the electrical isolation of the various supply sections by means of phase separation sections. During the journey, the train passes under several phase separation sections from which the frequent supply interruptions are observed at the locomotive pantograph.

3.4.3 Voltage and Current Harmonics

The distortion of voltage and current waveforms in AC traction systems is caused by many factors. The traction substation (TS) supplying power to the catenary wire is not a pure sinusoidal source itself. A certain quality of power is conveyed through the network feeding the TS and is affected by the number of non-linear devices present on the network and the unbalanced conditions of the power supply system [7, 9, 74]. Typical frequency spectra of the voltage signal measured under no load conditions in a TS indicate that the 2^{nd}, 3^{rd}, 5^{th}, 7^{th}, 11^{th} and 13^{th} harmonics are the main background harmonic voltages of the network [75].

Locomotive traction converters are the main generators of harmonic currents flowing into the overhead contact line (OCL). Generally, the characteristic harmonics produced

by these converters are known. Phase controlled converters using thyristors produce low order harmonics comprising the 3^{rd}, 5^{th}, 7^{th}, 11^{th} and 13^{th} order harmonics, whereas modern four-quadrant-converters (4QC) based on pulse-width modulation (PWM) control techniques generate high frequency components around the switching frequency and multiples of the switching frequency as characteristic harmonics [10, 74, 76]. A common 4QC power electronic system that is widely used in 25 kV 50 Hz locomotives is shown in Figure 3.8.

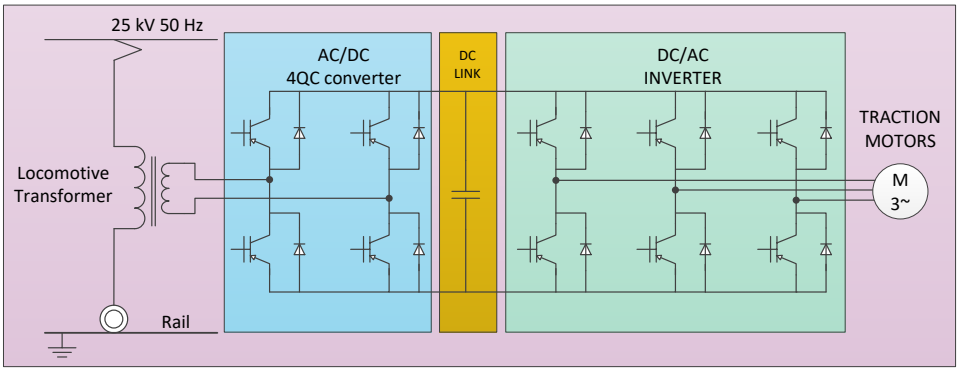

Figure 3.8: Four-quadrant-converters (4QC) power electronic system used in AC locomotives in 25 kV 50 Hz rail network.

In addition, auxiliary converters together with electronic devices with non-linear characteristics inside the train are all sources of distortion for incoming AC signals.

The inrush current of a locomotive transformer is another periodic harmonic source generator in AC traction systems. During a journey, a train has to pass several times under phase separation sections of the power supply network [73]. During this time, the feeding of the main transformer inside the locomotive is interrupted for several seconds [13]. After the train leaves one of the sections supplied by one phase and enters the next section supplied by the next phase, the main transformer of the locomotive is re-energized. The magnetizing current of the transformer produces low order current harmonic frequencies up to 300 Hz [29, 74, 77].

Less periodic, but frequent components are the harmonics and interharmonics injected by time varying phenomena. Arc events due to pantograph bounces [19], and other oscillatory transients, produce low to medium frequency components [7, 10]. Series or parallel resonances also easily change the amplitude of the harmonic components, influencing the overall frequency spectrum of the signals seen at the pantograph [9, 10, 73].

Other phenomenon such as rapid changes of the magnitude and phase angle of fundamental and harmonic components, related to the variability of the traction load and regenerative braking processes, are all temporary sources, which also give rise to harmonics and interharmonics [14]. For convenience, Table 3.5 summarizes the harmonics encountered in 25 kV 50 Hz rail networks together with their sources. Figures 3.9 and 3.10 present typical voltage and current frequency spectra, representing a portion of the coasting phase of a running locomotive [63].

Table 3.5: Harmonic sources in 25 kV 50 Hz railway systems.

Harmonics	**Harmonic Sources**
Background harmonics	Unbalance condition and the presence of non-linear devices in the power supply system
Characteristic harmonics	Locomotive traction converters of type phase controlled or 4QC
Characteristic harmonics	Auxiliary converters of the train
Current harmonics	Electronic devices with non-linear characteristics
Current harmonics	Power supply interruption and re-energization of the locomotive transformer
Harmonics and interharmonics	Initiated by time-varying phenomena such as arcs, transients and resonances
Harmonics and interharmonics	Due to rapid changes of magnitude and phase angle of fundamental and harmonic components

It can be observed that the low order voltage and current harmonics, below 1 kHz, have higher magnitudes than harmonics in the rest of the spectrum. This is probably due to the influence of characteristic harmonics generated by the locomotive traction converter.

In contrast, DC railway network signals are characterised by different characteristic harmonics, where the most dominating frequencies are those introduced by the AC/DC rectifier located in TS to produce the DC voltage supply of the rail network.

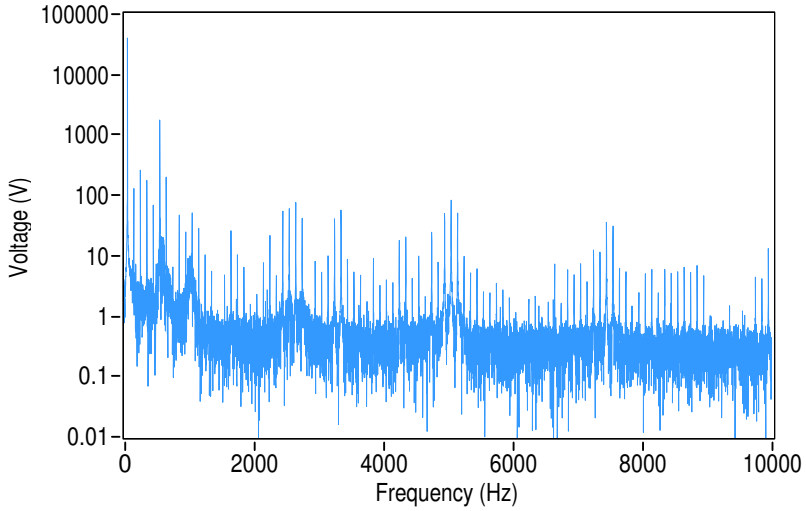

Figure 3.9: A typical voltage spectrum in 25 kV 50 Hz rail networks.

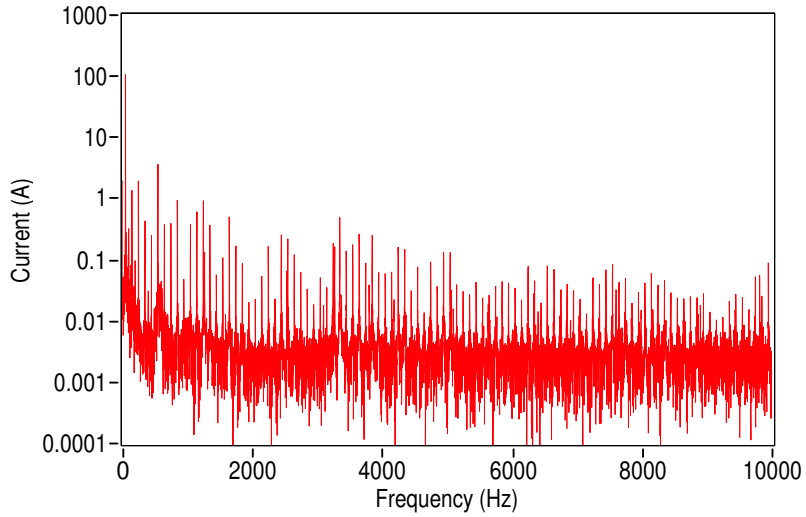

Figure 3.10: A typical current spectrum in 25 kV 50 Hz rail networks.

A typical rectifier-filter block widely used to power DC railway systems is presented in Figure 3.11. It consists of a six-pulse rectifier and an output LC filter to smooth the voltage ripple. The characteristic frequency of this DC voltage ripple is 300 Hz [78].

Frequency spectra of voltage and current waveforms recorded on-board train at pantograph level [64] in Italy, at a 3 kV DC railway network are presented in Figure 3.12 and 3.13. Each spectrum represents only one portion (0 to 2 kHz) of the total

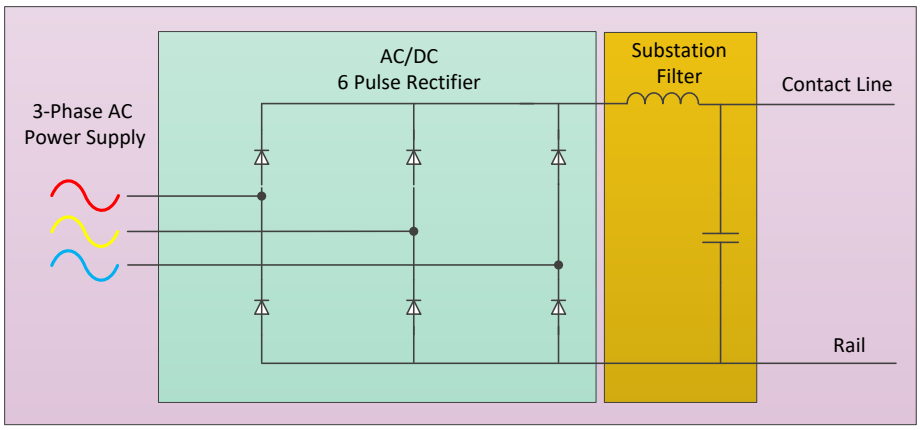

Figure 3.11: Substation rectifier used in TS of DC rail network.

frequency range, to indicate the 300 Hz component and its multiples at 600 Hz, 900 Hz, and 1200 Hz in the voltage, which are of course reflected on the current signal too. These frequency components are characteristic harmonics in this DC power supply railway configuration. Alternatively, a 600 Hz component and its multiples can be found in the current and voltage spectrum if a 12-pulse rectifier is employed in the TS.

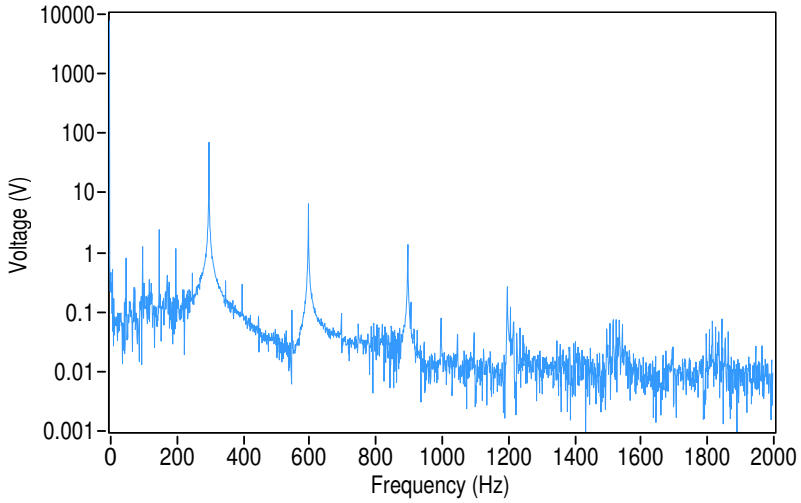

Figure 3.12: A typical voltage spectrum in 3 kV DC rail networks.

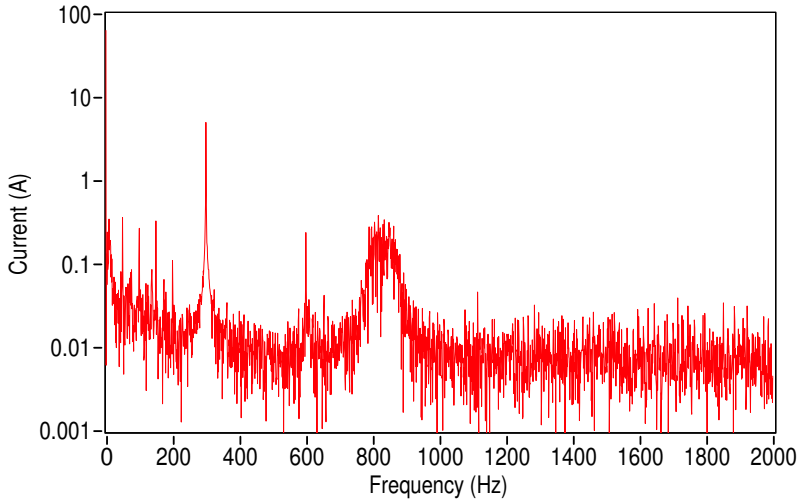

Figure 3.13: A typical current spectrum in 3 kV DC rail networks.

Other temporary non-characteristic frequency components can appear in the spectrum and are associated with the occurrence of short-time PQ events such as voltage transients and arcing [19, 78, 79]. These phenomena can give rise to a broadband of frequency components and resonances that, in turn, can amplify the magnitude of specific frequencies [80, 81].

3.4.4 Electric Arcs

Electric arcs in railway transportation networks is one of the most unwanted phenomena because it can damage the contact quality between the pantograph and the OCL, and at the same time can produce a wide band of conducted short-time PQ events that can propagate throughout the network.

An electric arc happens whenever there is contact interruption between a moving pantograph of a running train and its OCL that conducts the energy from the TS to the traction drives of a train.

The main causes that give rise to such contact interruptions are associated with mechanical oscillations of the train [20], horizontal zigzag movement of the OCL [21], and faults or incorrect adjustment in the pantograph operating system [82].

3.4.5 Resonances

Resonances in electrified railway networks are another unwanted and unpredictable phenomenon because, when occurring, they can produce a high current or high voltage at inductors and capacitors within network components, overvoltages at specific locations of the network, and line overcurrents. If a resonant frequency exists at a specific harmonic frequency, the harmonic magnitude will enlarge significantly, influencing the frequency spectrum of the signal and increasing the overall THD [10, 80].

Resonances are excited by harmonics or other frequency components of the network, produced by traction or auxiliary converters of the train, or from the background harmonics incoming from the high voltage supply network. Resonances also are triggered by the electric arcing phenomenon occurring between the OCL and the train pantograph, as shown in [79] where the natural resonance frequency of the locomotive input filter has been excited every time an electric arcing occurred in a DC railway system.

In DC traction systems, resonances are caused as a result of the presence of DC-side traction substation output filters, to locomotive input filters, and to the combination of electrical properties of the OCL [80]. Whereas, in AC traction systems, resonances are associated with the OCL and the network components.

Usually these resonances are distinct in the frequency domain; however, as shown in [80, 83], OCL resonant frequency can change significantly and is influenced by the locomotive position with respect to feeding substation. The closer the locomotive is to the substation, the higher is the resonant frequency of the OHL, and vice-versa.
In addition, the position of the resonance frequency also varies with the presence of different number of trains [10], and together with antiresonance frequency have shown to be sensitive to the change of the electrical properties of the line [81].

3.5 Solutions to Enhance the PQ in Railway Networks

In the previous section, an overview of the sources of current and voltage harmonics encountered in typical 25 kV 50 Hz, and 3 kV DC railway networks has been provided. It has been shown that harmonic sources can range from relatively basic and expected

causes to the less characterizable and unpredictable, usually excited by a variety of short-time PQ events.

To mitigate these unwanted phenomena and system resonances, and consequently improve the PQ of these grids, several techniques are proposed by the research community to attenuate harmonic currents generated by traction converters, unbalance issues, and background harmonics coming from the three-phase upstream power grid. These include:

- Traditional passive filtering approach to reduce system harmonic impedances through a combination of single-tuned filters and high pass filters [10, 84–86], usually located at traction substations.
- Active filtering approach to prevent filter detuning that is, however, more expensive than the passive filtering approach [74].
- Active compensation techniques using a static VAR compensator to improve power factor and regulate the voltage level, combined with filtering to attenuate the resulting harmonics [70, 87, 88].
- Hybrid solutions consisting of a combination of an active filter with a voltage source inverter to inject harmonic currents and compensate harmonic distortions, and passive filters to attenuate other harmonics [8, 89].
- From the locomotive traction drive itself by using one LCL filter to attenuate characteristic harmonics generated by the PWM locomotive converter [90].
- Using specially connected transformers known as balanced transformers to minimise the unbalance of the three-phase power supply system feeding the 2×25 kV 50 Hz rail supply system, and to provide reduction of harmonics [70, 91, 92].
- Railway power conditioner to compensate harmonic currents, unbalance, and reactive power [8, 70, 93].
- Using a co-phase power supply system to provide active power balance, reactive power compensation, and harmonic filtering [8, 70, 94].

Despite the proposed solutions, limiting the harmonic distortions in rail networks still remains a challenge. This is because, on one hand, there is still a variety of mixed old and new locomotives operating in the same network having different characteristic harmonics to deal with and, on the other hand, the simulated models employed for harmonic analyses and mitigation techniques do not fully represent all the possible loading and operating modes of the locomotives of a real rail network.

The variety of short and wide-range of PQ events will always exist in railway networks, and with the new developments and integration of power electronics, more disturbances are expected. This situation obviously, brings challenges to measurement systems and algorithms for a proper and accurate characterisation in real-time of PQ in railway networks. Actual challenges of the PQ measurement methods when applied to railway networks are reported in the following section of this chapter.

3.6 Issues with Existing Measurement Methods

In this section, the peculiarities of the PQ phenomena encountered in railway networks are discussed in the context of the challenges they bring for existing standardised measurement algorithms. The need to adjust these methods and provide new methods for a proper and accurate characterisation of railway signals is highlighted.

3.6.1 Characterisation of Voltage Dips Voltage Swells and Voltage Interruptions

Power quality (PQ) phenomena superimposed on voltage and current signals of transmission and distribution electricity grids, due to their non-stationary characteristics and random nature, introduce challenges in measurement, monitoring and characterisation. Although complex, established approaches in international standards define PQ indices, testing and measurement methods, e.g. IEC 61000-4-30 [14], IEC 61000-4-7 [15] and IEEE Std. 1159 [29].

For the European public electricity networks, EN 50160 [28] defines a minimum set of characteristics that electrical utility companies should guarantee to customers.

While in fixed conventional electricity grids, PQ disturbances are well known and have been extensively researched [24,42,43,95–97], including the definition of quantities and indexes, for AC traction systems these issues are still under consideration and have been only preliminarily considered in the literature [11, 98].

There are no standardized procedures for measurement and evaluation of PQ for railway applications: EN 50163 [47] determines the voltage and frequency characteristics of the railway traction supply, whereas EN 50388 [73] deals with some quality requirements at the interface between the traction unit and fixed installations, focusing on the train power factor and giving only guidelines for the assessment of harmonics, in particular in relation to voltage instability.

Some literature deals with PQ issues of AC 50 Hz traction systems, focusing on the statistics of harmonics along a network and for different operating conditions [11, 99]. Such literature proposes and discusses measurement solutions, including practical aspects [30, 100], and considers solutions to PQ compensation, especially for the interface with the utility [7, 101]. However, no standards focus on PQ measurement techniques for railway applications, either for DC or AC systems.

There are several proposed methods in the literature for voltage dip, voltage swell, and voltage interruption detection and evaluation for conventional AC electricity grids, though each has its limitations. In such a context, the method based on peak voltage evaluation [102, 103], although easy to implement, is sensitive to noise and unable to detect events of short-time duration.

The methods based on discrete Fourier transform (DFT) [104, 105] are not able to provide accurate results for non-stationary signals and are measurement window size-dependent. They are also prone to the picket fence effect (the phenomenon where the information for a frequency component present in the signal is not available due to the limited frequency resolution of spectral analysis) and the spectral leakage effect [106] when implemented over one cycle due to poor frequency resolution. More improved results have been achieved when using the short-time Fourier transform (STFT) technique for tracking the variability of voltage changes. Even this method has shown to be window size-dependent.

Based on discrete wavelet transform (DWT) [103, 104, 107, 108] other methods have been proposed for voltage event detection. They seem to be effective in detecting and analysing voltage events when tested with simulated signals, but fail to discriminate the considered events from other disturbances due to the sensitivity of its coefficients from noise and other high-frequency components present in the real signals.

The Kalman filtering technique also has been proposed to detect and analyse the properties of the signal during disturbances [103, 104]. This method can determine the voltage magnitude, phase angle, and the point-on-the-wave where the event begins and ends, and can calculate the time duration of the disturbance. This method provides good results, but the main issue with this method is its high computational requirement [108].

The point-on-the-wave method for determination of the instant where the voltage dip starts and ends has been considered in [109]. This method fails when determining the point where the voltage dip ends for developing voltage dips (multistage dips) or slowly recovering voltage dips such as those associated with transformer energising and motor starting.

Two different approaches have been proposed in the literature to detect voltage dips in three-phase systems based on Park transform, and in single-phase systems based on Hilbert transform. Both techniques calculate the signal envelope to detect voltage dip and voltage swell occurrences [105]. The method based on the Hilbert transform seems to introduce oscillations on the signal envelope following signal transitions from one magnitude to another.

The properties of a voltage dip, a voltage swell, or a voltage interruption, including the dip magnitude, the swell voltage, and the time duration of the event, have been conventionally quantified by using the rms method (where the rms value is quantified over one complete cycle) [14]. The detection capabilities of the method are analysed in [110–112]. It has been shown that due to method dependency on the measurement window size and on the time interval chosen to update the rms values, short-duration events (10 ms to 15 ms) with low magnitude changes might pass undetected. Also, the method cannot indicate the instant where the voltage event starts and ends, leading

to event duration errors and detection time delays between 5 ms to 15 ms depending on the point of the wave where the voltage event commences. Event time duration has to be accurately evaluated by PQ instruments because this is one of the indices (along with voltage variation magnitude) used to assess the performance of equipment and power systems. Usually, electronic components do not tolerate even short voltage dips, and when the voltage dip occurs, the operation of the electronic component is affected. Therefore, if a PQ instrument cannot accurately calculate the event-time duration, the network-connected equipment performances and specifications under PQ disturbances would not be correctly attested. The detection time delay can only be important if the rms voltage magnitude is used by a control system to compensate for voltage variability. However, due to its implementation simplicity, speed of calculation, and robustness, this is the preferred worldwide acceptable method used by standardised PQ instruments.

Railway electric supply networks are characterized by peculiar PQ phenomena [9]: trains are a moving source, interacting with TSs, OCLs and other trains within the same supply section. Trains continuously exchange power during acceleration, coasting and notably during regenerative braking [113, 114], giving rise to an energy flow that deviates from the most intuitive process from TS to the train, but may be in the opposite direction (back to the TS), or directly exchanged between trains. This producer-consumer behaviour of the locomotive with the rest of the system is characterized by harmonics, interharmonics, dips, swells, oscillatory transients and arcing, which further deteriorate the power quality of the railway grid.

It is observed that electric signals of railway networks are characterised by short variations in voltage magnitude and frequent periodic voltage interruptions due to specific characteristics of the network (e.g. “phase separation sections”, also named as “neutral sections”), and specific operating conditions (e.g. pantograph detachment from the OCL). Dips and swells shorter than 1 cycle are not accurately characterised by the measurement method proposed in IEC 61000-4-30 [14]; hence methods using shorter calculation intervals are needed for a closer tracking of the voltage dips and swells, to further understand the phenomena, and to allow a better assessment and

classification of PQ events. Furthermore, an analysis technique is needed regarding voltage interruptions, differentiating those caused by the network configuration from other voltage variations.

3.6.2 Characterisation of Harmonics

3.6.2.1 Characterisation of Voltage and Current Harmonics

Railway electrical networks are characterised by significant distortion levels that are very high compared to other public electrical networks. AC locomotives, depending on the converter system used, may draw or produce large harmonic currents and can be affected by the quality of the power supply voltage. As a phenomenon, harmonics are described and the possible sources of disturbances are presented in detail in the literature [4, 10, 74, 75, 115, 116]. References [4, 76] focused on harmonic patterns produced by different types of converters employed in locomotives.

Voltage and current harmonic behaviour in AC traction systems has previously been studied by a broad research community. In this context, much effort has been made in designing appropriate and representative 25 kV 50 Hz electric rail network models. Through simulations, the impact of harmonics generated by locomotives having either AC electric traction motors [117] or DC traction motors [118] on the 110 kV 50 Hz upstream power supply electric grid has been studied. It has been also possible to identify characteristic harmonics emission levels produced by traction units and quantify their influence on the excitation of network components natural resonance frequencies [10, 119, 120]. The latter considerations have been particularly important for network planning, decision making or proposing relevant harmonic and resonance mitigation techniques on actual running rail networks [8, 84, 87, 89, 90, 99].

Measurement based PQ and harmonic analysis can be performed either by analysing recorded voltage and current quantities in railway electrical networks, as reported in [9, 11, 30] concerning different countries, with different supplied voltages and frequencies to identify relevant disturbances, or by using off-the-shelf PQ analysers [85, 86, 121] to then propose relevant mitigation techniques. Therefore, it is common practice to evaluate the harmonic emission levels and other relevant PQ indices in a real rail operating network

by using standardised [14, 15] PQ analysers and following general acceptable [29, 122] recommendations. These instruments employee measurement methods described in international standards IEC 61000-4-30 [14] and IEC 61000-4-7 [15] with respect to 50/60 Hz public AC power supply systems.

However, these standards are not specially designed for railway applications, and presently, there is no standard or measurement procedure that defines acceptable metrics for electrified railway networks [16, 17]. An initiative to define PQ metrics was presented in [16, 17], where some PQ disturbances and their corresponding standardised measurement algorithms were discussed, slightly modified, and proposed to be applicable to AC 16.7 Hz and DC traction power supply systems.

In such a context and considering both the relevance of harmonics and the need for a more accurate assessment of their emission levels, this thesis also evaluates the accuracy of standard voltage and current harmonic measurement algorithms [14, 15] when applied to 25 kV 50 Hz rail electrical waveforms.

Correct and accurate application of harmonic measurement algorithms in railway power networks is needed to reflect the time varying nature of frequency components [9], and for real-time harmonic analysis. Therefore, different time-aggregation intervals for PQ instrumentals are investigated as part of this thesis. This will allow a better characterisation of significant levels of distortion and consequently a better understanding of the negative effects such as overheating, losses, vibration, and the malfunction of electronic devices, caused by the presence of harmonics on the rail power system components. Effective measurements will also enable improved compliance verification of equipment ratings with standardized local regulations.

3.6.2.2 Characterisation of Harmonic Power

In addition to voltage and current harmonics, harmonic active power in 25 kV 50 Hz rail electrical networks is also evaluated. Harmonic power flow by considering the sign of active power harmonics [123, 124] has also been analysed. Due to large levels of distortion produced by locomotives in AC traction systems, harmonic active powers can potentially have an impact on the power meter of the train.

The corresponding levels of harmonic energy will be measured by energy meters [27], specified by the European Commission [125] to be installed in all trains for the purpose of establishing a fairer trade of electrical energy based on real energy consumption. This harmonic energy can potentially be reflected in the electricity usage of the train as an added financial cost inadvertently absorbed due to the presence of non-fundamental energy generated by other trains or external disturbances. This absorption, and hence the financial cost, depends both on the train running mode and on the network topology. The cost can significantly increase when a train passes from one part of the railway network to another part with a more distorted electrical supply as in [11] or older locomotives having DC traction motors that operate under the same supplied section [85, 86, 118, 121].

To prevent this potential energy cost issue and establish a fairer trade of electrical energy, an analysis performed on 12 train journey recordings is undertaken to investigate whether the need for improved energy meter strategies that reflect better the relevant and correct cost of power usage exists.

3.6.3 Electric Arcs Between Pantograph and Contact Line

3.6.3.1 Arc Definition

Electric arcs in railway transportation networks are physically defined as electric discharges occurring in a conductive ionizing gas, known as plasma, between the pantograph contact strip and the OCL [126]. Figure 3.14 presents three different stages being the arc initiation, the arc burning, and the arc extinction phases of a DC arc-fault created in a laboratory environment by using the pull-apart arc generation method.

An air gap forms during pantograph detachment and consists of three regions: anode, cathode, and plasma column. The anode region and the cathode region are characterized by a nonlinear voltage drop, and the plasma column region is characterized by a linear voltage drop. The latter is a function of physical distance between the two electrodes and the physical properties of the plasma [126].

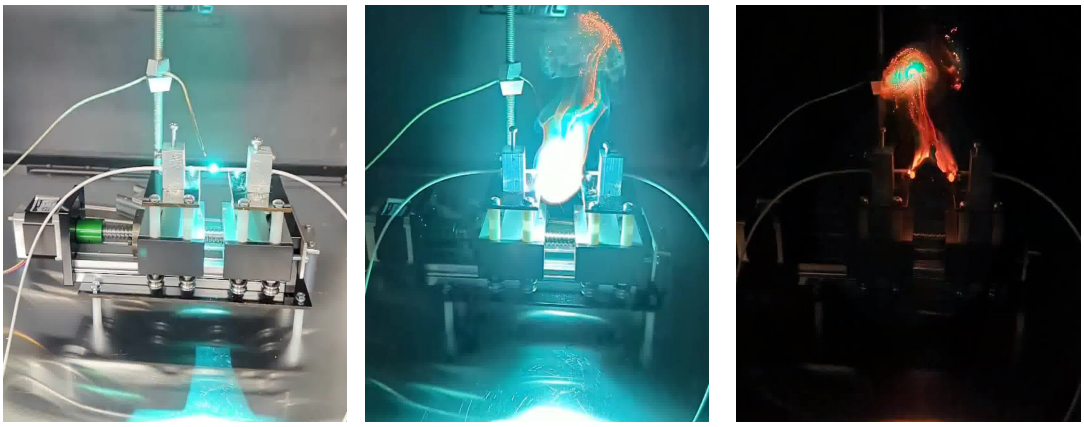

(a) Arc initiation (b) Arc burning (c) Arc extinction

Figure 3.14: Three development stages of an arc fault disturbance.

3.6.3.2 Arc Occurrence Mechanism in Railway Network

Arcs occur because of the inability of the pantograph to continually stay attached to the contact wire. One of the main reasons causing this contact interruption is the mechanical oscillation of the train caused by the irregularity of the track geometry [20], and abrupt variation of the height of the contact wire, mainly when trains enter tunnels [127].

In order to avoid rapid consumption of the pantograph contact strip, the contact wire is distributed in a zigzag manner throughout the track as presented in the diagram of Figure 3.15. Consequently, the pantograph follows this zigzag movement, and when the contact wire approaches the extreme ends of the strip an increased air gap is developed between the pantograph and OCL, which causes an arc. This has been simulated and confirmed experimentally in a laboratory environment [21, 128].

Another relevant cause of electric arcs is a fault in the pantograph mechanism or an incorrect adjustment of its operating system [82]. These cause either a low contact force to be exercised by the pantograph to the OCL, which in turn has a negative effect because it weakens the contact point and so the air gap increases, or it produces a high contact force that progresses the wear of the contact wire [129]. This wear deteriorates the contact quality and as a consequence electric micro-welding phenomena occur [130], which makes the occurrence of arcing more frequent. The arc occurrence mechanism is

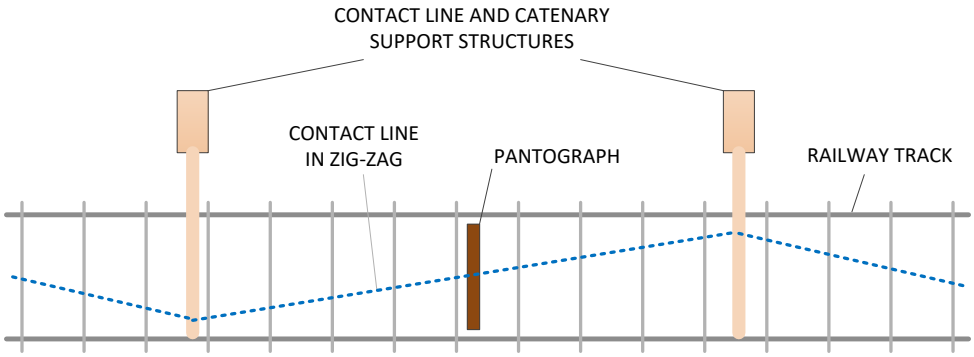

Figure 3.15: Distribution of contact wire in zig-zag.

also negatively affected by factors such as increased train speed, the collected traction level current, as well as poor weather conditions including strong winds, snow, and ice [21, 82, 128, 131].

3.6.3.3 Impact of Electric Arcs in Railway Network

Electric arcs are notorious for producing electromagnetic phenomena which propagate to the entire railway network. A wide range of injected electromagnetic frequencies have been observed during arc occurrence some of which can excite resonant frequencies of the employed network components (such as filters and contact lines) [18, 132], together with DC components induced in AC signals as a result of current interruption due to arcing [133]. Other conducted electromagnetic disturbances resulting from arcs are voltage transients and oscillations [21,132,134]. Low and high frequency oscillations spanning up to hundreds of MHz due to arcing phenomenon [20, 135] have been electromagnetically radiated to nearby circuits, and potentially interfering with signaling and radio communications systems [18–22, 136]

3.6.3.4 Detection of Electric Arcs in Railway Network

Smooth dynamic interaction between the contact strip of the pantograph and the OCL is important for the safe and efficient performance of electrical train transportation

services. A reliable contact contributes to minimising short-term power quality events and establishing good quality current collection to power the train [131, 137]. Indeed, a continuous mechanical sliding contact distinguishes high and poor quality current collection performance [127, 130, 138, 139].

However, it is unlikely that continuous contact can be maintained for an entire train journey due to mechanical oscillations of the train [20], horizontal zigzag movement of the pantograph [21], and faults or incorrect adjustment in the pantograph operating system [82]. Therefore, contact interruption between pantograph and OCL will occur leading to arcing phenomena which in turn causes a number of unwanted issues such as: conducted short-term power-quality events; current flow disturbances; undesirable radiated electromagnetic emissions [18–22]; increased temperature at contact points [140]; increased wear on contact wire and contact strip of the pantograph [21, 22, 138], and electric micro-welding phenomena [130].

It is worth mentioning that continuous and steady development of wear on the contact wire and contact strip of a pantograph can damage the pantograph frame and the contact strip, deteriorate the quality of current collection, and result in serious consequences leading to service interruption [21].

Standard EN 50367 [131] considers either the measured vertical contact force exercised by the pantograph to OCL or the percentage of arcing (ratio between the total duration of all arcs to the total run time) as an assessor of pantograph current collection quality. Therefore, arc detection in railway electrical networks, including their geographical localisation and characterization in terms of time duration, are fundamental for the assessment of the contact wire lifetime, pantograph lifetime and consequently for the entire safety and performance of the train transportation service. Furthermore, arc detection and characterization has a direct impact on lowering the cost of periodical maintenance which can often be expensive [141, 142].

Due to the relevance of arcs and the impact on general power quality in electrified transportation services, much effort has been devoted to arc identification techniques by the research community.

In general, arc detection techniques can be grouped into three main categories:

those based on image processing of recorded videos; those based on emission evaluation of physical quantities such as light, temperature and radiated electromagnetic field; and those based on the processing of electrical quantities such as voltage and current signals.

In this context, [141] proposed the usage of image processing algorithms to detect arcs occurring in a pantograph-catenary system. This method requires a video camera to be installed close to the pantograph. Video frame images are processed by an algorithm in order to detect pantograph movement with changes in the surrounding background of the processed images attributed to arc occurrence. Reference [143] proposed the application of threshold values to binary converted frame images, where the evaluated ratio of white pixels to black pixels is considered as an index of arc occurrence.

Barmada et al. [142], initially proposed the use of a Support Vector Machine (SVM) based classification algorithm to detect the presence of arcs. Extracted features of pantograph recorded voltage, pantograph current, and signals from phototube sensors were used to support the proposed algorithm. The method has been shown to achieve an arc detection accuracy of 80%. Later on, Bermada et al. [144], proposed the use of clustering techniques to detect arcs by considering only the current signals, this avoiding the deployment of phototube sensors. Current signals were processed and grouped in 4 classes which indicate both the presence and magnitudes of the detected arcs.

In reference [133], the authors developed a new arc detection technique by analysing the recorded locomotive current. It was observed that arc occurrence causes significant injection of a DC component into the AC current signal, due to increased disturbances in the transformer magnetizing circuit. This proposed method requires accurate knowledge of the network infrastructure and the speed of the running train in order correlate and distinguish DC components caused by other factors, for example by the presence of phase separation sections. As a consequence, the method cannot be successfully applied for arc detection in cases when trains cross multiple power separation sections [13], and for example, when crossing borders from one country to another within Europe [11, 12].

Light emission (ultraviolet emission) produced by arcs and measured by photo-

tube sensors has been proposed in [127] as an appropriate measurement system for arc detection. Similarly, in Standard EN 50317 [137], a light detector for measuring predefined light wavelengths emitted by copper material under arcing is proposed. Despite the fact that an additional measurement sensor is needed, the proposed technique requires different sensors or sensors with appropriate wavelength tuning due to different material-to-material emission characteristics. For example when trains need to travel from one particular section characterised by copper contact wire material, to another section characterised by aluminium alloys or aluminium conductor steel reinforced contact wires [138], or for example when trains enter tunnels, and an aluminium overhead conductor rail substitutes a traditional copper contact wire [133].

Significant temperature changes developed at the contact point between pantograph strip and OCL occur during arc occurrence have been exploited by the proposed method in [140] for monitoring the current collection quality of a pantograph-catenary system. Images from a thermal camera installed close to the pantograph continuously recorded and fed a number of arc detection image processing algorithms. The temperature of the contact point was identified by using an edge detection algorithm (Canny algorithm), and the Hough transform for continuous detection of OCL movement. The main issue with this particular method appears to be the high computational burden.

Reference [135] proposes a new method for arc detection by analyzing the spectral content of the electromagnetic field radiation caused by the arc occurrence. The radiated signals were captured by an antenna and processed for the determination of possible characteristic radiated frequencies. A wide range of measured frequencies were observed in relation to arc occurrence with the main peak located around 18 MHz. A possible limitation of method is related to the fact that all analyzed arcs were created in a laboratory environment. Arcs occurring in practical rail systems may have different radiated characteristic frequencies, and be influenced by factors such as the length of OCL, number of trains, respective train positions, and network topology of the employed converters, etc.

The quality of the current collection has also been evaluated by the use of wavelet multi-resolution analyses [139]. Recorded current signals were decomposed to a 4th

level, and then a comparative analysis by considering the energy of the signal quantified through Parseval's theorem employed to discriminate arc occurrences from electric welding phenomena [130]. Although the comparative analysis shows good results, it limits itself only to detecting the electric welding phenomenon. In addition, it is known that wavelet coefficients are prone to noise levels and other disturbances [104, 108]. Hence, the effectiveness of the method to discriminate against other possible common phenomena in electric railway systems, for example, the presence of current spikes is still an open question.

Another interesting approach for arc detection has been proposed by measuring the vertical displacement and lateral accelerations of the OCL when the pantograph passes [82]. The proposed method clearly does not directly detect an arc event, but its consequences are evaluated. Large deviations of the displacement and acceleration have been associated to pantographs with contact strip degradation or defects, and hence the method supports maintenance activities.

Clearly, early-stage defect detection in contact wire and pantograph strip can prevent excessive wear in the entire pantograph-catenary system, and help maintenance service improve scheduling of inspection work. To this end, this thesis also proposes a new method for arc detection in DC railway systems.

The proposed technique does not require any external equipment to be installed on the train (such as sensors, cameras, or antennas), because it is based on signal processing of measured pantograph current only. Furthermore, it does not employ extensive processing techniques, which results in a low processing overhead, and therefore it can be implemented relatively easy in real-time. The number of arcs per kilometre can be also calculated to allow a reliable estimation of the current collection quality index, and consequently form a valuable assessment of the entire pantograph-catenary system.

3.6.4 Geographic Localisation of Electric Arcs in DC Railway Networks

In Section 3.6.3, several methods proposed in the literature for arc detection have been described. All these methods have been developed to support pantograph-catenary condition monitoring. The current collection quality index resulting from the processing of the number of arcs detected in the railway line, even if this has supported the maintenance services of railway companies to schedule OCL inspections [130, 139, 140], has not been able to determine the arc localisation along the railway line. Consequently, entire OCL inspections have been undertaken periodically to identify damages to the network components or the contact line itself. This action, besides being expensive and slow, also requires the transportation service of the railway line in question to be interrupted.

One initiative to estimate the arc location in DC railway networks and enable OCL inspections at specific line positions, has been presented in reference [23]. By exploiting the locomotive position-dependent OCL resonant-frequency curve, occurred arcs at different locations within the first half of the railway line were shown to trigger a known OCL resonant-frequency. This approach can identify the arc location over half of a railway line. In the second half of the line, the resonant-frequency curve has shown a repetition of the values of the first half. Therefore, this method cannot indicate half of the line in question.

A second initiative to identify the train position and correlate that with the arc occurrence has been presented in [140]. However, the method has shown to be network-dependent as it can only identify the locomotive position in the case of railway lines with portal structures.

In this thesis, the information of the speed profile of the locomotive has been considered to identify the train position along the track. This feature is used to extend the capability of the newly proposed arc detection method. Together they form an enhanced condition monitoring tool for the pantograph-catenary system of DC railway networks. It has the potential to reduce maintenance costs and improve the reliability

of the network.

A GPS signal to obtain the precise location of the locomotive has not been considered because the GPS signal can lost when the trains run inside tunnels.

3.7 Chapter Summary

In this chapter, an overview of actual railway traction power supply systems is provided. It has been shown that different voltage levels and frequencies have been implemented in different European countries. The choice was usually driven by technical and economical factors. An overview of the percentiles of the electrified railway networks to the total railway networks in European countries is also provided. A larger implementation of the electrified railways is expected in the coming years, as a more efficient, safer, comfortable, and cleaner transportation service.

It was shown that a variety of PQ disturbances occur in electrified networks. The main sources of these have been discussed and presented. Usually these disturbances are time-varying in nature and can be excited by various rolling stock electronic drives, or by other external factors.

Although several mitigation techniques have been proposed, they are unlikely to limit all the PQ disturbances in railway networks. For example, limiting harmonics will remain a challenge due to a variety of mixed type locomotives operating under the same network, and the unpredictable occurrence of the short-time PQ events that usually amplify or initiate other frequency components. Likewise, limiting the electric arcing phenomenon that is usually followed by other conducted phenomena (transients, resonances, etc.,) will be impossible due to mechanical oscillation of the train, or other contributors.

All these PQ phenomena with their peculiarities have been shown to present challenges to standardised measurement methods described in IEC 61000-4-30. In particular, the processing techniques used to evaluate PQ phenomena, although standardised, are not explicitly designed for railway applications and are not appropriate for accurate characterisation, classification, and real-time tracking that is required for the variability of disturbances in railway signals. Also new methods are needed to detect and localise

certain PQ disturbances, like electric arcs or voltage interruptions caused by neutral sections that are characteristics in railway networks.

A detailed survey of the literature has been provided to highlight the key gaps in knowledge, and the opportunities to address these gaps. These issues, and their solutions, will be treated in detail in the following chapters of this thesis.

Chapter 4

Improved Evaluation and Classification of Voltage Interruptions, Voltage Dips and Voltage Swells in 25 kV AC Traction Systems

4.1 Introduction

Power quality (PQ) phenomena characterizing the voltage and current signals of railway electricity networks differ from those present in transmission and distribution electricity grids. It is observed that electric signals of railway networks are characterised by short variations in voltage magnitude and frequent periodic voltage interruptions due to specific characteristics of the AC network.

Presently, there are no standardized procedures focused on PQ measurement techniques explicitly for railway applications. This chapter evaluates whether the standard power quality measurement algorithms used in monitoring 50 Hz electrical grids are sufficient for an accurate evaluation and classification of PQ indices of voltage dips,

swells and interruptions present in 25 kV AC 50 Hz railways. Recommendations are therefore provided for PQ measurement algorithms for AC railways.

4.2 Typical Voltage and Current Waveforms

This section presents the main characteristics of the pantograph voltage and current waveforms recorded at various European 25 kV railway networks. Voltage and current waveforms, presented and used for the analysis of the PQ indices, are part of the waveform database of the 16ENG04 MyRailS project [145], which have been recorded using a data acquisition system (DAQ) sampling at 50 kS/s installed on-board the train.

Figure 4.1 and 4.2 represent the voltage and current waveforms acquired at a pantograph during a train journey of approximately 18.5 minutes. This journey spans over all the possible running modes of a train: acceleration (100 s to 300 s), coasting/cruising (600 s to 680 s and 700 s to 870 s), braking (320 s to 330 s, 540 s to 550 s and 860 s to 950 s) and stationary (0 s to 100 s and 320 s to 450 s) to refer to the most evident time intervals, where each is characterized by a different current absorption pattern.

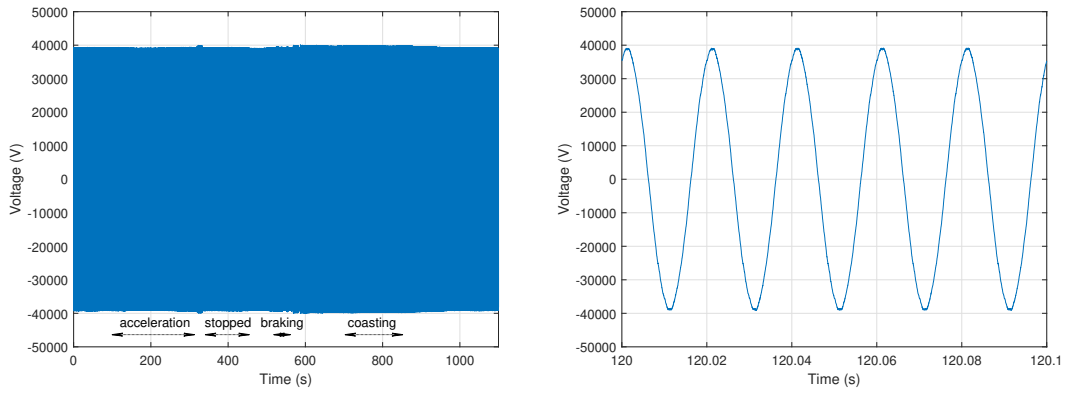

(a) Complete voltage waveform. (b) Five cycles of voltage during acceleration.

Figure 4.1: Instantaneous voltage at the pantograph.

During normal operation conditions, the voltage level at the OCL is different from the nominal voltage for AC 50 Hz systems set out in EN 50163 [47] and reported in Table 3.3. The OCL voltage is normally ranging between U_{min1} and U_{max1}. This

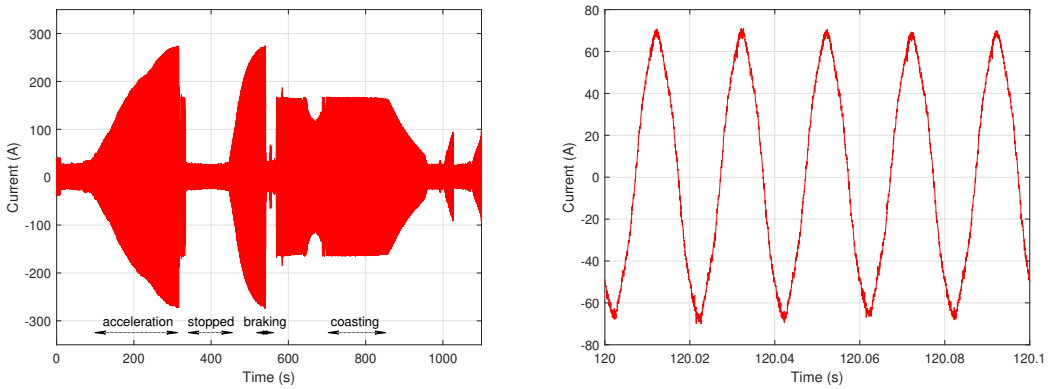

(a) Complete current waveform. (b) Five cycles of current during acceleration.

Figure 4.2: Instantaneous current at the pantograph.

voltage is affected by the voltage changes at the primary side of the TS, which are due to voltage regulation mechanisms and caused by traffic overload (when an unusual number of trains occur in the same supply section with significant power absorption).

Figure 4.3 represents the r.m.s values of voltage and current magnitudes, measured over a 10-cycle time interval, as recommended by [14]. As can be seen, the voltage remains above the nominal value of 25 kV and close to the highest permanent voltage U_{max1}. This is quite a common phenomenon in railways, where system parameters are sized for the largest traffic load attainable.

A clear dependence in the current on the operating mode of the train can be seen in Figure 4.3. This dependence also affects the voltage level at the pantograph. This is obvious, especially during the braking stage (320 s to 330 s, or 540 s to 550 s), where an immediate reduction of the absorbed current, produces a voltage raise of approximately 300 V.

Figure 4.4 represents the dynamic impedance at the locomotive pantograph, defined as Z = V/I, and calculated for the fundamental phasors. The V-I curve indicates how the non-linear behavior of the load changes over the recording period. Different slopes at various time intervals can be observed, where slowly decaying and rising exponential curves are associated with the acceleration stages (100 s to 300 s, and 440 s to 540 s) and the slowly braking stage (860 s to 950 s), respectively.

The abrupt changes in the impedance curve are mainly related to the rapidly decreasing

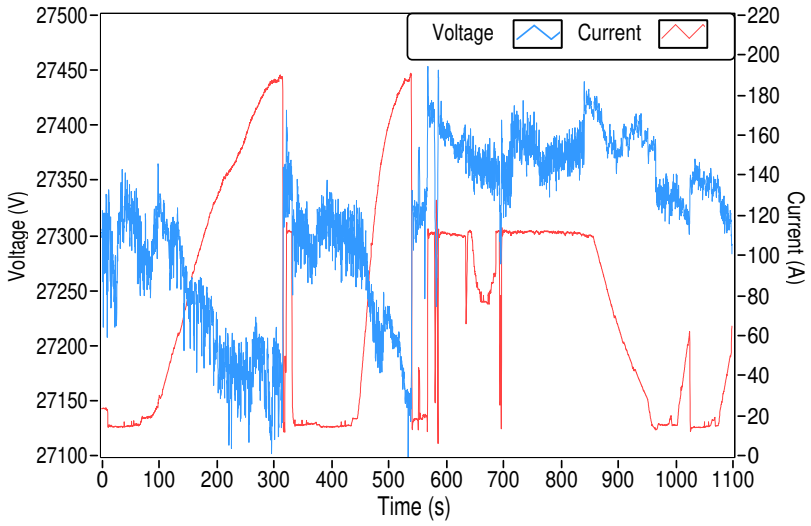

Figure 4.3: Voltage and current r.m.s value at a pantograph level.

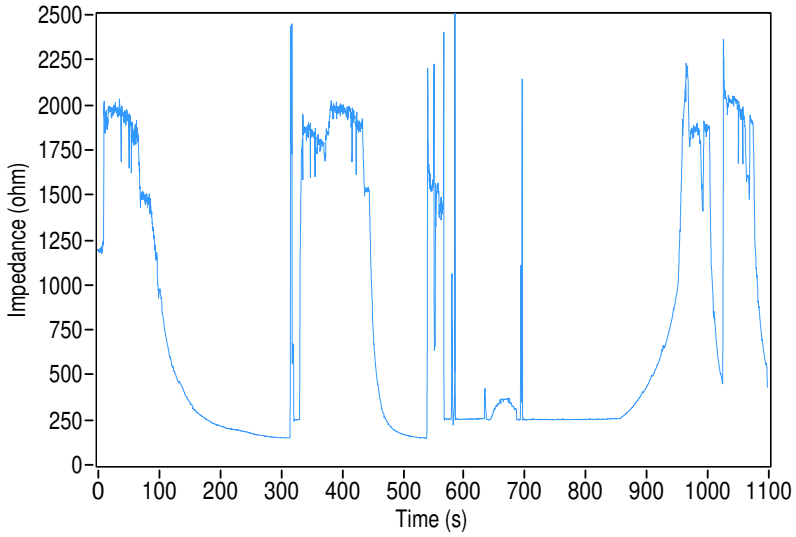

Figure 4.4: Dynamic impedance of the traction unit.

current magnitude. In general, a poor positive correlation of 0.12 exists between the impedance curve and the voltage magnitude curve, in contrast to a strong negative correlation of -0.86 between the current magnitude curve and the impedance curve, indicating that non-linearity is affected more by the absorbed current than the supplied voltage.

4.3 Improved Detection of Supply Voltage Interruptions

Supply interruption in transmission and distribution grids is a phenomenon caused by faults in the system, failure of equipment and tripping of protection devices installed in the network. In AC traction systems, supply interruption of the locomotive is periodically caused due to the phase separation sections, as part of the power supply network, and is governed by EN 50388 [73]. The measurement method specified in IEC 61000-4-30 [14] is normally used to detect and measure voltage interruptions in electricity grids. Although it is a standardized and broadly used method, it is not suitable for the typical disturbances experienced in AC railways as shown in section 3.6.1, because it will not be able to discriminate between events caused by neutral sections and by other sources.

This section proposes a new algorithm for voltage interruption discrimination, which is designed to be applied to AC 25 kV 50 Hz systems but without the drawbacks of conventional approaches. In Figure 3.2 a common power supply configuration has been presented, where TSs were approximately evenly spaced along the railway line to feed independent supply sections [7, 101].

To reduce the unbalance on the three-phase power supply system caused by single phase loads, each TS is connected to different pairs of the utility phases and this requires electrical isolation of the various supply sections by means of phase separation sections. During the journey, the train passes under several phase separation sections from which frequent supply interruptions are observed at the locomotive pantograph.

By definition, a supply interruption is the condition when the voltage magnitude at the supply terminal becomes less than 1% of the nominal value, shown in Table 3.3, [47]. In Figure 4.5 and 4.6 examples of two voltage interruptions for two successive phase separation sections are represented. The events are characterized by a time duration of about (7 to 8) s.

According to EN 50388 [73], the power consumption of the train must be brought to zero before the train passes under a phase separation section to avoid arcing, and the main circuit breaker on board is open. Usually this is done automatically by on-

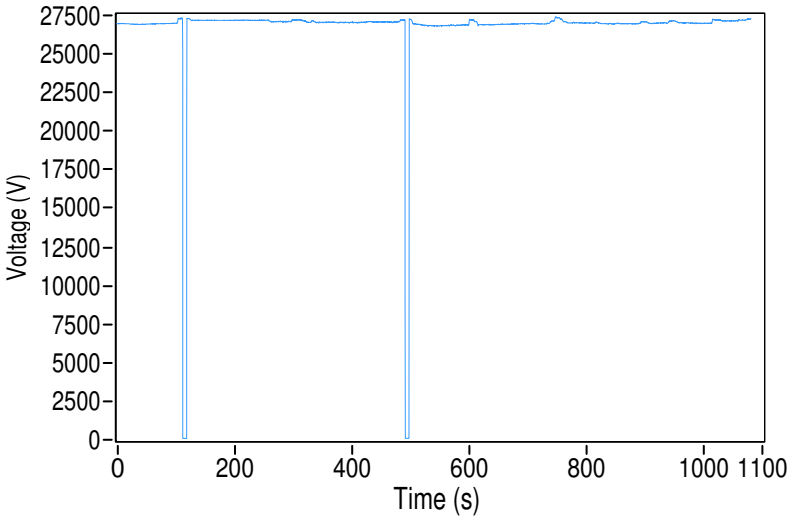

Figure 4.5: Supply voltage interruptions registered in segment 1 of the network.

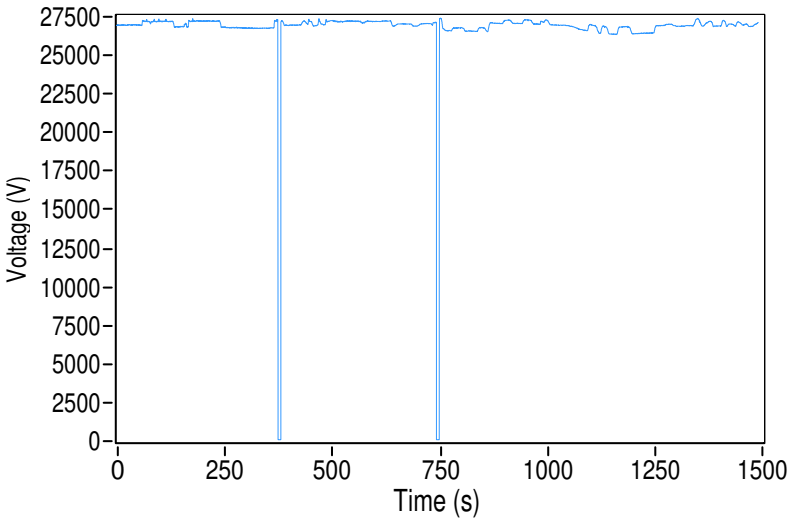

Figure 4.6: Supply voltage interruptions registered in segment 2 of the network.

board devices and triggered by control signals. The time domain signals show that the current magnitude was reduced to zero before the train enters the phase separation section. Figure 4.7 and 4.8 show both voltage and current behaviour in the time domain before entering the supply section 1 and 2 of the line, respectively.

As the main circuit breaker of the locomotive is still on, the voltage signal (present for some additional cycles) continues to supply the locomotive transformer, and that

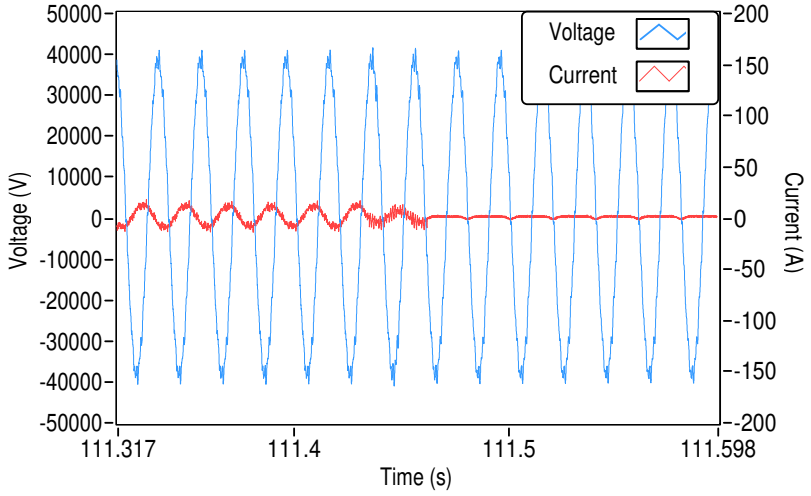

Figure 4.7: Voltage and current before interruption 1 in segment 1.

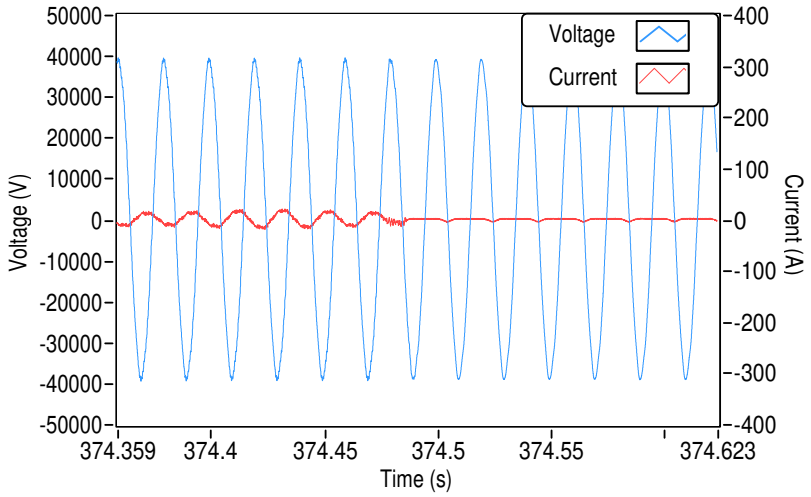

Figure 4.8: Voltage and current before interruption 1 in segment 2.

causes the no-load current of the transformer to be visible after 111.45 s and 374.5 s, respectively in the figures. The same behaviour in the time domain is common to other waveforms in the available database.

It is therefore useful for a supply interruption detection algorithm to consider not only the voltage, but also the current, as a supplementary piece of information to determine the cause of the event. Figure 4.9 presents the flow chart of the proposed technique, with the algorithm steps as follows:

1. Extraction of 1 cycle of voltage and 1 cycle of current from the database;
2. Voltage and current rms values are calculated;
3. Voltage magnitude is compared with the interruption threshold;
4. If the voltage magnitude is below the set threshold, the current magnitude of the previous cycles is checked;
5. If the current magnitude on each of the previous 5 cycles is less than 1 A, the voltage interruption is attributed to phase separation section; otherwise the voltage interruption is caused by other factors;
6. The algorithm iterates by sliding the window along the waveform by 1 cycle until the end of the record is reached.

The proposed algorithm has been tested with voltage and current records obtained from the said project database. It is observed that this algorithm can differentiate voltage interruptions based on their cause, i.e. due to network configuration (namely phase isolation) or other phenomena. Furthermore, the algorithm does not employ extensive processing techniques, and therefore it can be implemented relatively easy in real-time.

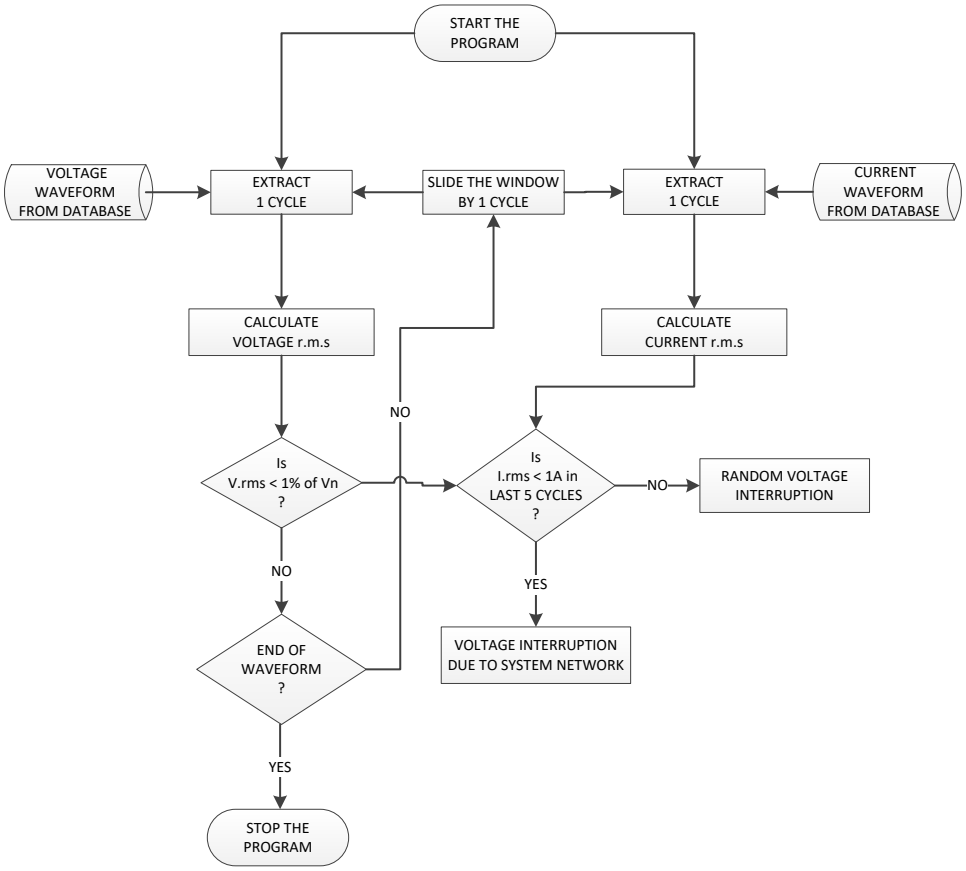

Figure 4.9: Flowchart of the proposed measurement technique for classification of voltage interruptions.

4.4 Improved Characterization of Voltage Dips and Swells

All railway electrification systems experience short variations of the voltage magnitude. Dips and swells of less than 1 cycle and frequent transients shorter than half a cycle affect the waveform and the rms value of the measured quantity. Because of such short durations, the measurement method proposed in the IEC 61000-4-30 [14], i.e. rms voltage measured over 1 cycle, does not accurately characterize these phenomena in 25 kV AC traction systems. For this reason, methods using shorter calculation intervals for closely tracking short variations of the voltage magnitude are needed.

This section considers using a half-cycle window length and analyses the impact that it has on calculation of the rms value for dips and swells. Recommendations are proposed for the method to be used by PQ monitoring instruments designed for AC electric railway applications, to address the gaps with established methods.

In AC traction systems, voltage dips are often caused by large loads switching on simultaneously, such as when several locomotives are starting to run at the same time or when passing under a phase separation section and connecting to the same supply section. The latter may also cause voltage swells, depending on the position along the line, as demonstrated in [68], due to resonance phenomena.

In general, voltage swells and slower voltage rises are mainly associated with regenerative braking and switching off of locomotive onboard loads. With a behaviour similar to MV distribution networks, a voltage dip may be also caused by faults in other sections of the network, where a sudden voltage reduction is present before the fault is cleared, which is coupled through the high voltage feeding network (often arranged as a HV bus feeding some TSs in parallel).

By definition, voltage dips and swells are temporary reductions or increases of the voltage magnitude below 90% or above 110% of the nominal voltage, respectively [28]. Dips and swells are characterized by residual voltage and maximum swell voltage, respectively, and by time duration. Both phenomena are classified according to these characteristics, by referring to Tables 5 and 6, of [28]. Thus, correct classification requires a high level of sensitivity and accuracy to voltage changes.

Methods based on rms calculation, fundamental extraction and estimate, or more directly on processing of the instantaneous peak value are reviewed in [146], although the definition of swell or sag is still based on the rms value as per existing standards.

The work in [147] provides a clear representation of the performance and accuracy of algorithms based on rms calculation (both sliding window and synchronized versions) used to estimate voltage dips, including frequency deviation among the considered sources of error. It is observed that AC railway systems may show significant variations of the instantaneous fundamental frequency, especially for those weakly connected or completely separated from the national grid, such as 16.7 Hz systems [148]. For 25

kV 50 Hz systems, variations of the fundamental frequency are minor because of the connection of the traction systems with the main 50 Hz power system [149].

Methods based on a half-cycle and 1-cycle window for rms value calculation are considered. Even though both methods are standardized [14,150], the method proposed in [14] (using a 1-cycle window) is mostly used by instruments for measuring PQ indices and to interpret the results in electricity grids.

The effects of the window size are evaluated in terms of classification accuracy of the measured quantity, sensitivity with respect to voltage changes, and estimated time duration of the event; results are shown in Figure 4.10 to 4.12 for some events captured within the available database recordings. In the case of voltage swells shown in Figure 4.11 and 4.12, both events are followed by interruptions, therefore the recovery of the signal does not occur after the swell.

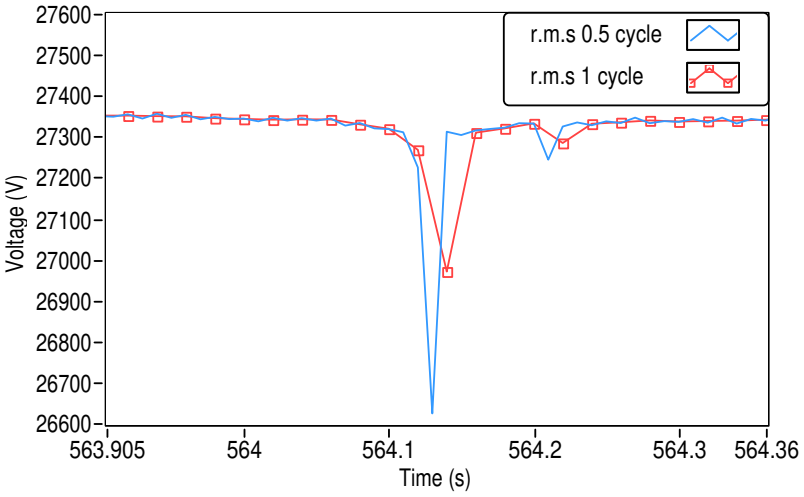

Figure 4.10: Voltage dip measured as r.m.s value over 1 cycle and half cycle.

Such events correspond to the overvoltages observed in [68]. Figure 4.10 shows the difference in magnitude for a voltage dip event using a 1-cycle and a half-cycle window. Strictly speaking, this event cannot be classified as a dip because the reduction in magnitude does not go below 90% of the nominal voltage; the same may be observed for the two swells shown in Figure 4.11 and 4.12. The time-domain representation of the voltage swell presented in Figure 4.11, is indicated in Figure 4.13. As can be seen,

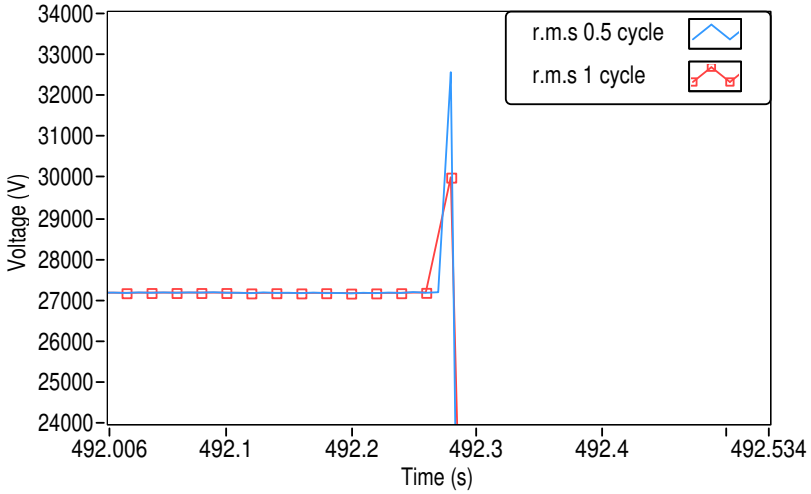

Figure 4.11: Voltage swell measured as r.m.s value over 1 cycle and half cycle.

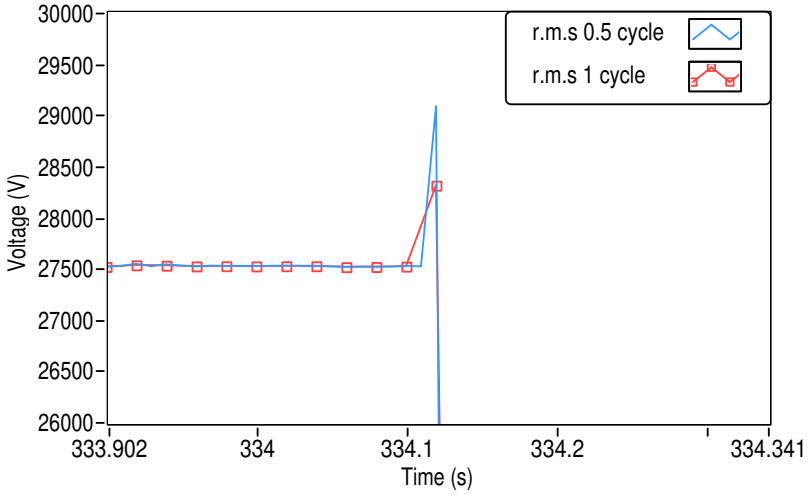

Figure 4.12: Voltage swell measured as r.m.s value over 1 cycle and half cycle.

the instantaneous voltage rises following the second half-cycle of the last complete cycle of the waveform. As the voltage swell is not severe, the one cycle rms method does not fully evaluate its magnitude, whereas the half-cycle performs better.

All examples highlight the clear difference that the time window size has on the classification accuracy of the estimate. The half-cycle measurement interval is more sensitive to voltage variations and hence faster in detecting the occurrence of voltage events. In terms of time duration, dip and swell events with fractional cycle duration

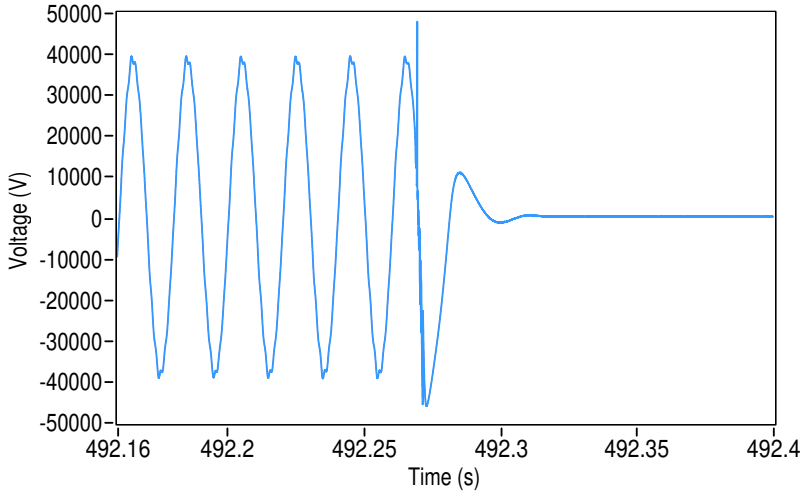

Figure 4.13: Time-domain representation of the voltage swell observed in Figure 4.11.

will be rounded up to one cycle, or to an integer number of cycles; the characterization using half cycles is more accurate (by approximately a factor of two) yet could not be calculated over a shorter window in order to preserve the significance of rms concept.

Since the sensitivity to voltage changes and the detection speed improves with the half-cycle rms method, then also the classification accuracy of the event according to Table 5 and 6 of EN 50160 [28] is improved. The event presented in Figure 4.11 will not be considered a voltage swell if measured in 1 cycle, because the swell voltage will be slightly less than 110% of the nominal value, whereas using a half-cycle window, it will be registered as a swell and with a voltage larger than 120% of the nominal value.

This analysis has shown that the measurement method using a half-cycle window produces more accurate results in terms of magnitudes and time duration for characterizing dips and swells in AC railway systems. Also, it provides a faster response to event detection as it is more sensitive to voltage variability. The DC component, 2^{nd} harmonic, etc, are not constraints, as would be for protection systems that need to extract the fundamental component. By definition, the rms includes harmonics, interharmonics, and other types of disturbances [14].

4.5 Chapter Summary

This chapter has evaluated whether or not the standard power quality measurement algorithms used to monitor 50 Hz electrical grids are sufficient for an accurate evaluation and classification of power quality indices of voltage dips, voltage swells and voltage interruptions in 25 kV AC traction systems. Some characteristics of typical signals and possible network configurations have been presented and discussed, in order to understand the sources behind the events.

For voltage interruptions, an improved estimation technique (including a cross check of the absorbed current behaviour) allowing understanding and classification of different phenomena on the network related to voltage interruption has been presented and discussed. This technique is able to identify voltage interruptions related to the network configuration, and specifically due to phase separation sections.

Due to the characteristics of the signals present in railway systems, it was observed that the measurement methods for the characterization of dip and swell phenomena proposed by the IEC 61000-4-30 standard are not sufficiently accurate for 25 kV AC traction systems. The risk is an underestimate of amplitude and time duration, for which the use of shorter integration intervals has shown to provide better classification accuracy and a faster response time to event occurrence.

The improved proposed technique for voltage interruption estimation and differentiation, and the recommendation provided for voltage dip and voltage swell evaluation over a shorter measurement interval equal to half-cycle, can contribute to an improved appreciation of signal characteristics and consequently to a better correlation of their impact on rail network assets as well as on the operation and the electrical insulation system of the locomotive.

Chapter 5

New Post-Processing Intervals for Improved Estimation of Harmonics Emission Levels – Harmonic Analysis and Considerations on Harmonic Power

5.1 Introduction

Railway electrical networks rated at 25 kV 50 Hz are characterised by significant levels of voltage and current harmonics. These frequency components are also time varying in nature due to the movement of trains and changing operational modes. Processing techniques used to evaluate harmonic results, although standardised, are not explicitly designed for railway applications, and the smoothing effect that the standard aggregation algorithms have on the measured results is significant. This chapter evaluates the application accuracy of standardised power quality (PQ) measurement algorithms, for

evaluation of harmonics in 25 kV 50 Hz rail networks, and proposes a new aggregation time interval for future rail PQ measurement instruments.

5.2 Voltage and Current Harmonic Analysis

This section presents the harmonic analysis of voltage and current waveforms as measured on a locomotive which has been identified as having a phase-controlled converter from the harmonic content. All signals are measured at the pantograph level in various European 25 kV 50 Hz railway networks. It aims to provide an overview and a quantitative assessment of harmonic emission levels present in AC 25 kV 50 Hz rail networks.

The analysed waveforms are recorded by a data acquisition system (DAQ) sampling at 50 kS/s installed on-board the trains [31, 145]. The spectral analysis of the sampled voltage and current waveforms is performed by the STFT algorithm. A Hanning window function is chosen to reduce the spectral leakage and improve the accuracy of the fundamental and harmonics components. The size of the time window was chosen to be 10 cycles in order to maintain a frequency resolution of 5 Hz as recommended by IEC 61000-4-7 [15]. The signal and window function are multiplied and then processed by the algorithm in order to produce the Fourier coefficients. Next, the time window slides on the signal by a half cycle (10 ms) to better track the dynamics of the time varying components. Harmonics represented by their RMS values, for voltage and current waveforms, up to the 50th harmonic order are calculated as required by IEC 61000-4-30 [14].

Figure 5.1 presents an example of the fundamental voltage and current magnitudes for one selected train journey of approximately 9.5 min. Significant time variation of the load gives rise to the voltage variations seen in Figure 5.1. A voltage interruption occurred between 325 s and 332 s, which was caused by the phase separation section of the power supply network. Different current absorption patterns are presented in Figure 5.1, caused by different operating modes of the train. These are: smooth acceleration; coasting; several braking stages; and stationary.

Figures 5.2 and 5.3 present respectively the results of harmonic voltage and current

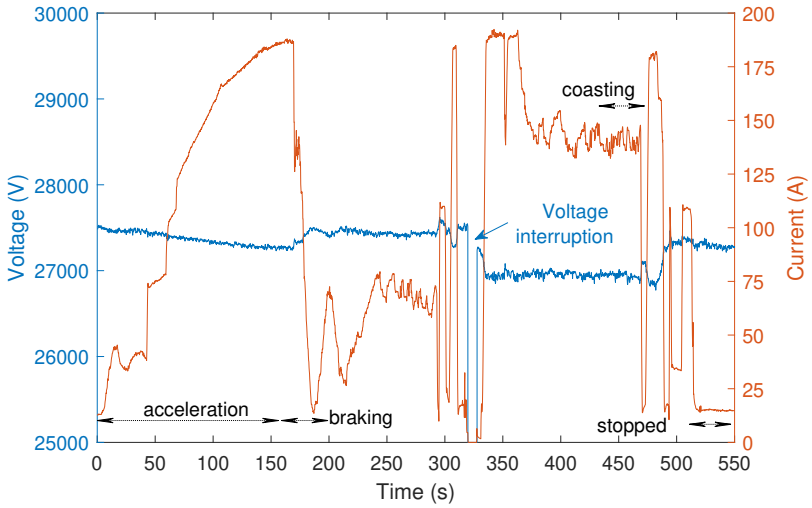

Figure 5.1: Voltage and current fundamental components.

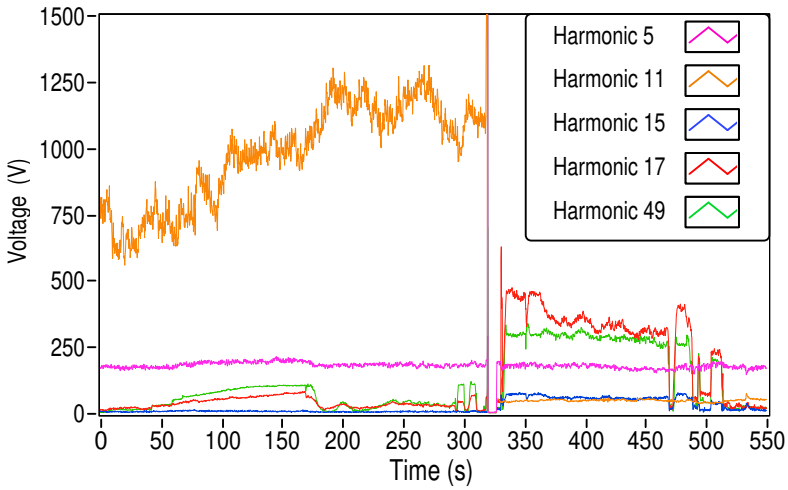

Figure 5.2: Voltage harmonics during the train journey.

variability for the most significant harmonics during the considered train journey. As is typical in power systems, the most dominant harmonics contained in the voltage and current waveforms are the odd harmonics, whereas even harmonics are negligible.

To appreciate the distortion levels, Figure 5.4 presents the voltage and current THD calculated from the RMS values of the harmonics. The large values of current distortion (28% at 187 s and 35% at 295 s) are expected in AC rail networks where a locomotive behaves as multiple current sources at several harmonic frequencies, giving

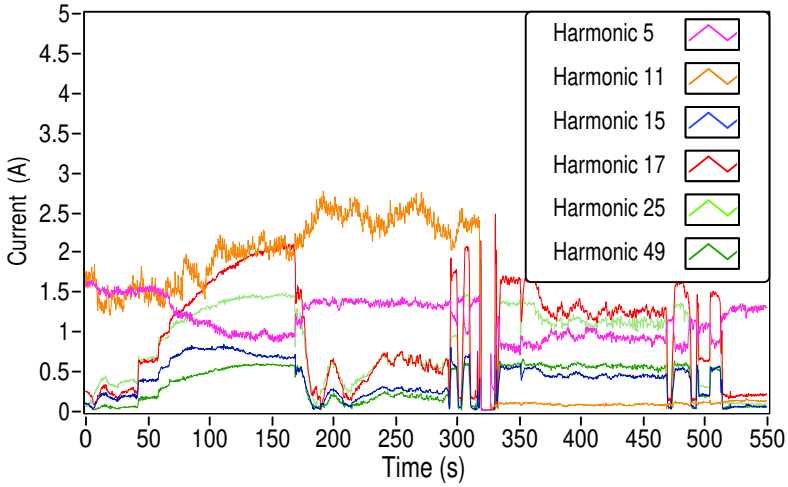

Figure 5.3: Current harmonics during the train journey.

rise to voltage distortions at the pantograph level that propagate throughout the electric

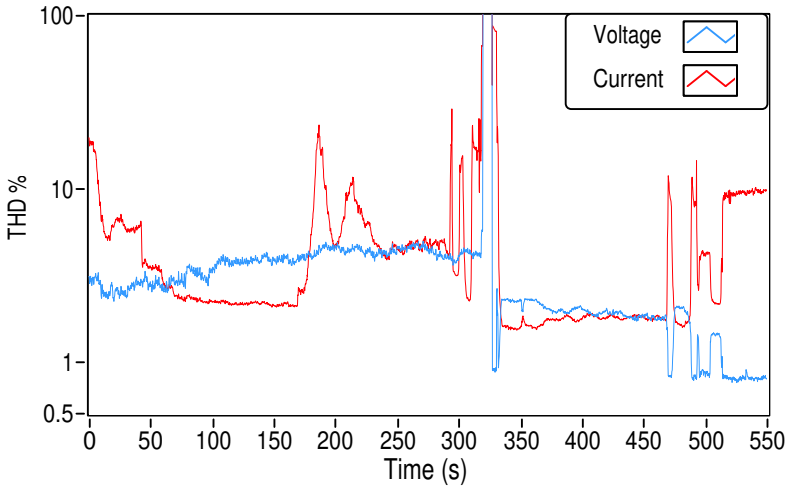

Figure 5.4: THD of voltage and current.

rail network. In Figure 5.4, the large spikes in voltage and current THD observed between 325 s and 332 s are associated with the voltage interruption caused by the phase separation section of the power supply network. As can be seen, the voltage and current waveforms are characterized by time varying frequency components.

To understand whether the current harmonics are generated by the locomotive trac-

tion converter or generated by the network, a correlation analysis for each of the current harmonics, with respect to the fundamental current harmonic at 50 Hz, is performed by using Pearson's correlation coefficient. The correlation analysis presented in Table 5.1 shows a strong positive correlation of the 15^{th}, 17^{th}, 25^{th}, 33^{rd} and 49^{th} current harmonics with the fundamental current harmonic, which is graphically presented in Figure 5.3. The rest of the current harmonics as denoted by their correlation coefficients in Table 5.1 are less significant but still strongly correlated with the train operation conditions.

Table 5.1: Correlation analysis of harmonics with fundamental.

Harmonic order	**Pearson's correlation coefficient**
5	-0.51
15	0.91
17	0.94
21	0.88
23	0.86
25	0.98
27	0.88
31	0.71
33	0.98
35	0.78
37	0.79
43	0.76
45	0.86
49	0.95

It is clear that almost all these current harmonics are generated by the locomotive converter and are typical characteristic harmonics generated by a phase controlled converter. An exception (by looking to Figure 5.3) is the 5^{th} harmonic current which has a weakly negative correlation with the fundamental current. The 5^{th} harmonic current, which does not follow the pattern of the fundamental current, may result from a possible combination of the harmonic current generated by the locomotive converter with the background harmonic of the same order. This is confirmed by a voltage correlation analysis, where a strong positive correlation of 0.86 exists between the 5^{th} harmonic voltage and the voltage fundamental.

The harmonic analysis presented in this section indicates that although significant emission levels are present in AC traction systems, understanding their influence on the rail network can be achieved through a correlation analysis. However, this requires PQ instruments installed onboard trains.

5.3 A Comparative Analysis of Measurement Intervals

Despite improvements in the harmonic measurement techniques given in Section 3.6.2.1, an important factor to be considered is the accuracy of the processed output results. PQ measuring instruments that are in conformity with Class A measurement [14] are required to aggregate (using the square root of the arithmetic mean of the squared input values) the measurement results without time gaps in two time intervals of 150 cycles for 50 Hz signals and 10 min, before making them available to the end user. The smoothing effect that the aggregation process can have on the measurement results may be negligible when such PQ instruments are intended to analyse electrical networks with low and slowly varying levels of distortion. In contrast, rail electrical networks are characterised by signals having time-dependent frequency components with large values of harmonics distortion. Hence, aggregation intervals shorter than 150 cycles are needed to better evaluate the presence of time varying harmonics in such networks.

This section then presents a comparison of harmonic and THD measurement results obtained by the standard aggregation measurement method and when applying a shorter aggregation time interval.

In Figure 5.5, a comparison of the measurement results for the 17^{th} harmonic current (being the most significant harmonic generated by the locomotive during the train journey) obtained by using different time intervals to aggregate the results is presented. There are clear differences both in magnitude and in the time duration of the estimated harmonics. Magnitude differences vary from 2.15 A to 1.81 A and 1.1 A, whereas calculated areas under the curves vary from 9.2 Ampersecond (As) to 10.2 As to 13.5 As respectively when estimated over 10 cycles (no aggregation), aggregated over 50 cycles, and aggregated over 150 cycles.

Figures 5.6 and 5.7 present examples of the THD results calculated over the same

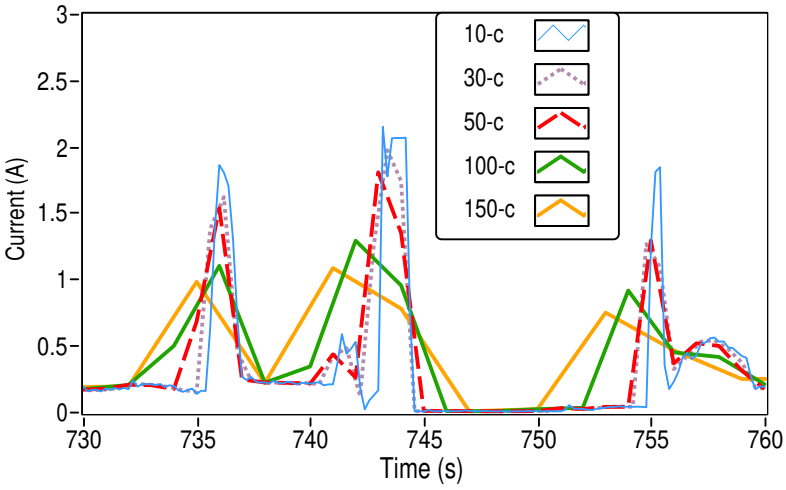

Figure 5.5: The 17th harmonic current measured over 10 cycles and aggregated over 30, 50, 100 and 150 cycles.

aggregation time intervals. Significant differences of more than 10 % can be observed from the figures between the measurement results obtained by aggregation over 10 cycles and over the standard 150 cycles. It is clear that harmonic and THD measurement results, aggregated in 150 cycle time intervals [14], cannot track the true dynamics of the signals, the timescale of which is considered 200 ms corresponding to the measurement interval for 50 Hz signals. This is due to the significant smoothing effect that the standard aggregation algorithm [14] has on the measurement results, causing all time varying components to be underestimated.

In addition, a long aggregation time interval introduces an integration slope error (slopes become more linear; compare for example the yellow curve with the red or blue curve in Figure 5.5) that results in different calculated areas under the curves, indicating that the results are not comparable.

These findings are also supported by simulations. Ten different scenarios have been created where artificial harmonic emission has been injected onto a sinusoidal waveform. A 17^{th} harmonic current was temporarily inserted on the fundamental signal with a time duration varying from 0.5 s to 5 s in steps of 0.5 s, respectively for every scenario. In this analysis, only the 50-cycle and 150-cycle time aggregation intervals are considered. Estimated harmonic magnitudes, areas under the curves, and their respective relative

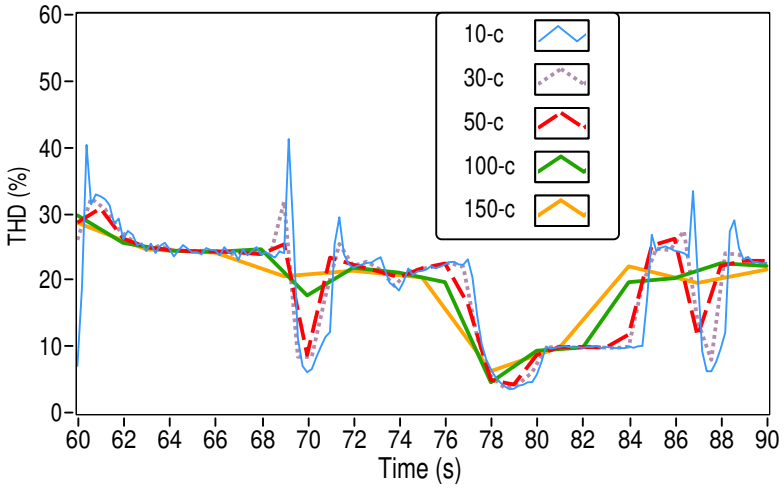

Figure 5.6: Current THD results measured over 10 cycles and aggregated over 30, 50, 100 and 150 cycles. The figure represents the time interval between 60 s to 90 s.

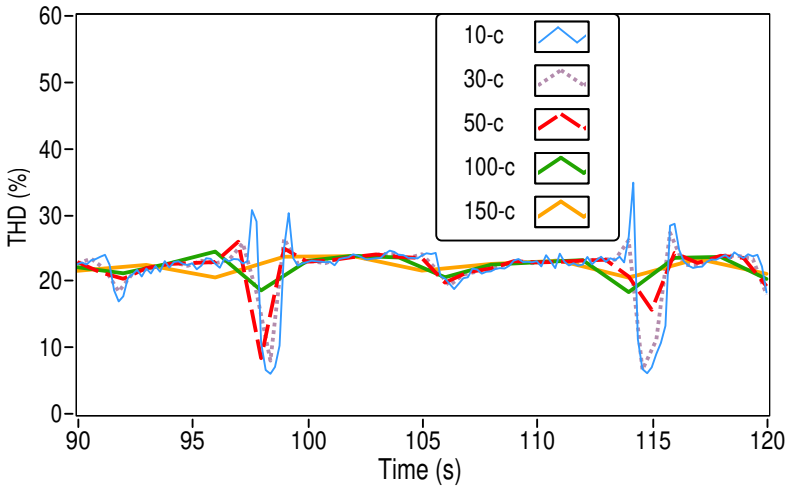

Figure 5.7: Current THD results measured over 10 cycles and aggregated over 30, 50, 100 and 150 cycles. The figure represents the time interval between 90 s to 120 s.

errors are recorded respectively for the two considered aggregation time intervals and are graphically presented respectively in Figures 5.8, 5.9 and 5.10.

As presented in Figure 5.8, the level of 17^{th} injected harmonic current was constant and equal to 0.1 A in each of the considered scenarios. As the time duration of the considered harmonic increases with the increasing number of scenarios, the magnitude of aggregated harmonic current increases until it reaches a saturation point (scenario

no. 4). This point corresponds to an injected harmonic current of a time duration of 2 s. Under this point (scenarios no. 1, 2, and 3) the estimated harmonic magnitude departs from the true value for the 50-cycle time aggregation interval case. Consequently, all time-varying harmonics of time duration shorter than 2 s that may occur in real electrified rail networks will be underestimated regardless of which time interval has been used to aggregate the results. Figure 5.8 also indicates a major difference in harmonic magnitude curves estimated with the standardised aggregation time interval [14], and the newly considered 50 cycles time interval. The 50-cycle time aggregation interval is able to better track the dynamics of the signals and can reflect the true signal magnitude if the disturbance time duration is at least 2 s long. In contrast, the 150 cycles aggregation time interval [14] requires at least 5 s of injected harmonic in order to reflect that magnitude accurately.

Figure 5.9 presents the calculated areas under the curves produced by the 50-cycle and 150-cycle time aggregation interval for every scenario. In this graph, the true-area curve represents the area created by the 10 cycles harmonic estimated values as per [14]. This reference curve has been included to highlight the differences arising from the utilisation of the two aggregation time intervals. The offset among the curves as was mentioned earlier is due to integration slope error.

It is worth mentioning that the 50-cycle aggregation time interval allows more accurate values of curve areas to be calculated. Relative errors of the considered indices for both the aggregation time intervals are represented in Figure 5.10.

The shorter aggregation time interval of 50 cycles for 50 Hz signals offers improved accuracy of the estimated magnitude values and closer tracking of short-time varying components. It significantly reduces the signal magnitude and curve area error for short time disturbances of time duration 0.5 s to 1.5 s and brings the magnitude error to zero for disturbances lasting from 2 s and upward as indicated in Figure 5.10.

Clearly, this is more useful for adoption in PQ instruments designed explicitly for railway applications, because it allows a better correlation of electrical and thermal stresses impact caused by harmonics on network components. Shorter aggregation time intervals also have the ability to establish a closer correlation of the event or the

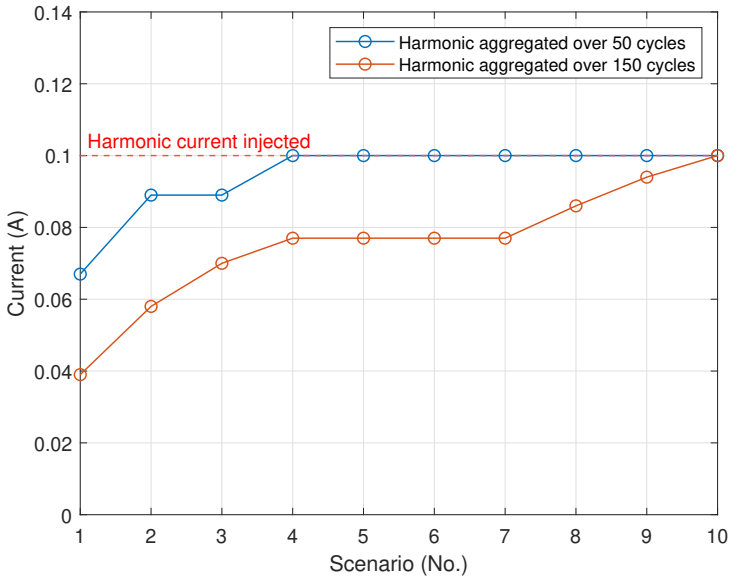

Figure 5.8: 17th harmonic currents magnitudes aggregated over 50 cycles and 150 cycles curves.

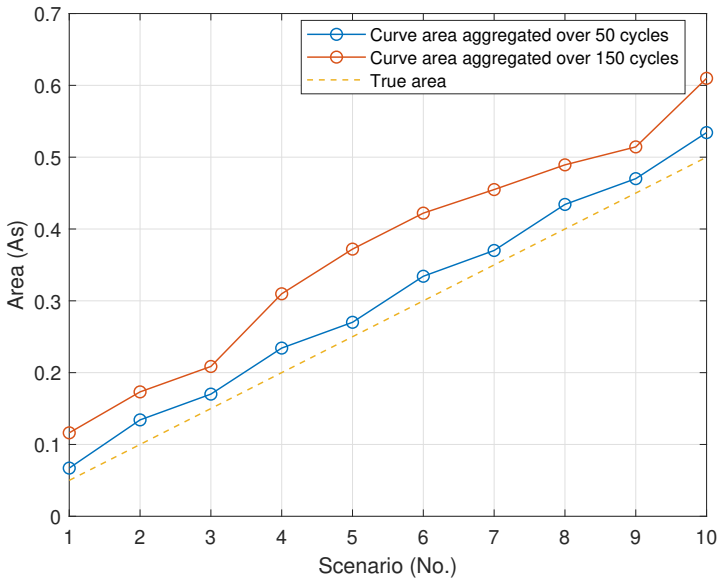

Figure 5.9: Areas under the curves calculated for each scenario by considering 50 cycles and 150 cycles time aggregation intervals.

phenomena with its time of occurrence. Therefore, a 50 cycle aggregation time interval can reduce the time localisation uncertainty by a factor of three compared to a 150

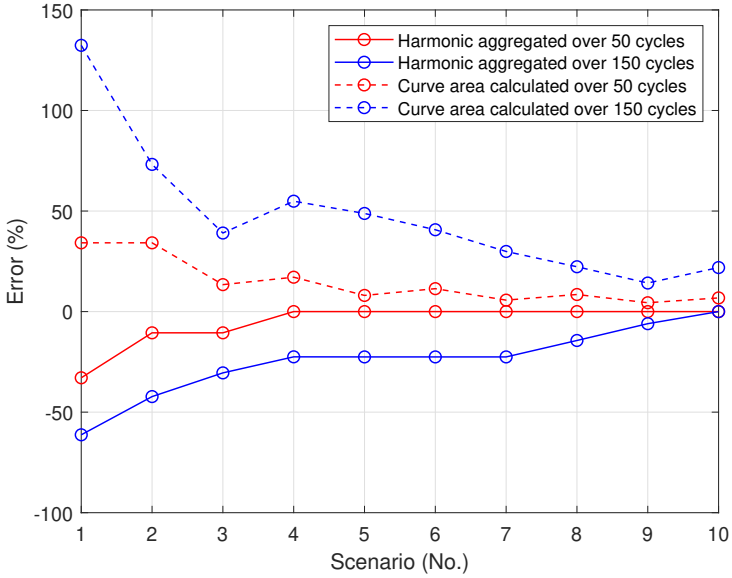

Figure 5.10: Relative error curves for harmonic magnitudes and curve areas calculated over 50 cycles and 150 cycles time aggregation intervals.

cycle aggregation.

5.4 Harmonic Power Flow Analysis

Non-fundamental active power impacting the measured electrical energy together with absorbed and regenerated active power for all the considered train journeys is evaluated in this section. The formula of calculating the non-fundamental active power is presented in Appendix A. The active power flowing bidirectionally during acceleration, coasting and regenerative braking is measured by energy meters to calculate consumed and regenerated electrical energy. Simultaneously, the harmonic active power, flowing from the train to the utility or exchanged between other trains and vice versa, is also being measured. EN 50463-2 [27] considers the technical and metrological requirements for new energy meters to be installed in every train as required by the European Commission [125], for measurement and billing purposes. However, EN 50463-2 [27] does not prescribe a separation of the fundamental active energy from the active energy. As a consequence, energy meters will count both fundamental and non-fundamental energy generated by other trains, leading to potentially erroneous evaluation of energy usage.

This section evaluates the non-fundamental active power to quantify the impact on the energy accumulated by any installed energy meters, with a view to recommend appropriate measurement procedures for a fairer measurement and costing of electrical energy.

As examples, Figures 5.11 and 5.13 represent the results of fundamental active power for two different train journeys (Journeys 1 and 12). Voltages and currents magnitudes are determined using the DFT algorithm over a 10 cycle measurement time interval as required by IEC 61000-4-30 [14]. Both figures indicate likely running modes of the train, that is acceleration, coasting characterized by constant active power and braking characterized by negative power where the fundamental active power is delivered back to the network.

Harmonic power flow variability for the two journeys is presented in Figures 5.12 and 5.14. This analysis has considered harmonic power up to the 50^{th} harmonic order. The figures represent the active power flow of the most dominant harmonics carrying

active power. As indicated by these figures, active harmonic power is present in these traction systems and can flow in the same direction with the fundamental active power; for example, as can be seen in the case of the 11^{th} harmonic (see Figure 5.12) or flow in the opposite direction as shown by the 17^{th} harmonic of Journey 1 and Journey 12. In other words, this indicates harmonic power flows outside the train toward the network (distorting the network, given by a negative value), or from the network to the train (distorting the train, given by a positive value).

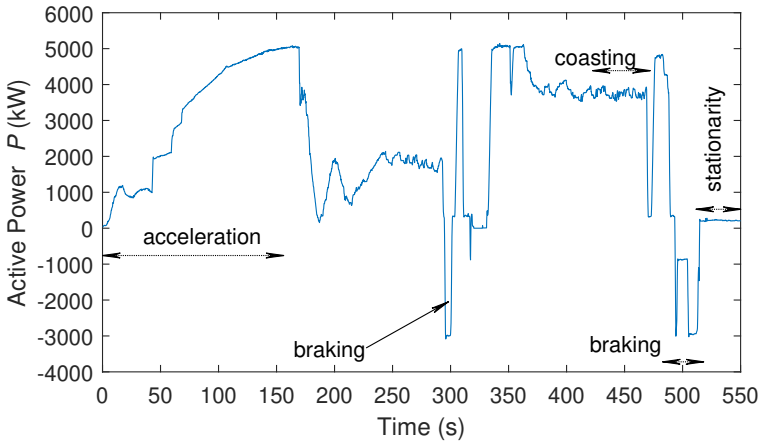

Figure 5.11: Fundamental active power consumed and regenerated of journey 1.

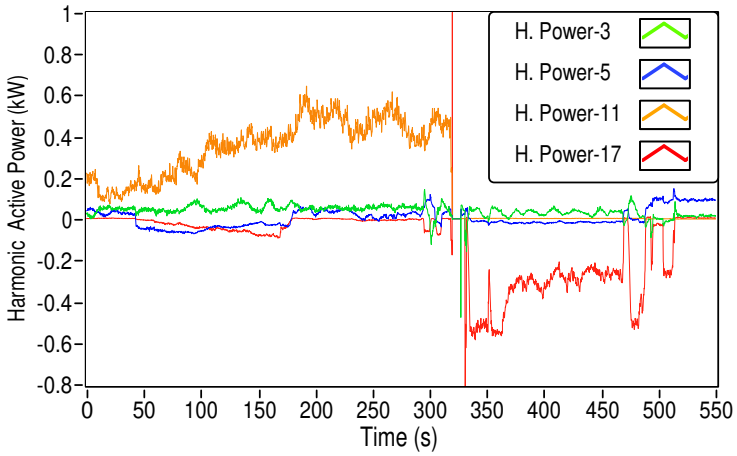

Figure 5.12: Harmonic power, 3^{rd}, 5^{th}, 11^{th} and 17^{th} of journey 1.

Less dominant harmonics carrying negligible active power in journey 1, are the

9^{th}, 23^{rd}, 25^{th}, 35^{th}, 45^{th} and 49^{th} harmonics. All these harmonic powers have a negative value and consequently the locomotive distorts the fundamental component. Harmonic powers of the order 5^{th}, 7^{th}, 13^{th} and 19^{th} fluctuate between positive and negative values during the journey. At these frequencies, the locomotive distorts the fundamental component and is affected by the distortions of the supply network. It may be noted that the 3^{rd} harmonic power has a positive value, meaning that the network distorts the locomotive at this harmonic. Regarding journey 12, harmonics carrying negligible active power are the 19^{th}, 21^{st}, 23^{rd}, 25^{th}, 27^{th}, and 49^{th} harmonics which have a negative value. Harmonic power of the orders 5^{th}, 13^{th} and 15^{th} fluctuate between positive and negative values during the journey, whilst the 3^{rd} and the 33^{rd} harmonic powers have a positive value.

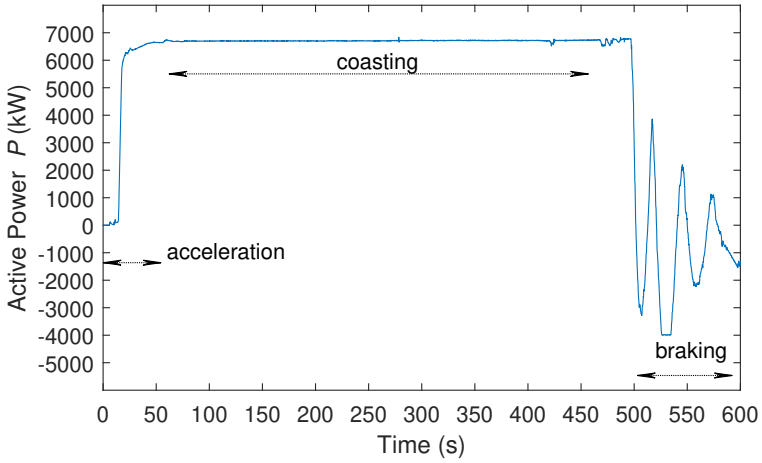

Figure 5.13: Fundamental active power consumed and regenerated of journey 12.

Non-fundamental active power P_{H}, positive active power P_{+} (consumed power), and negative active power P_{-} (regenerated power) are calculated as average values of the instantaneous power over 10 cycle intervals and reported for the 12 recorded train journeys in Table 5.2 together with corresponding non-fundamental active energy E_{H}, positive active energy E_{+}, and negative active energy E_{-}. For journey one shown in Table 5.2, the information is interpreted as follows: the train has completed a trip with a time duration of 9.5 minutes; during this trip, the active power P_{+} (calculated over every 10 cycles intervals) consumed by the locomotive is 2475.3 kW; the active power

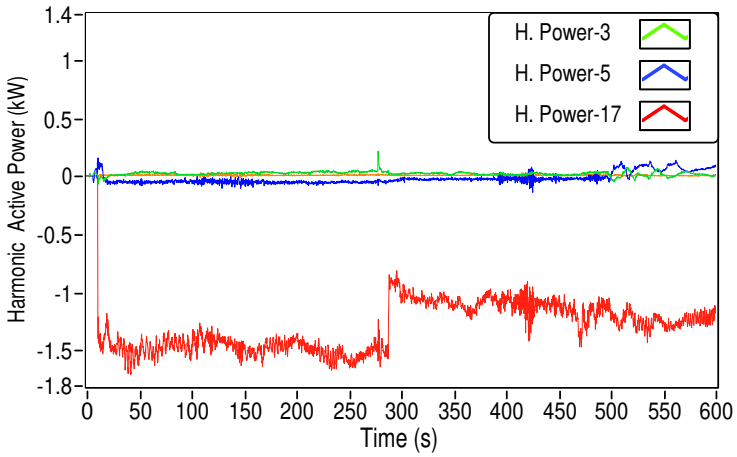

Figure 5.14: Harmonic power, 3$^{\text{rd}}$, 5$^{\text{th}}$, and 17$^{\text{th}}$ of journey 12.

P_{-} (calculated the same as P_{+}) regenerated by the train and fed back to the network is -98.4 kW; the non-fundamental active power P_{H} (calculated as presented in Appendix A) is +0.13 kW —(the positive sign indicates that the network is distorting the train); the active energy E_{+} consumed by the locomotive is 393.8 kWh; the active energy E_{-} regenerated by the train is -15.7 kWh; and the non-fundamental active energy E_{H} is 0.02 kWh.

The level of non-fundamental active power P_{H} reflects the active power carried by all frequency components of the signal, excluding the fundamental, for the reported period of time (journey time). As energy meters according to EN 50463-2:2017 [27] will not separate the non-fundamental energy from the total active energy, they will continuously count it as generated by other trains. This issue can be even more obvious when trains of different owners share the same network and pass from one part of the rail network to another with a more distorted electrical supply, as for example when they cross relevant borders and countries [11].

Although for several journeys, as presented in Table 5.2, harmonic power may reach larger values for short periods, the corresponding harmonic energy as indicated in the last column of the table remains below the maximum percentage error limit of the energy meter, decided to be 1.5 % for active energy according to EN 50463-2:2017 standard [27]. Therefore, the financial cost of both inward and outward energy flows

Table 5.2: Positive active power, negative active power, non-fundamental active power, positive active energy, negative active energy, and non-fundamental active energy.

Journey No.	**Duration minutes**	P_+ **kW**	P_- **kW**	$P_{\mathbf{H}}$ **kW**	E_+ **kWh**	E_- **kWh**	$E_{\mathbf{H}}$ **kWh**
1	9.5	2475.3	−98.4	0.13	393.8	−15.7	0.02
2	18.5	1098.8	−906.9	−0.29	338.8	−279.6	−0.09
3	10.0	2430.4	−338.2	0.14	405.6	−56.4	0.02
4	4.2	4135.8	0.0	0.16	289.3	0.0	0.01
5	13.3	3833.2	−4.7	0.19	852.7	−1.0	0.04
6	13.0	5009.5	−430.9	1.14	1085.1	−93.3	0.28
7	9.7	2145.5	−207.5	−0.02	347.3	−33.6	0.00
8	4.1	3127.5	0.0	0.43	216.1	0.0	0.03
9	18.0	2921.2	−103.9	0.25	878.6	−31.3	0.08
10	24.9	4019.8	−15.1	0.25	1668.0	−6.2	0.10
11	9.6	467.4	0.0	0.05	74.5	0.0	0.01
12	10.0	5299.7	−222.1	−1.25	908.3	−38.1	−0.21

of non-fundamental energy produced by other trains and other power sources remains insignificant. However, the results of this analysis were based on harmonic emission levels produced by only one locomotive type having a phase-controlled converter onboard. To consider whether or not the need exists to propose recommendations for improved energy meter strategies that better reflect the correct cost of power usage, analysis of harmonic power onboard other types of locomotives such as those having full-bridge rectifiers, and four quadrants converters is required.

The analysis of harmonic power flow is based on the evaluation of the sign of active harmonic powers [123], [124], and besides the economical interest, also has scientific importance. Trains running under the same supply section may be of different models, age, and employing different converter technologies on board, or similar models under different operating modes at the same moment in time. For example, one train could be accelerating while another is coasting or braking. In this scenario each locomotive will generate a set of characteristic harmonic currents of different magnitudes and at the same time will consume distorted currents generated by other locomotives. By calculating the active power carried by each harmonic frequency, it is possible to indicate specific frequencies where the locomotive distorts the network and frequencies

where the locomotive is affected by the network distortions, mainly produced by other locomotives. By periodically performing this evaluation, it is possible to quantify the significance of harmonic power and establish trends that indicate whether the network distortion influences are larger than those produced by the locomotive or vice-versa. This will allow a better understanding of electrical and thermal stresses caused by harmonic presence on network components. In such a context, network operators can rely on this data and use it for a better evaluation of the life time of the network components, and hence schedule more accurately maintenance services. An example of this trend is presented in Figure 5.15, where the 3^{rd}, 5^{th}, 11^{th} and 13^{th} harmonic active power components are presented for each journey. Although different journeys are presented, the trips are conducted by a single train onboarding a phase-controlled converter.

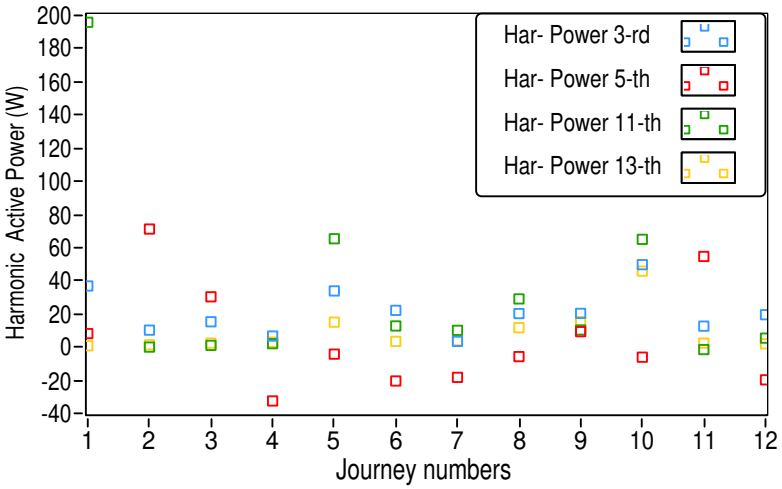

Figure 5.15: Trend of network influences. Harmonic active power 3^{rd}, 5^{th}, 11^{th} and 13^{th}.

As can be seen, the 3^{rd} harmonic active power for all 12 journeys has a positive value indicating that the locomotive is affected by the network distortions. A more fluctuating behavior is experienced by the 5^{th} harmonic active power where the network has a larger influence onto the locomotive in journeys 1, 2, 3, 9, and 11, whereas the locomotive has a larger influence onto the network in journeys 4, 5, 6, 7, 8, 10 and 12. At the 11^{th} and 13^{th} harmonic frequencies the network mainly distorts the locomotive

except in journeys 1 and 12 (for the 11^{th} harmonic active power), and in journeys 2, 3, 4, and 11 (for both harmonic frequencies) where no obvious influence of the network onto the locomotive and vice-versa is observed.

The magnitude of each active power harmonic changes during a journey (see Figure 5.12 and Figure 5.14) and between journeys as it depends on the number of trains running under the same supply section; their position with respect to each other; characteristic harmonics magnitudes and their respective phases; impedance variability of the OCL; and normally the presence and magnitudes of background harmonics. The influence of the above-mentioned factors on the magnitudes of harmonic power, however, has not been demonstrated here due to a lack of information about the locomotive position to the network, and the presence of nearby trains having a similar or a different converter type onboard.

This variability at each active power harmonic indicates a larger network influence on the train when harmonic active power has a positive sign (i.e. harmonic power flowing into the train) or the locomotive has a larger influence onto the network when harmonic active power has a negative sign (i.e. harmonic power flowing onto the network).

The main goal of analysing active harmonics powers is to support condition monitoring applications of network rail assets. However, other applications can benefit from making use of active harmonics powers and they are presented in the flow chart in Figure 5.16. As can be seen, the analysis of active harmonics powers is not limited only to the identification of sources of disturbances but also to supporting disturbance localisation methods and network operation policies for customers distorting the network.

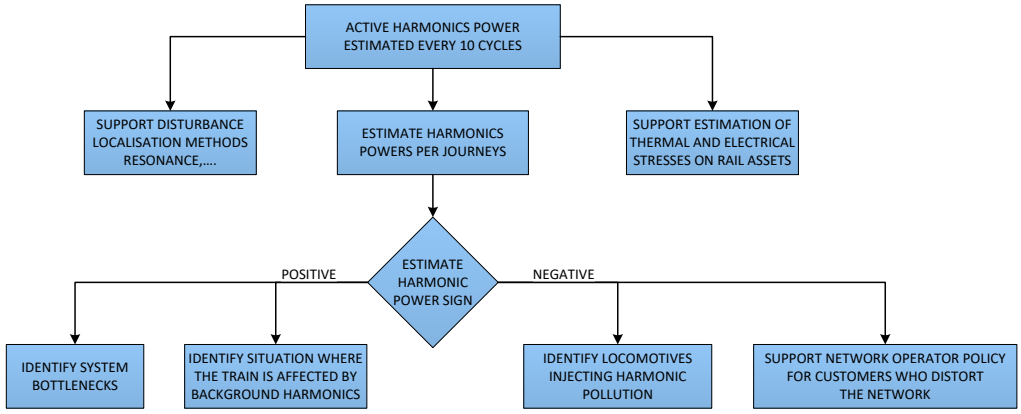

Figure 5.16: Flowchart of possible exploitation of active harmonics powers.

5.5 Chapter Summary

This chapter has evaluated the accuracy and applicability of standardised PQ measurement algorithms for the evaluation of harmonics in 25 kV 50 Hz rail electrical networks. It is demonstrated that a reduction in the number of cycles over which PQ measurements are made offers improved estimation accuracy of harmonic quantities and subsequently improved tracking of time varying frequency components. As a consequence, a shorter aggregation time interval, equal to 50 cycles for 50 Hz signals, is proposed for future rail PQ measurement instruments.

Based on the power analysis performed on 12 train journey recordings, evidence of negligible harmonic energy has been demonstrated to flow in and out of the train. Even though the level of non-fundamental energy is below the measurement accuracy of energy meters, the results cannot be generalised for every case because this analysis has considered only one locomotive type with a phase-controlled converter on board. Other converter-type technologies such as full-bridge rectifiers are still in use and are well-known to cause larger harmonic pollution than phase-controlled converters in the railway networks. Therefore, more analysis of non-fundamental energy needs to be undertaken onboard other types of locomotives in railway systems and for a variety of network loading conditions to consider whether or not the need exists to propose

recommendations for improved energy meter strategies that better reflect the correct cost of power usage.

It is also demonstrated that by evaluating harmonic active power, it is possible to identify specific harmonic frequencies at which a locomotive distorts the network, as well as harmonic frequencies where the locomotive is distorted by the network. Through trending the active harmonic power, it is therefore possible to measure and quantify the variability of the network distortion influences on both the network and on an individual locomotive, to identify locomotives that pollute the network, to identify on what line sections the train is affected by background harmonics, to understand and appreciate the electrical stresses and the potential heating caused by the presence of harmonics flowing on rail system network components, and to support condition monitoring applications.

Chapter 6

Novel Methodology for Arc Identification in DC Railway Power Systems

6.1 Introduction

Electric arcing due to contact interruption between the pantograph and the overhead contact line in electrified railway networks is an unwanted phenomenon which can have important consequences. Arcing events are short-term power quality disturbances that produce significant conducted and radiated electromagnetic disturbances as well as increased degradation on the contact wire and contact strip of the pantograph. Early-stage detection can prevent further deterioration of the current collection quality, reduce excessive wear in the pantograph-catenary system, and mitigate failure of the pantograph contact strip. This chapter presents a novel arc detection method for DC railway networks. The method quantifies the rate-of-change of the instantaneous phase of the oscillating pantograph current waveform during an arc occurrence through the Hilbert transform.

6.2 Time Behaviour of Voltage and Current Waveforms

This section presents the time domain characteristics of voltage and current waveforms measured at the pantograph of a locomotive operating on a 3 kV DC railway network in Italy. The waveforms used for this analysis are part of the database of [31, 145] and can be accessed online [151]. The waveforms are recorded using a data acquisition system (DAQ) sampling at 50 kS/s installed on-board the train.

Figures 6.1 and 6.2 present two examples of the measured pantograph voltages V_{p} and currents I_{p} for two different arc occurrences during the coasting phase of a running train. It can be observed that initially the pantograph voltage and current waveforms are relatively steady, indicating good and continuous sliding mechanical contact between the pantograph and OCL. When an arc occurs there is an immediate pantograph voltage V_{p} drop (V_{drop} 1). This behavior of pantograph voltage also has been observed in a previous study [126]. Due to contact interruption, the pantograph current I_{p} decreases because of the inability of the arc channel to conduct the level of current required by the traction drive of the locomotive. This current decrease in turn causes the stored energy in the magnetic field of the power system inductance to be released instantly [18, 21], and consequently causes the voltage spike (V_{spike}) shown in Figure 6.1 and 6.2 respectively.

After the first voltage spike, V_{p} continues to decrease almost linearly up to the point denoted as V_{drop} 2. This further decrease can be explained due to the increased gap between pantograph contact strip and the OCL, and this is again consistent with previous research studies [126, 128]. After this voltage drop (V_{drop} 2), the pantograph restores its contact with the OCL, producing a voltage transient followed by oscillations (see the blue line, V_{p}). This behavior is also confirmed by previous work [20, 21] and simulation [18] studies, and is a typical system response due to an applied transient or impulse. The oscillatory behavior of V_{p} is reflected in the current waveform, causing I_{p} to oscillate.

Figures 6.3 and 6.4 show recorded waveforms of two arc occurrences during two separate regenerative braking phases of the train. It is noted that the pantograph

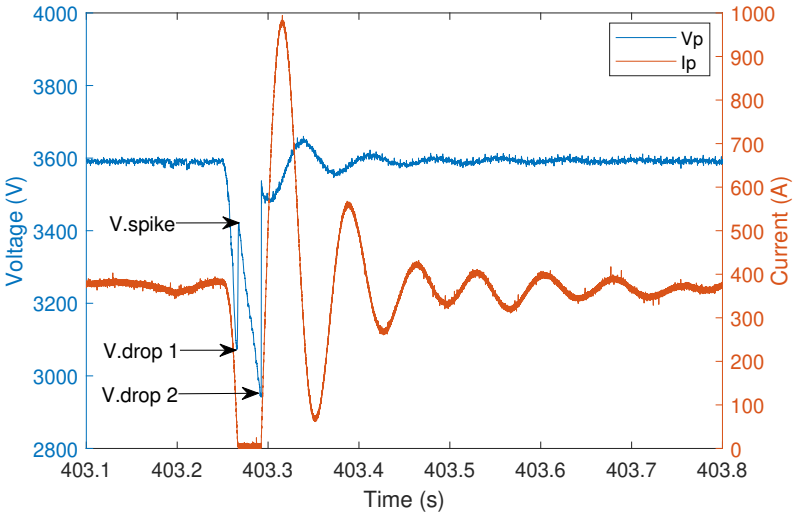

Figure 6.1: Time domain representation of pantograph voltage V_{p} and pantograph current I_{p} during arc event 3 occurred in a coasting phase.

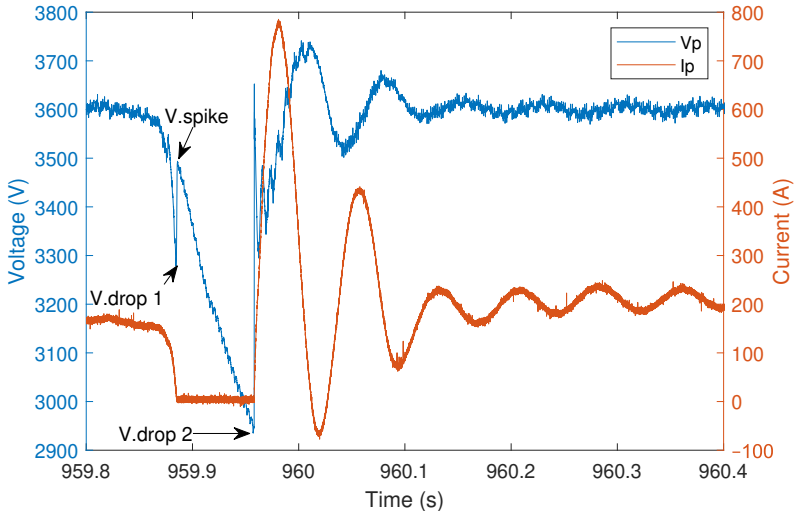

Figure 6.2: Time domain representation of pantograph voltage V_{p} and pantograph current I_{p} during arc event 5 occurred in a coasting phase.

currents have negative values indicating current leaving the train. In Figure 6.3, the arc is associated with a pantograph current magnitude decrease (from -280 A to -200 A approximately), causing a voltage spike (V_{spike}) due to the immediate release of stored energy in the magnetic field of the locomotive inductances. As soon as the contact restores, an immediate pantograph voltage drop (V_{drop}) occurs most likely caused by the

loading effect of the locomotive filter, and then followed by a low-frequency oscillation observed both in V_{p} and I_{p}.

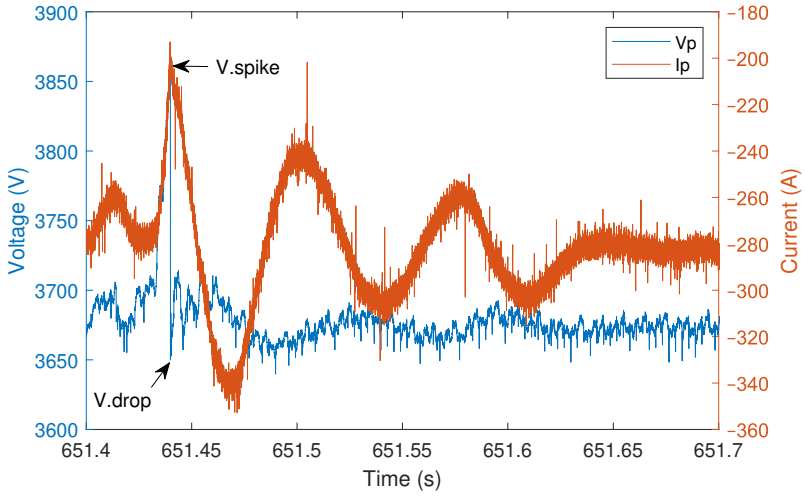

Figure 6.3: Time domain representation of pantograph voltage V_{p} and pantograph current I_{p} during arc event 7 occurred in a regenerative braking phase.

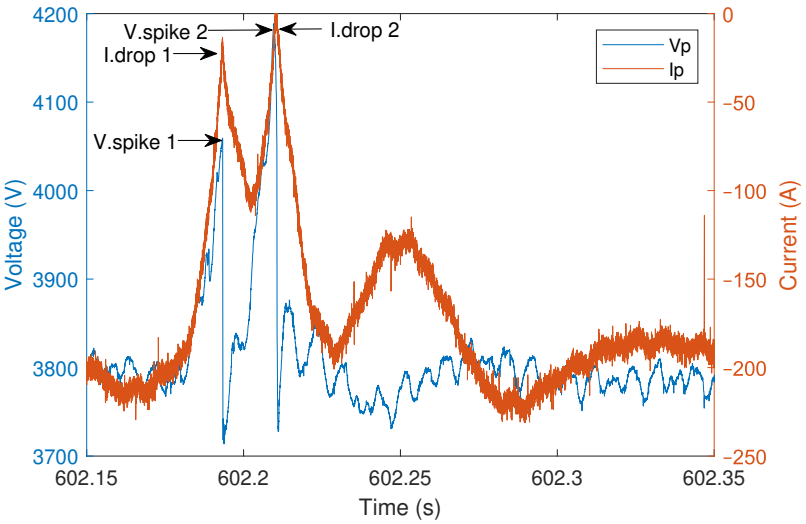

Figure 6.4: Time domain representation of pantograph voltage V_{p} and pantograph current I_{p} during arc event 9 occurred in a regenerative braking phase.

A more peculiar behavior of V_{p} and I_{p} due to an arc is presented in Figure 6.4, where the first pantograph detachment (characterized by an I_{p} magnitude decrease (I_{drop} 1) and V_{p} increase (V_{spike} 1) is followed by a second detachment (characterized

by I_{drop} 2 and V_{spike} 2) before the final restoration of the mechanical sliding contact.

Many other recorded arcs are considered for the analysis in this chapter. These arc events trigger similar oscillatory patterns experienced by the recorded quantities, which can be used as the basis of a detection algorithm. Based on these types of waveforms, the low-frequency oscillation characteristics have been exploited by the proposed arc detection method presented in the following section.

6.3 Arc Detection Method

The proposed detection method is based on the instantaneous phase evaluation of the low-frequency oscillations triggered by the arc fault. This feature was considered because of the significant change of phase of the waveform observed during an arc occurrence. Signal frequency also changes during an electric arc, but this feature is also common to other disturbances.

As the raw data recorded at the pantograph level are real-valued numbers, a mathematical operation is required to create an analytic complex valued signal, having both real and imaginary terms, thus enabling extraction of suitable phase information. In this analysis, the Hilbert Transform (HT) [152–154] is employed to quantify the instantaneous magnitude and phase of the considered time series waveforms. The HT is widely used in digital communication systems [155], mechanical vibration analysis [156], and has been recently proposed for Power Quality (PQ) disturbance monitoring [157, 158] and Phasor Measurement Unit (PMU) parameter estimation [159]. The HT is useful for analysing non-stationary time series data [160], and to detect short-time disturbances. In contrast, the Fourier transform and its short-time version assumes signal periodicity and are optimised for stationary signals analysis [157, 161, 162]. The lack of ability of Fourier analysis in detecting an arc occurrence in traction system is indicated in Figure 6.5. The frequency spectra before and during arc occurrence for two real waveforms containing electric arcs are compared. While for waveform 1, an increase in frequency spectrum (0 Hz to 400 Hz) occurs during an arc, for waveform 2, this change in spectrum is not visible. As will be shown later in the analysis waveform 2, which

was not detected by the Fourier analysis, will be detected by the proposed method.

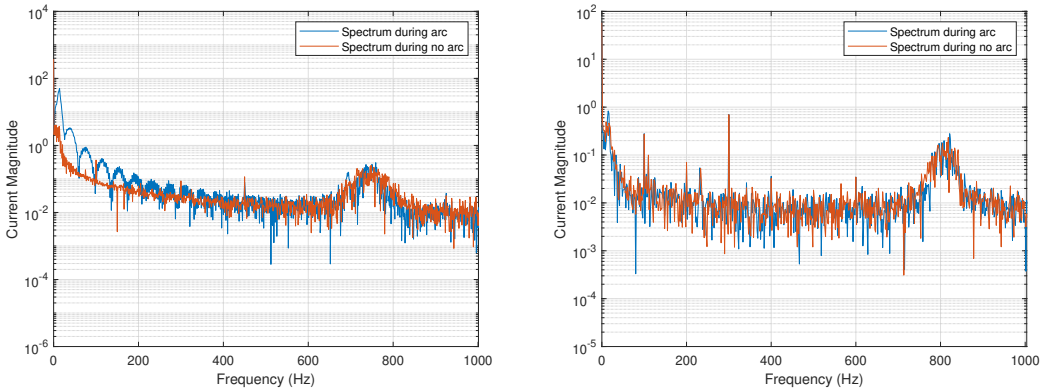

(a) Waveform 1.

(b) Waveform 2.

Figure 6.5: Spectrum of two waveforms analysed during arc and no arc occurrence.

Equation 6.1 depicts the general form of an analytic signal:

$$y(t) = y_{\mathrm{r}}(t) + \mathrm{j} \cdot y_{\mathrm{i}}(t) = y_{\mathrm{r}}(t) + \mathrm{j} \cdot HT\{y_{\mathrm{r}}(t)\} \tag{6.1}$$

where $y_{\mathrm{r}}(t)$ is the continuous time real signal, and $y_{\mathrm{i}}(t)$ is the imaginary terms of the analytic signal that is formed by the application of the HT on $y_{\mathrm{r}}(t)$ [152–155]. In the time domain the $y_{\mathrm{i}}(t)$ is formed by the convolution operation of $y_{\mathrm{r}}(t)$ with the function $1/\pi t$ [152], as shown in Equation 6.2.

$$y_{\mathrm{i}}(t) = y_{\mathrm{r}}(t) * \frac{1}{\pi \cdot t} \tag{6.2}$$

In the frequency domain, the HT operation introduces a constant phase shift of -90 degrees for every positive frequency component, and 90 degrees for the negative frequency components present in the signal. This is achieved by using either a digital Finite Impulse Response (FIR) filter [153, 155] or by using the Fourier transform approach [152]. In this paper the Fourier transform technique is employed to obtain the HT. This is normally implemented by the following steps:

1. Perform the Fourier transform on the real input sequence;

2. Set the DC and the Nyquist component to zero;

3. Multiply the positive frequency components of the spectrum by $e^{-\mathrm{j}(\pi/2)}$, and the negative frequency components of the spectrum by $e^{\mathrm{j}(\pi/2)}$;

4. Perform the inverse Fourier transform on the modified sequence to obtain the imaginary terms of the analytic signal.

Once the analytic signal is created, the instantaneous amplitude $A(t)$ (also known as envelope function of the signal), instantaneous phase $\phi(t)$, and the rate of change of the instantaneous phase (ROCOP) are computed by Equations 6.3, 6.4 and 6.5, respectively.

$$A(t) = \sqrt{{y_\mathrm{r}}^2(t) + (HT\{y_\mathrm{r}(t)\})^2} \tag{6.3}$$

$$\phi(t) = \tan^{-1} \frac{HT\{y_\mathrm{r}(t)\}}{y_\mathrm{r}(t)} \tag{6.4}$$

$$ROCOP(t) = \frac{\mathrm{d}\phi(t)}{\mathrm{d}t} \tag{6.5}$$

Considering the discrete sampled form $y_\mathrm{r}[n]$ of the real time continuous signal $y_\mathrm{r}(t)$, and its respectively calculated analytic signal $y[n]$=$y_\mathrm{r}[n]$+$j\cdot y_\mathrm{i}[n]$, Equation 6.5 takes the form of Equation 6.6

$$ROCOP[n] = \frac{\triangle\phi[n]}{\triangle t} = \frac{\phi_\mathrm{n} - \phi_\mathrm{n\text{-}1}}{\triangle t} \tag{6.6}$$

where n is the number of samples acquired in $y_\mathrm{r}(t)$; for a time sampled signal $\triangle t$ is the sampling time which is 20 µs, and $\triangle\phi$ is the difference in phase between successive samples.

A flow chart of the proposed algorithm is presented in Figure 6.6, where pre-filtering and post-filtering stages are used to attenuate the external noise of I_p waveform and the ROCOP noise, respectively. These stages are explained in detail in Section 6.5 of this chapter.

Figure 6.6: Flow chart of the proposed algorithm.

From the calculated properties, ROCOP was found to be a good indicator for arc detection in DC railway systems, as is presented and justified in the following section.

6.4 Results of the Proposed Method

Waveforms from pantograph voltages and pantograph currents have been recorded on-board a Trenitalia locomotive E464, and are categorized in two main groups [151]: arc waveforms detected during the traction/coasting phase that for convenience in the following analysis are identified as arc events 1 to 6; and arc waveforms detected during the regenerative braking phase identified as arc events 7 to 13.

Due to larger magnitudes and a longer time durations experienced by the arc-triggered oscillations, the following analysis considers the pantograph current as the quantity processed. Furthermore, by considering the current quantity, the method will be more immune to voltage disturbances such as voltage transients that may potentially compromise the accuracy of the method if V_{p} is considered.

Figures 6.7 and 6.8 present the instantaneous pantograph currents, together with instantaneous phase angles and instantaneous ROCOP values for all of the coasting and regenerative braking stage arc waveforms detected respectively.

To filter the incoming I_{p} waveforms from the external noise, a digital FIR filter of order 200 with cutoff frequency set at 100 Hz has been employed. In the next section an explanation for choosing the said order and cutoff frequency of the filter is provided. All the required calculations were performed in Matlab and LabVIEW programming using the HT toolsets provided in these programming environments. The Matlab code of the analysis is presented in Appendix B

The instantaneous phase angle calculations for each of the presented arc events in Figures 6.7 and 6.8 reflect the phase angle behavior during low-frequency oscillations

triggered by the arc events. To avoid ROCOP spikes due to phase angle jumps (passing from π to -π and vice-versa), the phase angle is unwrapped. The ROCOP calculations provide clear evidence of the presence of an arcing event in all the considered waveforms, despite the apparent noise levels seen in the waveform of Figure 6.7f. Noise may affect any arc detection triggering mechanism, but noise removal may be dealt with through appropriate filtering techniques. Arcs captured during the regenerative braking stage of the locomotive are also identified using ROCOP calculations as presented in Figure 6.8.

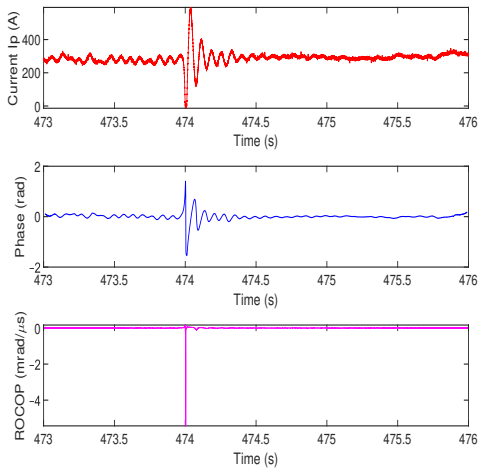

(a) Arc event 1.

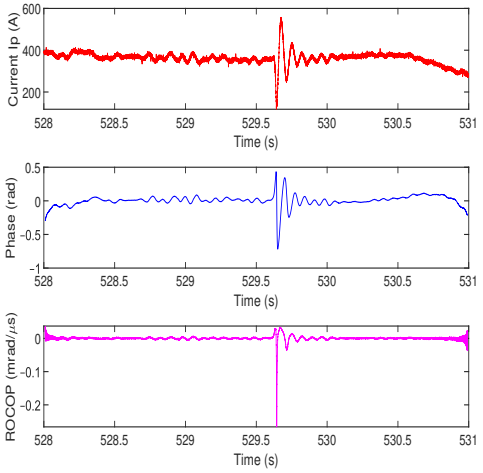

(b) Arc event 2.

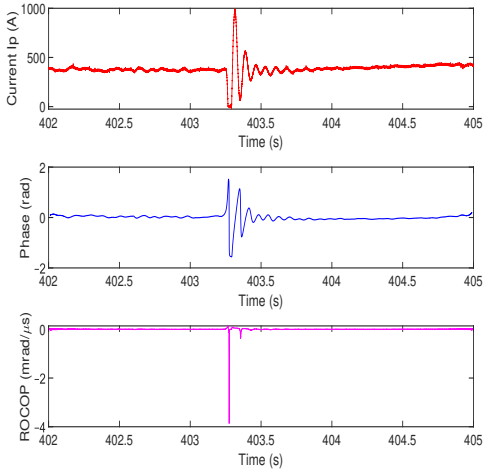

(c) Arc event 3.

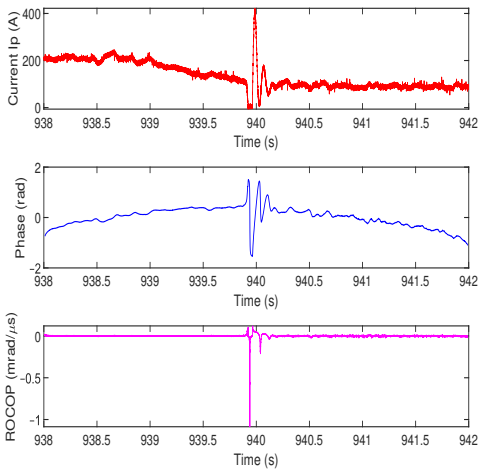

(d) Arc event 4.

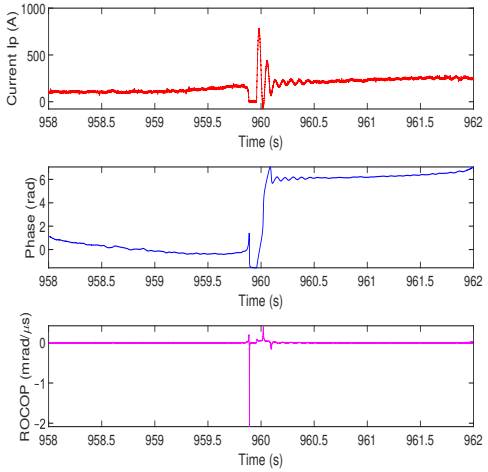

(e) Arc event 5.

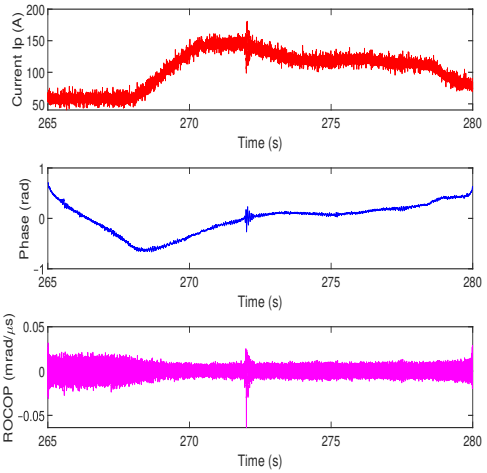

(f) Arc event 6.

Figure 6.7: Instantaneous recorded I_{p}, instantaneous calculated phase angle, and instantaneous ROCOP for all of the arcs detected during the coasting phase.

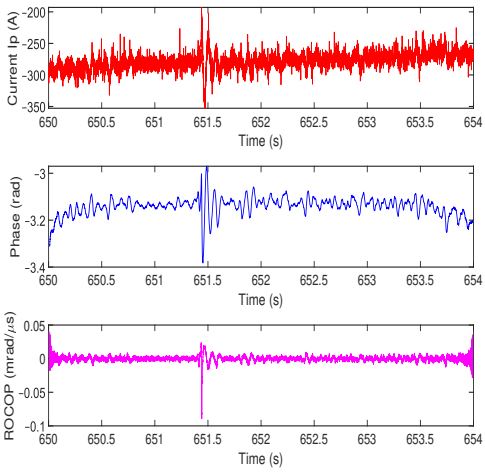

(a) Arc event 7.

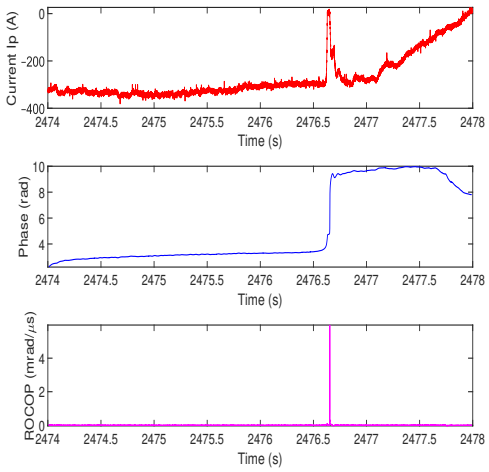

(b) Arc event 8.

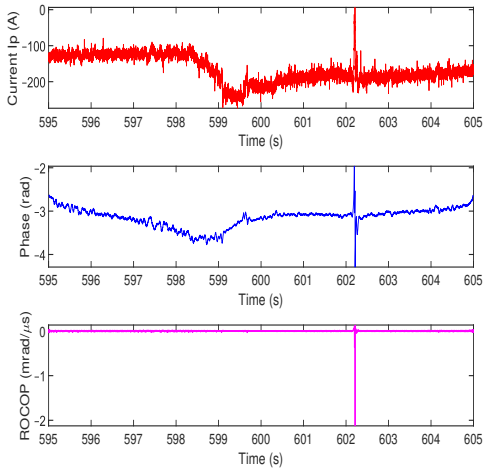

(c) Arc event 9.

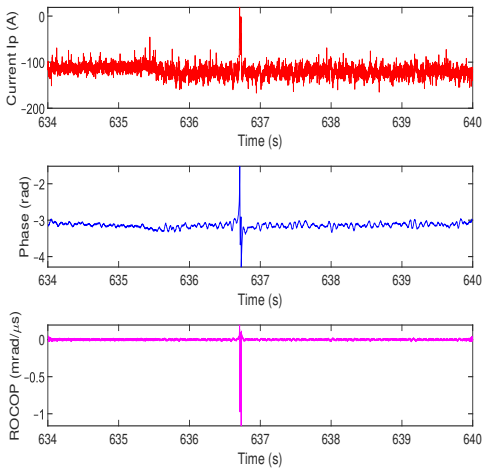

(d) Arc event 10.

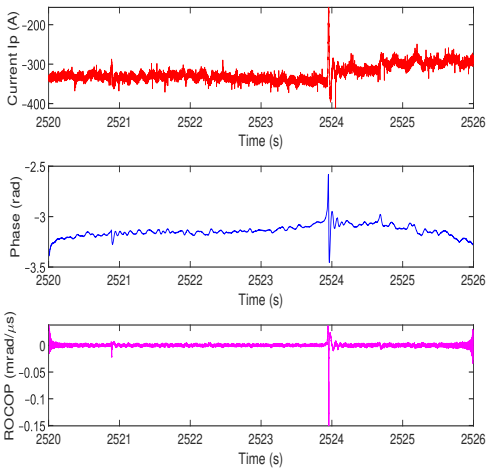

(e) Arc event 11.

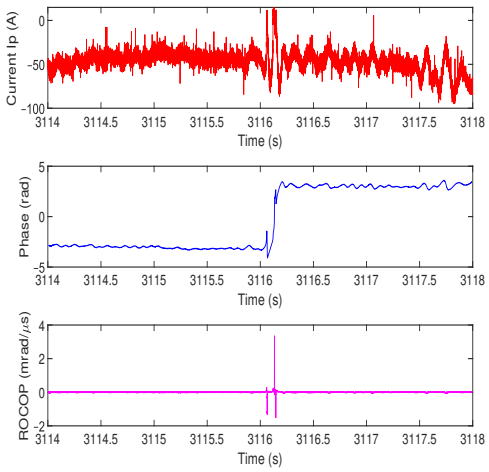

(f) Arc event 12.

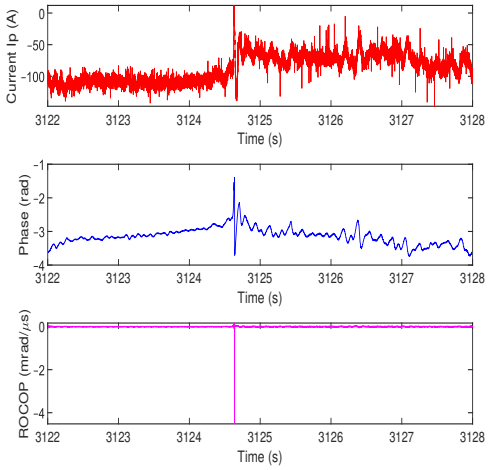

(g) Arc event 13.

Figure 6.8: Instantaneous recorded I_{p}, instantaneous calculated phase angle, and instantaneous ROCOP for all of the arcs detected during the regenerative braking phase.

Further to the arc detection, the method also can precisely localise in time the occurrence of the arc. This additional information can be useful to support, for example, future geographic arc localization algorithms. One such algorithm is presented in the next chapter of this thesis.

A possible reason for having such small variations in the magnitude of I_{p} (see Figure 6.7f) produced by non-significant arcs, can be explained with the locomotive position along the track and the level of current collected. By looking at Figure 6.7f, it can be observed that for the first 3 s (265 to 268) s the train has been stationary (probably waiting on a station), characterized by low traction current with significant distortion. A high level of distortion when trains are near stations has previously been observed in [114]. After the stationary phase, the train has started and accelerated for approximately 2 s to 3 s (268 to 270) s, leaving the station (confirmed by the very low train speed of 27 km/h reported in [151]). While leaving stations, trains at low speed often change track position which forces the pantograph to change the OCL and the train wheels to experience mechanical oscillations causing some minor arcs to occur.

The preliminary results of the proposed method indicate the need for a fine-tuning

of the algorithm to eliminate the noise level of calculated ROCOP (in Figure 6.7f) and to understand possible factors that may influence the effectiveness of the algorithm. These issues are considered in the next section of this chapter.

6.5 Sensitivity Analysis

The effects of signal magnitude, noise and the length of the considered waveform on the calculated ROCOP parameter are evaluated in this section. Pre- and post-filtering techniques are employed and presented for noise and harmonic attenuation of I_{p}, and smoothing of the phase derivative, respectively.

6.5.1 Pre-Filter Selection

To appreciate the harmonic presence and other frequency components of a DC rail network waveform, a typical frequency spectrum of I_{p} waveform during and after the arc event 1 is presented in Figure 6.9. The spectrum produced by the discrete Fourier transform (DFT) algorithm, has a frequency resolution of 1 Hz and is limited to 1000 Hz to clearly show the band of frequencies (5 Hz to approximately 250 Hz) excited by the arcing phenomenon. Within the frequency band, a particular frequency component (14 Hz) corresponding to the natural resonance frequency of the locomotive input filter [80, 132] is also excited, causing as a consequence a significant rise in its respective magnitude.

To filter the incoming I_{p} waveform from high frequency components and external noise, a digital Finite Impulse Response (FIR) filter is considered. The ROCOP signal to noise ratio (SNR) parameter was calculated for one of the arc events (arc event 1), by considering different filter orders (ranging from 10 to 300) and different cutoff frequencies (ranging from 50 Hz to 1000 Hz) to filter the incoming I_{p} waveform. The latter allows ROCOP SNR to filter-order response curves to be constructed for several considered cutoff frequencies (50 Hz, 100 Hz, 200 Hz, 300 Hz, 500 Hz and 1000 Hz) as presented in Figure 6.10.

The analysis shows that low cutoff frequencies are needed to avoid frequency com-

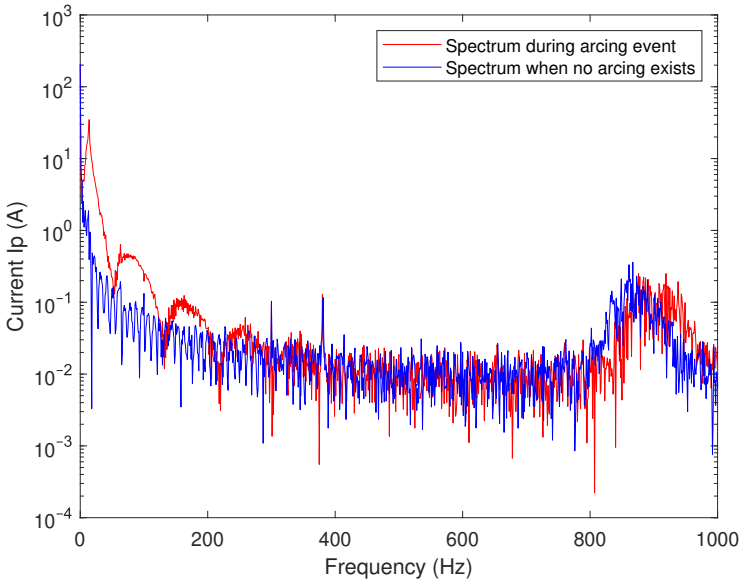

Figure 6.9: Frequency spectrum of I_{p} during and after arc occurrence.

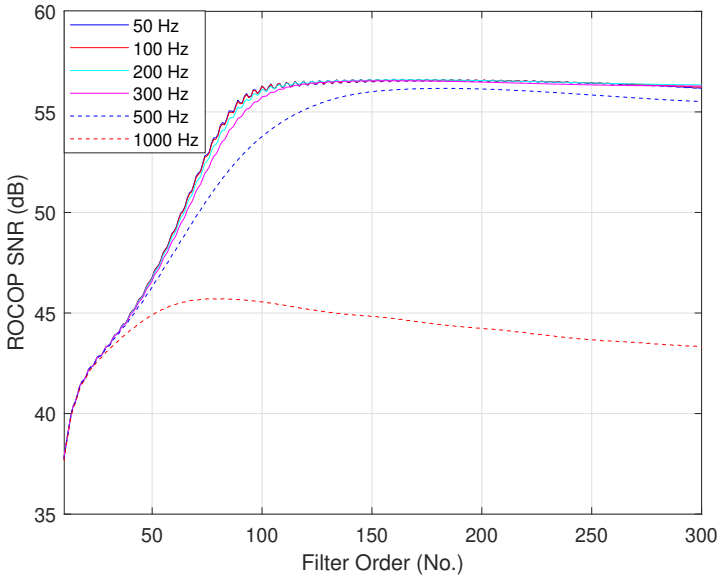

Figure 6.10: ROCOP SNR to filter order response curves constructed for filter cutoff frequencies of 50 Hz, 100 Hz, 200 Hz, 300 Hz, 500 Hz and 1000 Hz.

ponents and the noise infiltration into the ROCOP parameter. Cutoff frequency curves of 50 Hz to 300 Hz follow the same pattern and have negligible differences among them. This indicates that potentially any cutoff frequency (ranging from 50 Hz to 300 Hz)

can be employed, which provide similar reproduced results. Differences begin to appear when considering the cutoff frequency of 500 Hz and are more obvious for the 1000 Hz curve, reaching differences of more than 10 dB. This large difference is caused by the presence of a band of frequencies ranging from 850 Hz to 950 Hz approximately, as shown in Figure 6.9. The analysis also shows that higher filter orders provide larger ROCOP SNR, and the behaviour of the curve response is less fluctuating beyond the 150 filter order.

In this study, the filter order was selected to be 200, whereas the cutoff frequency 100 Hz. This cutoff frequency can also contribute to attenuate the 300 Hz component (as a result of the six-pulse rectifier installed in the electric substation) which is more distinctive when trains are near stations. The 300 Hz frequency component and other relevant components in I_{p} waveform of arc event 6, are calculated as a function of time by the short-time Fourier transform (STFT) algorithm and are presented in Figure 6.11 by the spectrogram plot.

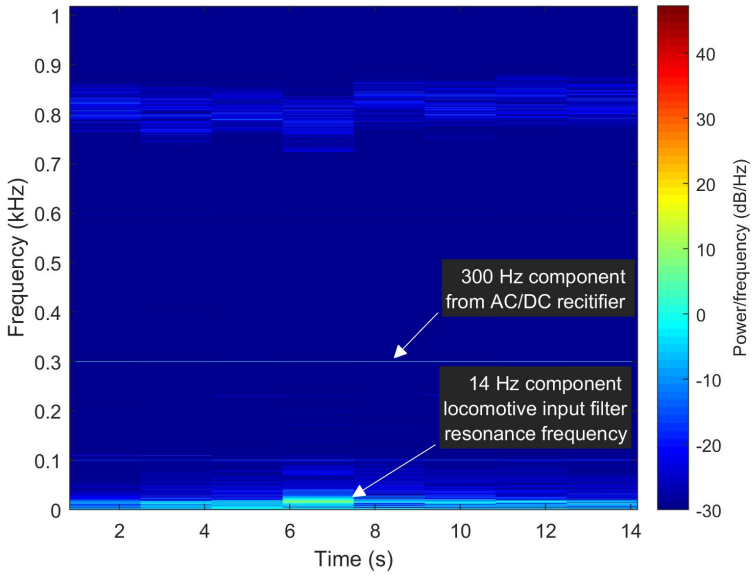

Figure 6.11: Spectrogram plot of I_{p} for arc event 6.

The plot estimates and localizes in time the frequency content of the considered waveform. It clearly indicates a 300 Hz frequency component, and a band of frequencies of 750 Hz to 850 Hz that are present continuously throughout the recording interval,

and a temporary 14 Hz frequency component, excited by the arcing event. It is clear that the 300 Hz frequency component and the band of frequencies ranging from 750 Hz to 850 Hz approximately are not affected by the arc occurrence (visible after second 6).

The selected filter parameters also have shown to remove more surrounding noise level in the ROCOP of Figure 6.7f.

6.5.2 Noise Sensitivity Analysis

To understand how noise affects the calculated ROCOP, a noise sensitivity analysis has been performed on I_{p} waveform of arc event 1. This analysis considers the white Gaussian noise because it is the most common type of signal noise found in electric system signals [153]. Furthermore, after pre-filtering of I_{p} it is considered that all that remains within the passband can be reasonably approximated by additive white Gaussian noise.

While different levels of noise have been added to the recorded I_{p}, the maximum absolute value of the calculated ROCOP has been recorded to allow the SNR-ROCOP response curve to be constructed. Figure 6.12, presents the SNR-ROCOP response evaluated for different noise variances corresponding to a SNR ranging from 100 to 35 dB. An almost constant ROCOP behavior can be observed in the interval of 100 to 70 dB. Below 70 dB, the ROCOP measured parameter experiences an increased variability leading to increased uncertainty of the measured parameter.

Although the analysis presented in Figure 6.12 is a good representation of the behavior of ROCOP magnitude at different noise levels, it does not represent the strength of the ROCOP magnitude itself to the surrounding ROCOP noise level.

Therefore, further analysis is required to represent the impact of the noise floor level (developed in relation to the noise level contained in the analyzed current waveform) on the measured parameter. Different levels of noise have been added to the I_{p} and the ROCOP SNR has been evaluated and presented in Figure 6.13 versus SNR corresponding to I_{p}.

As can be seen, the strength of the ROCOP magnitude to the ROCOP noise level is influenced by the increasing noise level in the I_{p} waveform. However, this influence

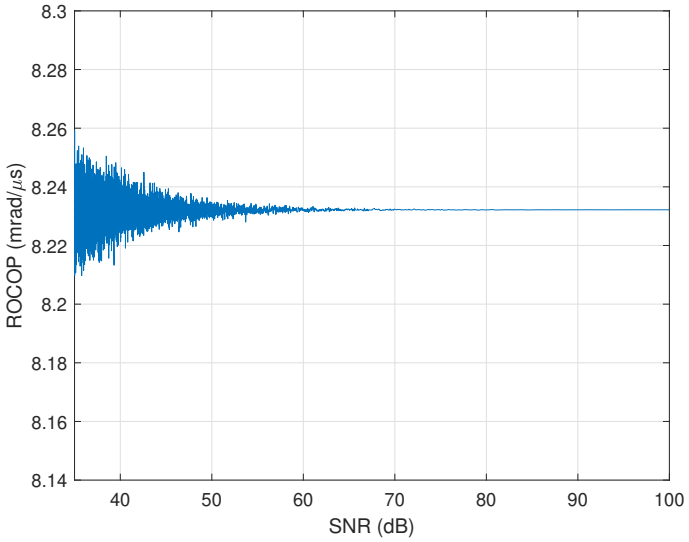

Figure 6.12: SNR-ROCOP response of I_{p} for arc event 1.

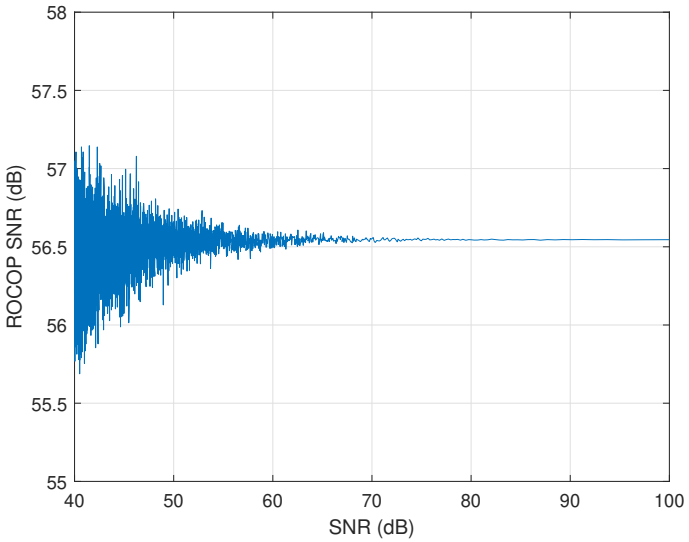

Figure 6.13: ROCOP SNR versus SNR of I_{p} for arc event 1.

is almost negligible in the interval of 100 dB to 70 dB, and small (approximately only ± 1 dB) from 70 dB down to 40 dB. This is because of the efficient attenuation effect the FIR filter has on the input waveform. Similarly, as observed in Figure 6.12, ROCOP SNR experiences an increased variability due to increased noise level starting below 70 dB SNR.

6.5.3 Post Filtering–ROCOP Noise Attenuation and Smoothing

The noise sensitivity analysis indicated an increase in the ROCOP noise floor level when externally applied noise magnitude increases. Because these noise levels can compromise any arc detection triggering mechanism, it is necessary to attenuate it as much as possible. Therefore, this subsection presents the use of a mitigation technique to further attenuate and smooth the noise level and fluctuations of the ROCOP calculated parameter observed in Figures 6.7f and 6.8a, allowing the algorithm to better interpret the processed data.

A moving average (MA) filter was considered to filter the ROCOP noise and spikes. As any type of filter, an MA filter offers various output responses for different filter order selection. To identify the behavior of the filter under different noise levels present on the arc event 1 waveform, and to provide assistance on the selection of the filter order for the required application, Figure 6.14 presents the relationship between the ROCOP SNR and the MA filter order for several filter response curves.

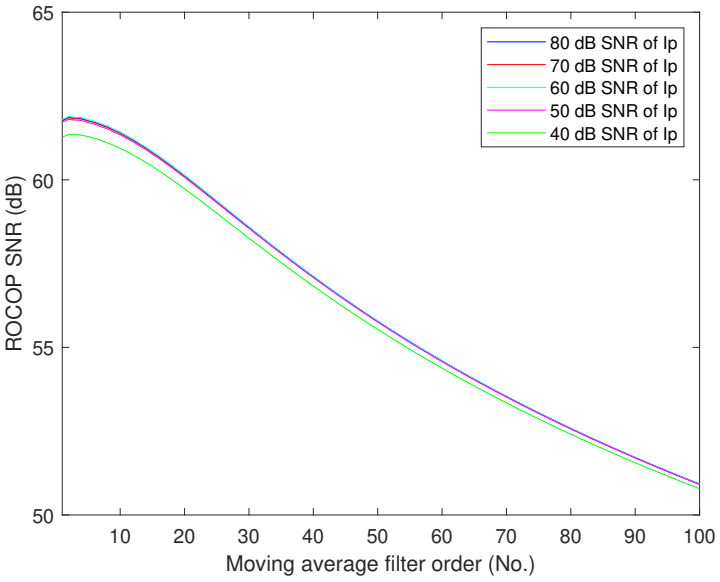

Figure 6.14: ROCOP SNR versus MA filter order for different SNR levels.

As can be seen, all the responses (corresponding to different noise levels present on I_{p}) follow the same decay and provide good attenuation (approximately 6 dB) when

considering the 50th filter order. Increasing the filter order from 50 to 100 provides an additional 4.9 dB attenuation respectively for signals having SNR noise levels of 80 dB to 40 dB. Several numerical simulations have been performed for the identification of the best MA filter order for all ROCOP curves presented in Figures 6.7 and 6.8. It was found that the 50^{th} filter order provides good attenuation of the ROCOP noise. An MA filter of 50th order requires 49 mathematical additions and one subtraction operation, and the computational demand increases with the filter order increase. However, when implemented alternatively using a recursive algorithm [163], the computational speed can reduce significantly with only one mathematical addition and one subtraction operation needed regardless of the filter order.

The absolute ROCOP calculated results filtered by the MA filter, for all the arcing captured events are presented respectively in Figures 6.15 and 6.16. These Figures clearly indicate the attenuation effect the MA filter has on the ROCOP noise. For example, the ROCOP noise level of Figure 6.7f has been considerably reduced, and as a consequence the ROCOP parameter during arcing is more clearly differentiated from the noisy environment.

Another important feature of the MA filter is the smoothing effect it has on the ROCOP fluctuations. For example, the ROCOP spikes resulting from current spikes in Figures 6.8a, 6.8d, 6.8f and 6.8g, are all smoothed by both FIR and the MA filter. Consequently, ROCOP spikes will not be counted as arcing events with a proper triggering level in place. These features of the MA filter provide significant advantages to an arc detection triggering mechanism allowing the rest of the proposed method to accurately identify the input data.

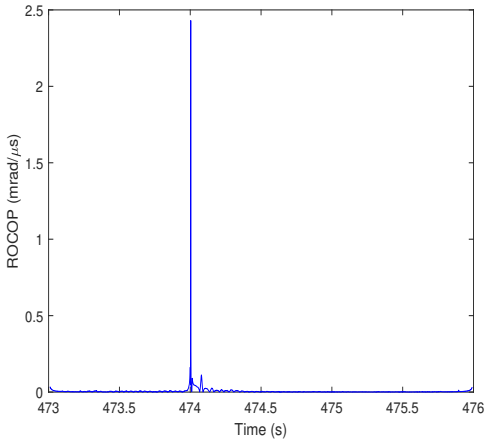

(a) Arc event 1.

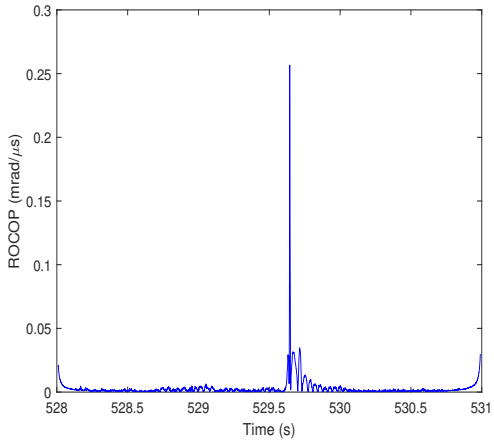

(b) Arc event 2.

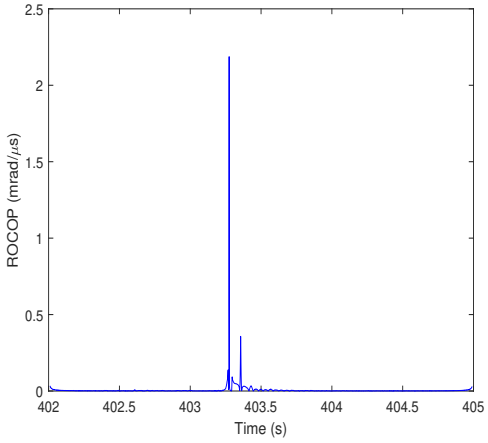

(c) Arc event 3.

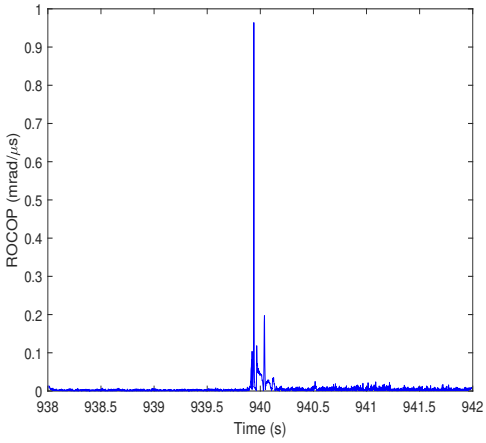

(d) Arc event 4.

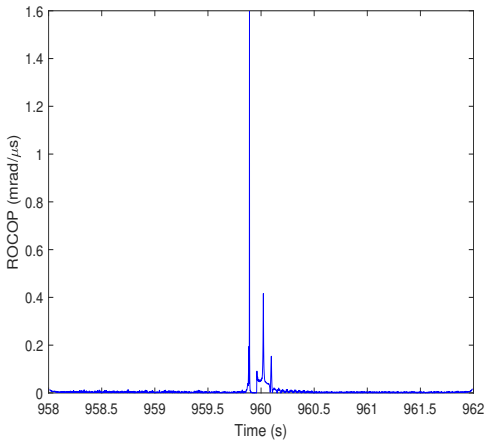

(e) Arc event 5.

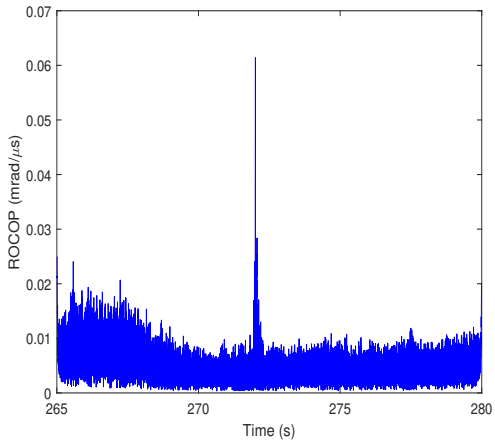

(f) Arc event 6.

Figure 6.15: Absolute instantaneous ROCOP after being filtered by the MA filter for the arc events 1 to 6.

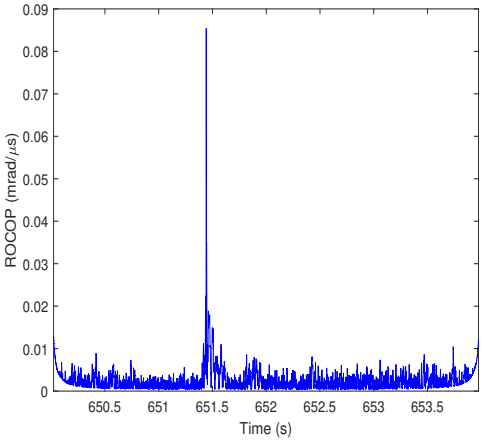

(a) Arc event 7.

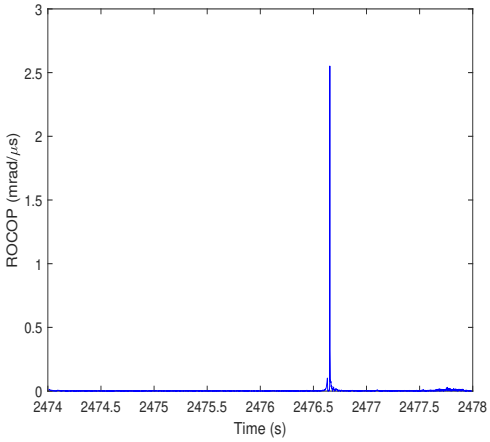

(b) Arc event 8.

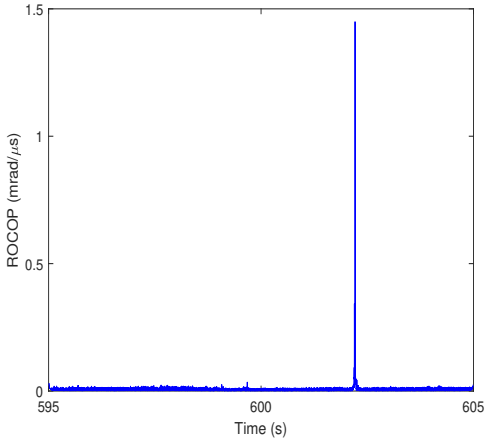

(c) Arc event 9.

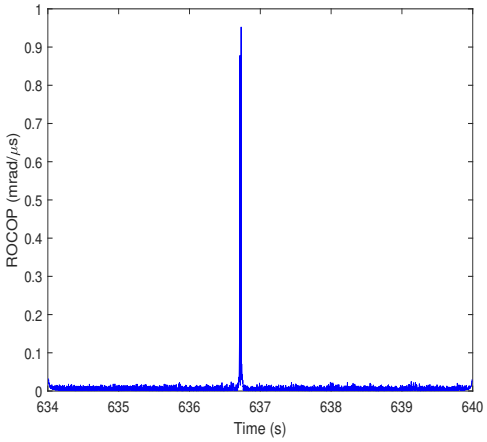

(d) Arc event 10.

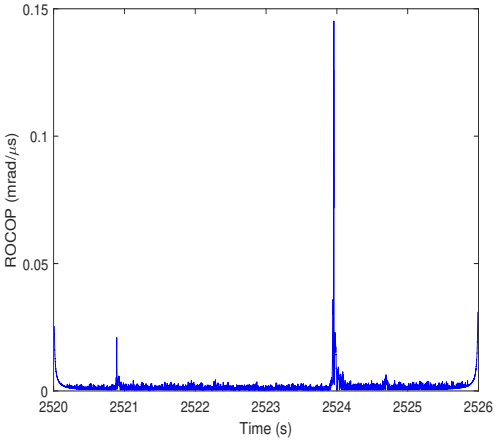

(e) Arc event 11.

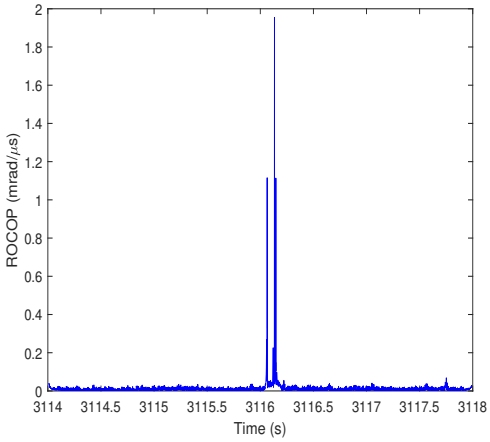

(f) Arc event 12.

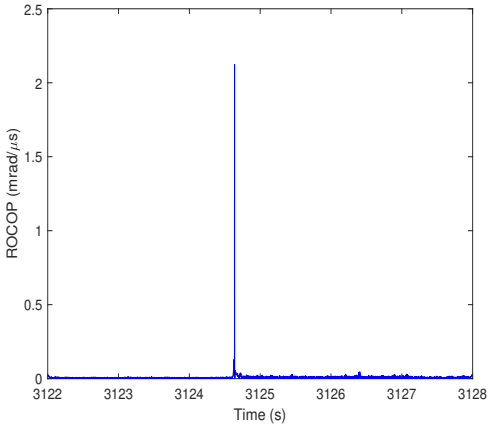

(g) Arc event 13.

Figure 6.16: Absolute instantaneous ROCOP after being filtered by the MA filter for the arc events 7 to 13.

6.5.4 Magnitude Sensitivity Analysis

The following subsection presents the influence of pantograph current oscillation magnitude on the arc detection capability of the proposed method. In this analysis, I_{p} of arc event 11 (recorded during the regenerative braking phase) has been considered because the current was not forced to zero during the arcing event, allowing a proper scaling of the oscillation magnitude.

The current oscillation instant during the arcing event was extracted, linearly scaled by a factor ranging between 0.9 to 0.1 in 0.1 steps, and then synthesized within the real data recordings to be used for testing the proposed arc detection method. The extracted portion of the current oscillation I_{p1} is presented in Figure 6.17, along with all the scaled versions denoted as I_{p2} to I_{p10}, corresponding to scaling factors 0.9 to 0.1, respectively.

The method was tested with all the 10 pantograph current versions, and the relationship between the calculated ROCOP SNR and the scaling factors is presented in Figure 6.18. ROCOP SNR values (for each scale factor) indicate the level of differentiation of the arc from the environment noise level, consequently, all the arcs have been

detected. A decrease is normally expected in ROCOP SNR with decreasing scale factors because the magnitude of the arc oscillation reduces significantly, for example to 36 A and 18 A (absolute values), respectively for scale factors 0.2 and 0.1 (corresponding to I_{p9} and I_{p10}) of Figure 6.17.

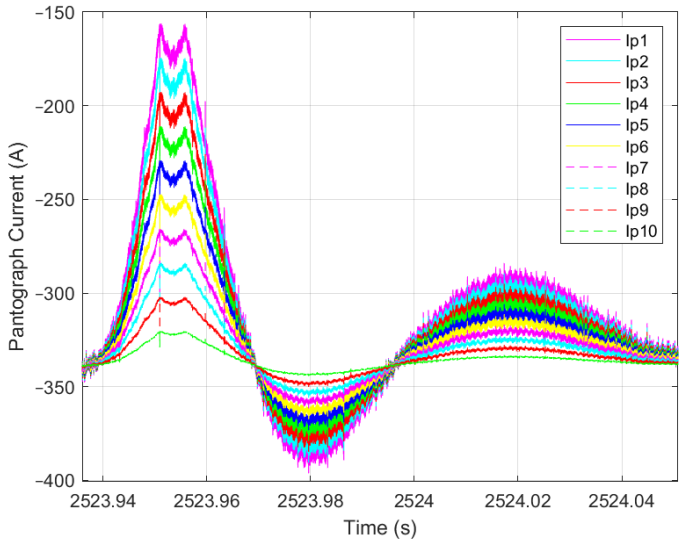

Figure 6.17: Pantograph current I_{p1} of arc event 11, along with scaled current versions I_{p2} to I_{p10}, respectively, for scaling factors 0.9 to 0.1.

This magnitude sensitivity analysis has shown that the proposed method is capable of identifying all arcing events having reduced oscillation magnitudes down to 18A. However, arcing events of such a small oscillation magnitude can be considered non-significant when compared to oscillation magnitudes of the real captured arcing events (arc events 1 to 13).

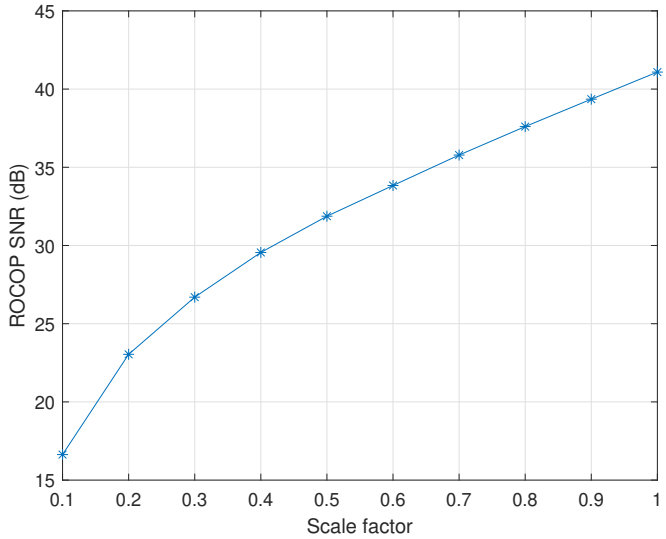

Figure 6.18: ROCOP SNR values versus the scaling factors for the considered arc event 11.

6.5.5 Signal Window Length Impact

The effect of considered waveform length on the ROCOP parameter is studied in this subsection. The pantograph current of arc event 1 has been considered for this analysis. Initially, the maximum ROCOP parameter observed within the time window processed waveform is evaluated for the total length of the recorded waveform (150,000 samples equals to 3 s). The waveform was divided into equal lengths through different consecutive time windows and processed by the proposed method.

The maximum ROCOP values for different fixed window waveform lengths are presented in Figure 6.19 (blue curve), where text annotations indicate the number of samples within each time window.

A small difference in ROCOP magnitude exists between a long window of 3 s and shorter windows of 1 s, 0.6 s, 0.2 s and 0.1 s corresponding to 50,000, 30,000, 10,000 and 5000 samples as presented by the blue curve in Figure 6.19. Decreasing further the length of the time window to 3000 samples, 1500 samples or 1000 samples produces a decrease in ROCOP magnitude. This behaviour is caused by short windows that fail to accommodate a complete arcing event. This is demonstrated when sliding windows

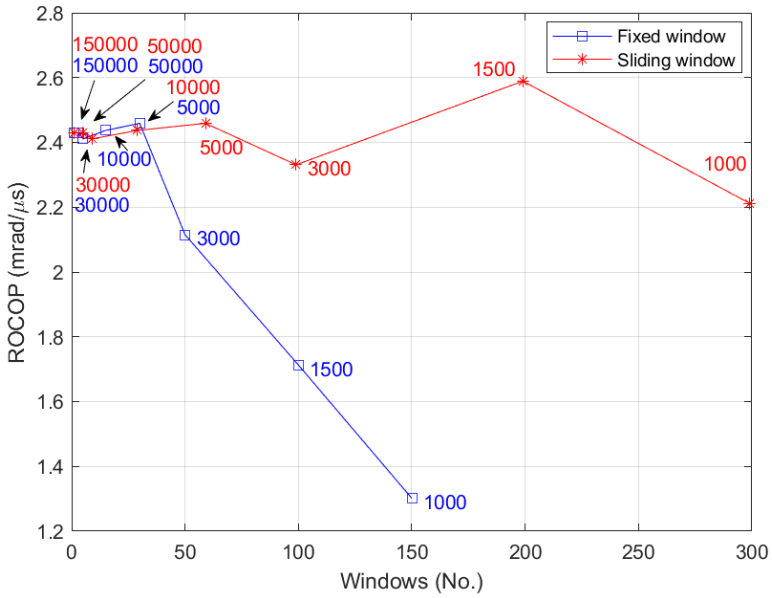

Figure 6.19: Maximum ROCOP values for different waveform lengths.

of 50% overlap are used (see the red curve in Figure 6.19), which better accommodate the arcing event for processing, and consequently produce ROCOP magnitudes of small differences for short windows. Based on this analysis, the one-second (equal to 50,000 samples) measurement window size was selected to detect electric arcs using the fixed window implementation and geographically locate their position along the line as presented in the next chapter of this thesis.

The analysis presented in this section has indicated that the proposed arc detection method is capable of detecting arcs of different magnitude at different noise levels in the DC rail network.

In addition, standard EN 50317 [137] requires the current collection quality of the pantograph-catenary system to be evaluated. For this purpose the percentage of arcing is proposed in [137], to be calculated as the ratio of total duration of all arcs to the total run time for pantograph current values above the 30% of the nominal current per pantograph. The proposed arc detection method clearly cannot evaluate the time duration of the arcs, but the detected arcs can be used to compute the number of arcs per kilometre, as an alternative criterion (also acceptable by standard EN 50317 [137])

for evaluating the current collection quality.

6.6 Chapter Summary

This chapter has presented a novel arc detection technique for DC railway systems. The method quantifies the instantaneous ROCOP of the pantograph current oscillating signal during the arc occurrence using the Hilbert transform. Real current waveforms measured at a 3 kV DC pantograph level of a running locomotive have been applied to test the performance of the algorithm, and it has been demonstrated that the phase derivative can detect and localize in time all the electric arcs occurring at both the coasting and regenerative braking phases.

The sensitivity of the algorithm to external applied white Gaussian noise, various synthesized oscillating magnitudes representing different arcing events, and the length of the considered waveform is also evaluated. It has been demonstrated that the noise level in the pantograph current has little influence in ROCOP parameter due to efficient noise attenuation provided by the FIR filter. ROCOP parameter measured for signals having SNR between 100 dB to 70 dB was highly repeatable, whereas, below 70 dB of SNR, the performance of the ROCOP technique is variable, leading to increased uncertainty.

A moving average filter was employed to attenuate and smooth the ROCOP noise level and spikes, and it was demonstrated that the ROCOP properties after the filtering stage were clearly differentiated from the rest of the noisy environment.

The magnitude sensitivity analysis has demonstrated that the proposed method is also capable to identify minor arcing events having oscillation magnitudes down to 18 A. These arcs are typical in very low train speeds and are probably caused when trains change the track position.

A small difference in ROCOP magnitude for different considered waveform lengths (3 s and 1 s, 0.6 s, 0.2 s and 0.1 s lengths) has also been demonstrated. For very short considered time windows (1000 to 3000) samples, it was shown that sliding windows outperforms fixed length windows because complete arcing events are better discovered, providing consistent results. A 200 ms window size has been proposed to detect the

electric arcing phenomenon in line with the typical window size commonly adopted in PQ instruments.

The DC arc detection method in this chapter provides a new tool for accurate condition monitoring of critical electrified rail infrastructure. This has the potential to enable predictive maintenance, thereby reducing operational costs and improving safety.

It is also worth noting that the proposed arc detection method is developed, tested, and evaluated with measured signals on a 3 kV DC railway system acquired onboard a single locomotive running along three different routes. Therefore, the proposed method is not dependent on the route and is expected to perform well in every 3 kV DC railway network because the power supply topology of such systems typically is formed by the same components (rectifier-filter block installed in TSs and standardised OCL distribution). Also, the method is considered independent of the locomotive type whenever the signals are measured at the pantograph level. The applicability of the arc detection method in other DC railway systems with a supply voltage of 1500 V DC or in other rail transportation systems (tramways and metros) needs validation with real arcing signals because the TS rectifier-filter block and the OCL characteristics can differ from those in 3 kV DC railway system.

Chapter 7

Detection and Geographic Localisation of Electric Arcs in DC Railway Networks

7.1 Introduction

Electric arcing in electrified railway networks is an unwanted phenomenon that cannot be eliminated. However, the consequences of continuous arc occurrence can be mitigated through predictive maintenance. In Chapter 6, a new arc detection technique to support pantograph-catenary condition monitoring has been presented and tested.

In this chapter, the capability of the proposed method has been extended to allow the geographical arc localisation information to be extracted. It can provide electric arc mapping to the railway track and, consequently, support condition monitoring of the rail network by allowing the network operator to understand where arcing events happen. It aims to reduce the operational cost, and increase the reliability of the DC rail network.

7.2 Proposed Arc Localisation Technique

As analysed in section 3.6.4, much effort has been devoted to arc identification techniques in railway electrified networks by the research community. The proposed methods, in addition to arc detection, aim to calculate a relevant index to quantify the current collection quality of the pantograph-catenary system. The index is used by railway companies to support predictive maintenance services. Contact line condition checks are usually performed periodically by specialised catenary equipment [130, 139]. The service is reported to be expensive, slow, and requires interruption of the particular lines of the transportation service [139].

The focus of previously proposed arc evaluation methods was only on arc detection, and little consideration is devoted to the geographical localisation of electric arcs in DC railway networks. An initiative to evaluate the arc location in DC railway networks is presented in reference [23]. In this study, a DC railway system consisting of two substations feeding a 20 km OCL and a locomotive is simulated in Matlab/Simulink. Arcing events at different positions along the line have been generated (at pantograph level), and the associated overhead contact line resonant-frequencies (RFs) have been measured. It allowed the creation of a resonant-frequency (RF) curve shown in Figure 7.1 relating together the OCL RFs with the arc position (estimated as locomotive position – km away from a particular substation).

In Figure 7.1, the respective RF curves show a monotonic increase up to halves of the line lengths. For the second halves of the lines, RF curves have shown a mirrored monotonic decrease. Because of this RF replication this method needs further improvement to differentiate which RFs belong to which half of the line.

A different approach to match the arcing occurrence with the train position along the track is briefly mentioned in reference [140], where the algorithm has shown the potential to count the train passage under the horizontal portals carrying the OCL for railway lines with portal structures only.

In this chapter, the speed profile of the locomotive has been exploited as a piece of supplementary information to derive the train position along the track, and correlate

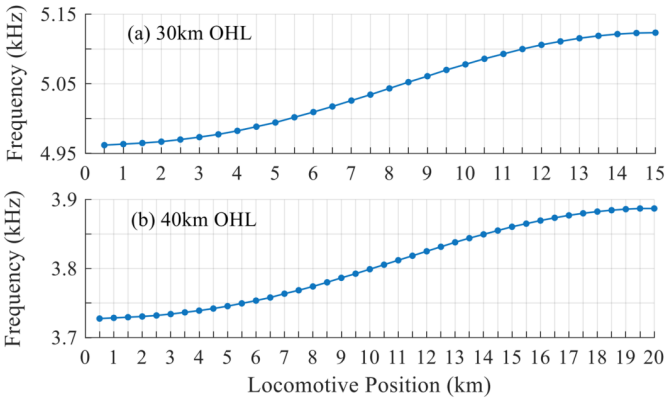

Figure 7.1: RF curves of a 30 km and 40 km lines split at different locomotive positions.

that with the arc occurrences detected with the method proposed in Chapter 6 of this thesis. However, the exact train position along the track cannot be accurately determined because there is no available information on the speed sensor accuracy used by the locomotive. The flow chart of the proposed algorithm is presented in Figure 7.2, with the algorithm steps as follow:

1. Extraction of 50,000 samples of pantograph current and locomotive speed signal from the database;

2. ROCOP according to the method presented in Chapter 6 is calculated;

3. Travelled distance according to Equation 7.1 is calculated:

$$L[n] = L[n-1] + \triangle s[n] \tag{7.1}$$

where $\triangle$ s[n] is calculated according to Equation 7.2

$$\triangle s[n] = v[n] \cdot \triangle t \tag{7.2}$$

where v is the speed signal; n is the number of samples acquired in the signal; for a time sampled signal $\triangle t$ is the sampling time which is 20 us; and $\triangle s$ is the instantaneous distance.

4. Calculate the difference $max - mean$ to link neighboring ROCOP samples to one arcing event;

5. If the $max - mean$ difference is grater than a threshold, an arc is detected at a specific kilometre position.

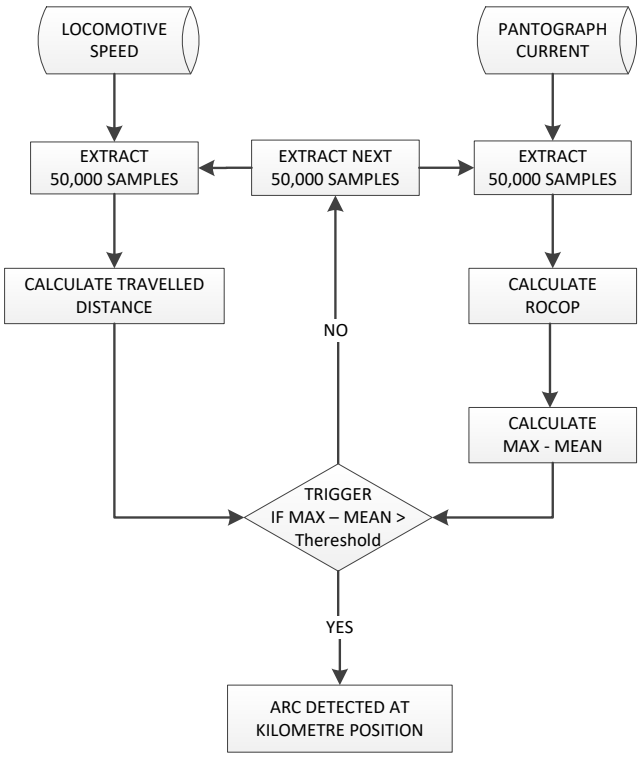

Figure 7.2: Flow chart of the arc detection and localisation algorithm.

This technique has the potential to permit OCL inspection at determined line positions only, without the need to check all the line and interrupt the transportation service for extended periods, thereby reducing the maintenance cost and improving reliability.

7.3 Considered Waveforms

This section presents the time behavior of the current waveform absorbed by the locomotive and the speed profile that will be considered in the remaining sections of this chapter to determine the geographic localisation of electric arcs detected. These waveforms are acquired on-board the train using a DAQ sampling at 50 kS/s. The considered railway line was Pisa–Collesalvetti, operating within a 3 kV DC railway network in Italy [19].

Figure 7.3, presents a portion of the current absorbed by the locomotive during the considered route. The corresponding speed profile of the locomotive is presented in Figure 7.4. As can be seen, the running mode of the locomotive varies during a journey and is characterised by several accelerating, braking, and stationary phases.

From the speed profile of the locomotive, the instantaneous distance of the locomotive using Equation 7.1 can be derived. The instantaneous distance allows the calculation of the travelled distance L as shown by Equation 7.2, and presented in Figure 7.5. For the considered portion of the journey, the locomotive has travelled approximately 13.5 km. It also has stopped for some time in two stations as annotated in Figure 7.5. The travelled distance will be used in combination with the arc detection algorithm to associate a geographic position in km to the detected arcs as shown in Figure 7.2.

In this analysis, the Pisa–Collesalvetti route has been selected simply because of the availability of the speed profile recorded on-board train. However, it is worth noting that during this portion of the journey, no arc has occurred. To enable the arc detection and localisation analysis, eight real electric arcs detected by the locomotive in other DC railway lines in Italy [151] have been inserted at different positions of the current waveform presented in Figure 7.3. The considered electric arcs are presented in Figure 7.6 and Figure 7.7.

The waveforms have been combined by following this procedure: the exact magnitudes of steady current waveforms before arc occurrences (see Figures 7.6 and 7.7) have been evaluated; similar current levels have been identified at different positions in the current waveform of Figure 7.3; the current waveform has been chopped at sev-

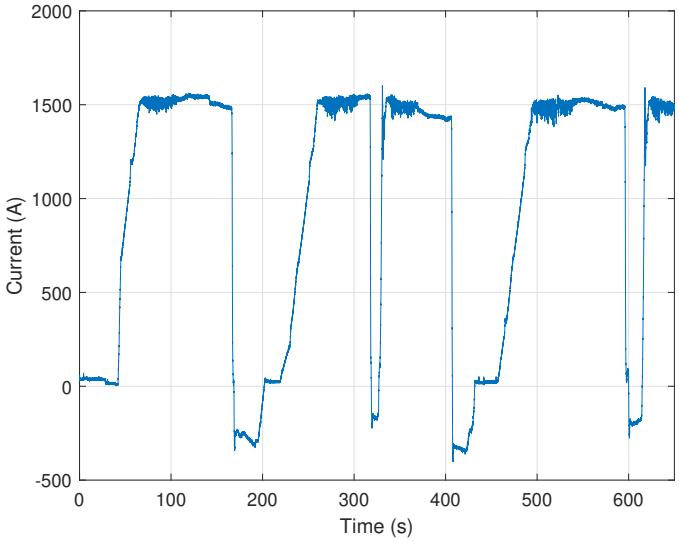

Figure 7.3: Pantograph current absorbed by the locomotive.

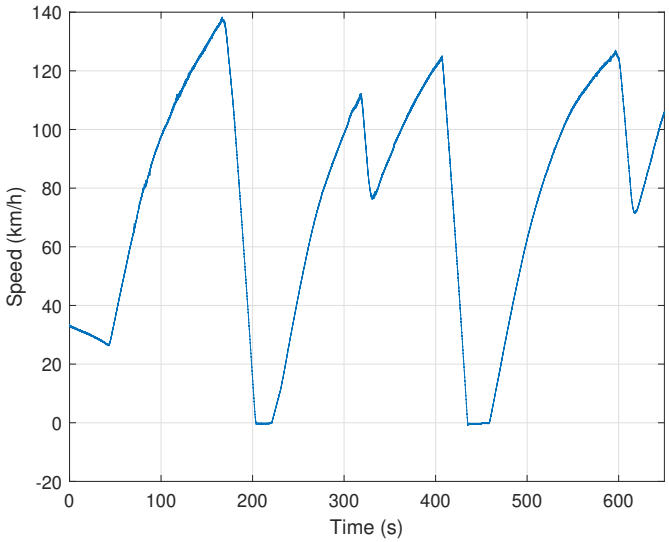

Figure 7.4: Speed profile of the locomotive.

eral positions and the electric arcs have been inserted one by one following the above procedure.

The electric arcs presented in Figure 7.6 and Figure 7.7, respectively, have occurred during the traction and braking phases of the running locomotive, and they have different characteristics such as duration and magnitude. They are selected to replicate as

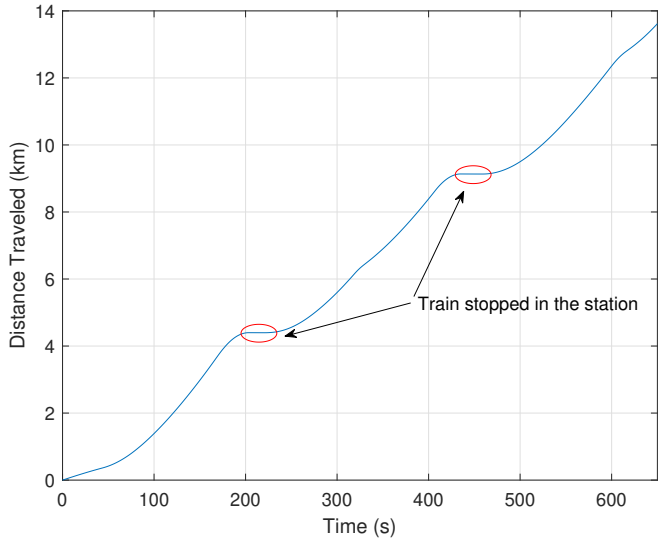

Figure 7.5: Distance travelled by the locomotive in km.

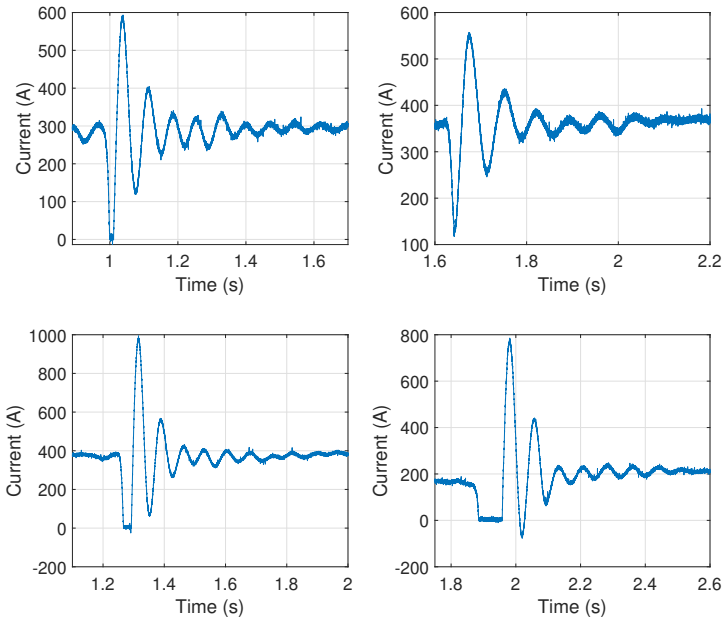

Figure 7.6: Electric arcs detected during the traction phases of a running locomotive.

much as possible a real situation of a pantograph current waveform in a DC railway network. These arcs are inserted in the Pisa–Collesalvetti current waveform as presented in Figure 7.8, and will be used to test the arc detection and localisation algorithm in

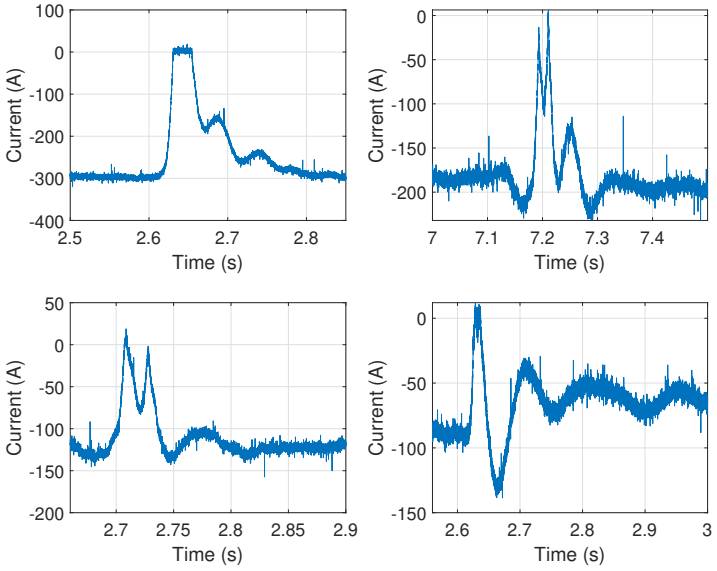

Figure 7.7: Electric arcs detected during the braking phases of a running locomotive.

the next section of this chapter.

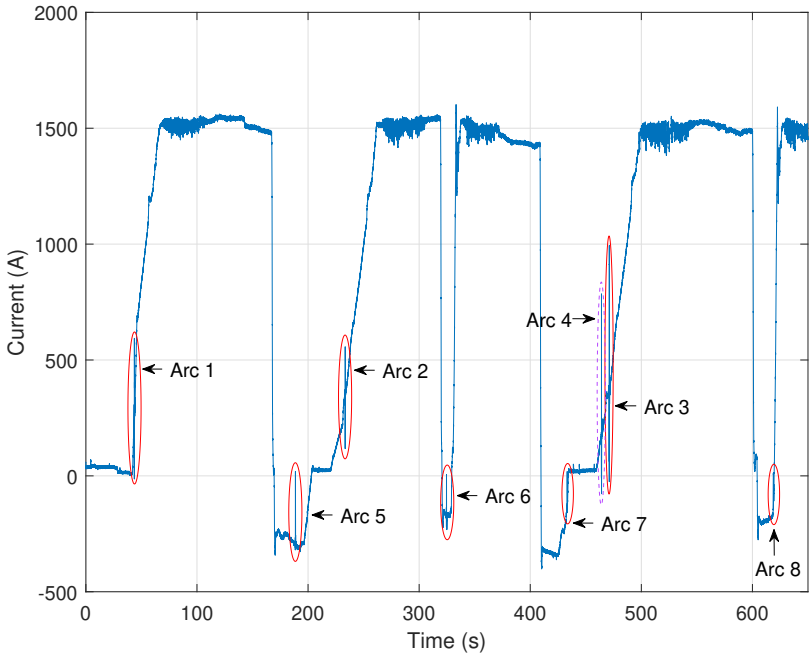

Figure 7.8: Pantograph current with electric arcs inserted.

7.4 Results of the Analysis

In the previous section, real electric arcs captured in a DC railway network have been inserted in a real pantograph current waveform. The reason for this is to test the performance of the algorithm in localising the geographic position of the arcs.

In Figure 7.8, arcs 1 to 4 correspond to the arcs captured during the traction phases, and as can be seen, they are inserted in the current waveform at different traction phases of the locomotive running in Pisa–Collesalvetti line. Similarly, arcs 5 to 8 are inserted in the braking stages of the locomotive noted by the pantograph current having negative values.

The results of only the arc detection processed by the arc detection and localisation algorithm are presented in Figure 7.9. The figure depicts the instantaneous pantograph current waveform, together with instantaneous phase angle and instantaneous ROCOP values. Figure 7.10 presents the absolute ROCOP calculated results after being filtered by the MA filter. As expected, the algorithm has detected all the arc events contained in the waveform.

As the ROCOP parameter contains instantaneous values, a mechanism is needed to link the neighboring samples (see the zoomed figure within Figure 7.10) having significant values, to one arc event only (represented by the maximum sample value), to simplify the detection mechanism. This is achieved by calculating the difference between the maximum value (max ROCOP sample) and the mean value calculated within each consecutive ROCOP window having 50000 samples. The difference of $max - mean$ for every 50000 samples is represented in Figure 7.11). This difference also further attenuates the ROCOP noise remaining after the final MA filter stage of the algorithm. As depicted by the zoomed inset figure, arc number four (occurred between 320 s to 330 s) has only one significant sample which represents the arc occurrence within the considered window. This approach helps resolve the requirement for a defined threshold to detect the arc occurrence along the railway line. By setting a threshold of 6-7 urad/us, and applying the current waveform, all the arcing events have been detected and their geographical positions have been identified by the proposed

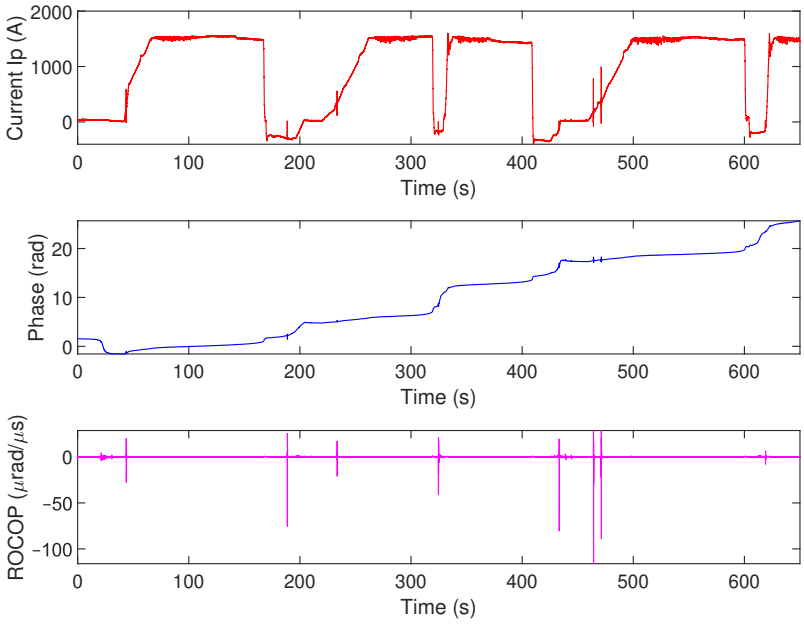

Figure 7.9: Instantaneous pantograph current Ip, instantaneous calculated phase angle, and instantaneous ROCOP.

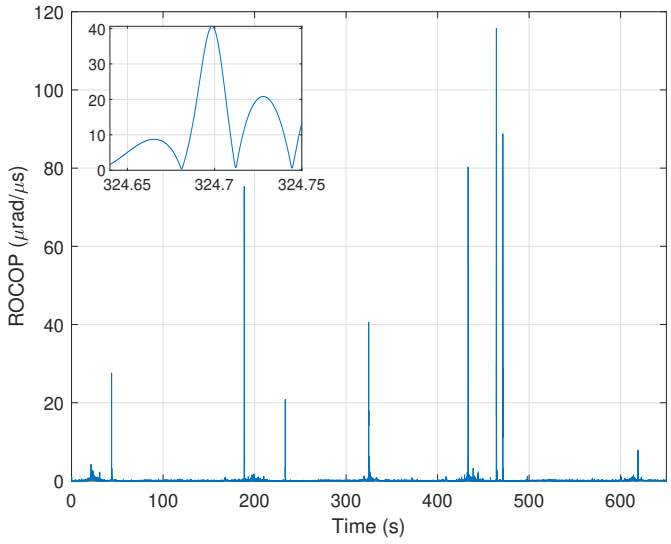

Figure 7.10: Absolute instantaneous ROCOP after being filtered by the MA filter.

algorithm in Figure 7.2.

The summary of results is presented in Table 7.1. The table indicates the position

in km where arcs have occurred, the train speed during the detected arcs, and the estimated error range. The error depends on the speed of the train as well as the measurement window size used in arc detection, which is equal to the instantaneous distance traveled $\triangle$ s[n]. By considering the measurement window size equal to 1 s, and the measured train speed of 26.84 km/h (or 7.5 m/s) corresponding to arc number one of Table 7.1, the localisation error ranges from -7.5 m (for arcs occurring at the start of the window) to 0 m (for arcs occurring at the end of the window).

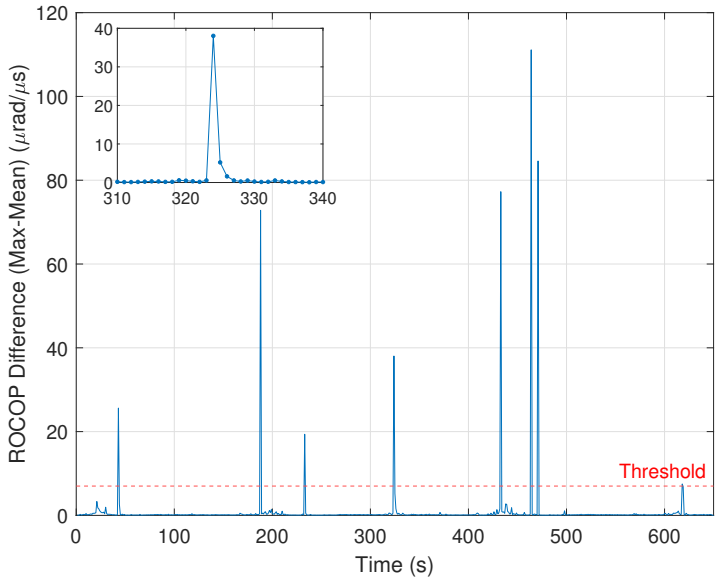

Figure 7.11: Max-Mean difference for every 50000 samples of the waveform.

Table 7.1: Localisation of electric arcs detected in a DC monitored railway line.

Arcs detected	**Occurred at**	**Train speed**	**Estimated error**
Arc 1	0.349 km	26.84 km/h	-7.5 – 0 m
Arc 2	4.239 km	67.33 km/h	-18.7 – 0 m
Arc 3	4.411 km	15.8 km/h	-4.4 – 0 m
Arc 4	6.289 km	91.54 km/h	-25.5 – 0 m
Arc 5	9.122 km	7.04 km/h	-2.0 – 0 m
Arc 6	9.129 km	8.75 km/h	-2.5 – 0 m
Arc 7	9.155 km	19.97 km/h	-5.6 – 0 m
Arc 8	12.82 km	71.91 km/h	-20 – 0 m

The analysis presented in this section allows to calculate the distribution of arcs per km as an indicator of the current collection quality of the pantograph-catenary system in DC railway networks. For the considered journey, the distribution of arcs per kilometre index is 0.59 arc/km, considering the 13.5 km locomotive travelled distance and eight arcs occurred.

7.5 Chapter Summary

In this chapter, the capability of the arc detection method proposed in Chapter 6 has been extended to allow the geographic localisation of electric arcs along a DC railway line. The speed profile of the locomotive has been used to derive the travelled distance of the train and support the localisation feature of the method.

To test the method, a real pantograph current waveform combined with eight injected real electric arcs to mimic a real situation of a pantograph current waveform disturbed by the electric arcing phenomenon has been considered. A mechanism to facilitate arcing detection also has been introduced. Combined with a threshold value, the method has indicated the ability to detect and localise the kilometric position of all of the arcs contained in the waveform successfully. The error of the method also has been evaluated. It has been shown that the error is dependent on the speed of the locomotive and the measurement window interval.

Even though the method has shown to be successful in detecting electric arcs and localising their kilometric positions, it has only been tested with combined signals (pantograph current signal and electric arcs detected in different DC railway lines). Other recorded waveforms containing electric arcs and speed profiles of the locomotives are needed to re-test the method. It can then be validated onboard the train, where a temporary video camera or a light sensor is required to check the results.

As arc detection allows estimating the current collection quality of the pantograph-catenary system and supporting better scheduling of a complete line inspection, arc localisation has the advantage to permit overhead line inspections at determined line positions only as indicated, for example, by a continuous arc occurrence at a specific line section. This way, the transportation service of the line in question will not be

interrupted for extended periods. Also, the expensive cost of a periodic line inspection will be significantly reduced. Overall, the reliability of a DC rail network will be enhanced.

Chapter 8

Conclusions and Further Work

8.1 Conclusions

In this thesis, PQ disturbances present in electrified railway networks have been discussed, presented, and analysed. Newly developed techniques to detect unique disturbances in AC and DC railway networks have been presented, and recommendations for PQ rail instruments have been provided.

In Chapter 1, evidence of the unique PQ phenomena encountered in AC railway signals, compared to disturbances present in transmission and distribution electricity grids, has been shown. In addition, the lack of a recommendation document describing the PQ measurement techniques in railway applications is emphasised. Therefore, a gap exists to better understand the PQ disturbances in railway networks and to evaluate if the measurement methods defined in IEC 61000-4-30 are appropriate enough for accurate characterisation and classification of PQ phenomena in AC railway signals. Furthermore, it has been shown that there is an industry need for new techniques in DC rail networks to enhance the pantograph-catenary condition monitoring, which is the primary objective of this research work.

Chapter 2 provides an overview of electrical measurements in power systems and briefly describes the importance of accurate and reliable measurements for different applications and studies. The PQ phenomena present in electric grids are introduced, together with a short definition and categorization based on their unique characteristics.

Standardised measurement methods along with other alternative techniques used for PQ disturbances evaluation also are presented and analysed.

A literature review of developments in electric railway networks has been presented in Chapter 3, including: traction power supply systems; the principal sources that produce PQ disturbances; PQ measurement techniques; and the present solutions to enhance the PQ of these networks. The challenges of standardised PQ measurement methods when evaluating the peculiar features of AC railway signals also have been emphasised, along with the need of having a cost-effective arc detection method for DC railway networks able to enhance the condition-monitoring of the railway infrastructure and lower the operational costs of the service.

Following on from the measurement challenges, an improved estimation technique for voltage interruption has been developed and presented in Chapter 4. It considers both voltage and current waveforms to identify those voltage interruptions caused by the phase separation sections as part of the network configuration and can discriminate them from other voltage interruption causes, allowing a better understanding of the phenomenon, an improved event classification, and a better correlation of their impact on rail network assets.

In Chapter 4, a comparison between the measurement methods based on half-cycle and one-cycle for the evaluation of voltage dip and voltage swell phenomena has revealed that the technique proposed by the IEC 61000-4-30 standard is not sufficient to provide a suitable classification accuracy and a fast-acting response to event occurrence for 25 kV 50 Hz traction systems signals. This is an important result which is crucial for future PQ measurement standards for rail systems. The measurement window size (of one-cycle) affects the magnitude accuracy and time-duration characteristics of voltage dips and voltage swells of short time-duration. The use of half a cycle integration interval has shown an improved evaluation accuracy for short-time events and a higher sensitivity to voltage variability of AC traction systems, allowing a better detection and classification of voltage events for an enhanced correlation of their effect on rail components as well as on the electrical insulation system of the locomotives.

The application of standardised measurement method for the evaluation of harmon-

ics in 25 kV 50 Hz railway waveforms is analysed in Chapter 5. The effects of several time-aggregation intervals on the measurement results have been evaluated. Significant differences have been observed between the measurement results made available over 150-cycles, and the measurement results aggregated over a shorter number of cycles. These findings have also been supported by simulations. It has been demonstrated that the time aggregation interval proposed by the IEC 61000-4-30 standard cannot track the true dynamics of the time-varying frequency components due to the smoothing effect of the algorithm. Consequently, a shorter aggregation time interval, equal to 50 cycles for 50 Hz signals, is proposed for future rail PQ measurement instruments, and it was shown to significantly reduce the harmonics magnitude errors for network disturbances of time duration shorter than 2 s, whereas for disturbances of time duration longer than 2 s the harmonics magnitudes errors were reduced to zero. The proposed interval allows a more accurate estimation of harmonic emission levels in railway systems, improved tracking of time-varying frequency components, and a better understanding of the negative effects of the harmonics on the network components.

Because significant levels of voltage and current harmonics exist in 25 kV 50 Hz railway networks, active harmonic powers of real train journey waveform recordings have been evaluated. The analysis has shown the negligible variability of harmonic powers flowing in and out of the train. The corresponding harmonic energy levels are below the measurement accuracy of energy meters for the locomotive type with a phase-controlled converter on board. However, other types of locomotives exist with different converter systems on board that are known to generate larger harmonic content in the rail network. Therefore, to prevent the energy meters of the trains from absorbing the non-fundamental energy produced by other trains on the system and to consider improved energy meter strategies that better reflect the correct cost of power usage, more analysis of harmonic powers onboard other types of locomotives and for a variety of network loading conditions is necessary.

A novel arc detection method for DC railway networks has been developed and presented in Chapter 6. The rate of change of instantaneous phase of the signal has been evaluated during arc occurrences using the Hilbert transform, and it was demonstrated

to successfully indicate of arc occurrence in all tested scenarios.

The method has been subject to an extensive sensitivity analysis comprising noise, magnitude variations, and various lengths of the considered waveforms. It also has been tested with real electric arcs captured from a 3 kV DC railway network. It has been demonstrated that the method is slightly influenced by the noise level of the input waveform thanks to a pre- and post-filtering stage. It can also detect minor arcs characterised by very small oscillation magnitudes, and is able to detect all arcs when sliding windows with 50% overlap are used. The method detects and identify the time of occurrence for all the real electric arcs captured during both coasting and regenerative braking phases of the running train.

The advantages of this method compared to other arc detection methods in the literature are:

- It is cost-effective because it does not require external equipment such as light sensors, video cameras, thermal cameras, or antennas to be installed on the train.
- Processes the pantograph current signal as the only input quantity and does not require any supplementary information to undertake the decision.
- It is simple and can be implemented relatively easily.

The proposed method has the potential to provide the number of arcs per kilometre, thereby reliably providing the current collection quality index for condition monitoring of the entire pantograph-catenary system of the electrified rail infrastructure.

Chapter 7 builds on the contributions of Chapter 6 to extend the capabilities of the arc detection method to also extract the geographical localisation of the occurred arcs along the traveled route. The technique exploits the speed profile of the locomotive to identify the kilometric position of the occurred arcs. It has been tested with a real pantograph current waveform containing eight injected arc events. Combined with a threshold value and a signal processing mechanism that facilitates arc extraction, the method has shown the ability to detect and identify the position of all of the electric arcs.

This novel arc localisation feature has the important benefit of permitting overhead line inspections at determined line positions only, thereby avoiding long interruptions of the transportation service because of the need for complete OCL inspections. It therefore has the potential to enable predictive maintenance, thereby reducing operational costs and improving safety and the reliability of a DC rail network.

In summary, this thesis has reviewed and analysed the application accuracy of standardised PQ measurement methods when applied to 25 kV 50 Hz railway waveforms. Modifications of the measurement methods are provided and a new techniques have been developed to better reflect the level of disturbances in AC traction systems. A novel arc detection techniques has been developed to support real-time condition monitoring of DC railway networks. Recommendations have been developed and provided for future PQ measurement rail instruments.

8.2 Further Work

8.2.1 Implementation and Validation of the Arc Detection Method in DC Railway Systems

In Chapters 6 and 7, the proposed arc detection and localisation method has been tested and evaluated with measured pantograph current waveforms containing electric arcs captured in a 3 kV DC railway system. This method now needs to be implemented in real instruments and integrated onboard a DC locomotive operative in a 3 kV DC railway system for online testing and validation. In such a context, a validation procedure must be developed in advanced where most probably, a temporary video camera or a light sensor will be required to check the results.

8.2.2 Application of the Arc Detection Method in Tramway and Metro Systems

Throughout the thesis, it has been shown that there is an industry need for new arc detection techniques in DC railway systems to enhance the pantograph-catenary condition monitoring and the reliability of the transportation system. Other rail-based trans-

portation systems, such as tramways and metros, operating at lower supply voltages also could benefit from the proposed arc detection method. However, direct application of the method in such systems is not straightforward because the network components and the OCL parameters can differ from those in the 3 kV DC railway system. Therefore, the method needs to be tested and properly adjusted to be successfully applied in metro and tramway systems.

8.2.3 Extending the Arc Detection Method for 16.7 Hz and 50 Hz Railway Networks

Due to the impact of electric arcs in railway networks, more work is needed to extend the applicability of the arc detection method to 16.7 Hz and 50 Hz railway systems. As the arc detection method proposed in this thesis is based on the rate of change of the phase evaluation of the pantograph current signal, in principle, the method would work in detecting electric arcs occurring in 50 Hz and 16.7 Hz railway networks. This is based on the fact that when an electric arc occurs in AC networks, the current will drop to zero, leading to detectable changes in the rate of change of the phase of the signal. In such a context, waveforms containing real electric arcs captured in 50 Hz and 16.7 Hz railway networks are needed to test the performance of the arc detection method.

It is known that electric arcs can impact the PQ of railway signals. Likewise, it can be assumed that PQ disturbances may affect the detection ability of the proposed arc identification method. For example, one of the challenges for the method could be the occurrence of phase jumps caused by faults in other parts of the AC three-phase grid where the method wrongly indicates the presence of an arc.

8.2.4 Standardisation of Arc Detection Measurement Method

As an electric arc in a railway network can be considered a PQ phenomenon, further work is needed to consolidate the work in this thesis to allow explicit arc detection methods to be added to the IEC 61000-4-30 standard, or other relevant standards applicable to electrified transportation systems.

Appendix A

Non-Fundamental Active Power Calculation

In this appendix, the mathematical formulas used to evaluate active power, fundamental active power, and non-fundamental active power from the voltage and current recorded waveforms are provided. These quantities will be the basis for the harmonic power flow analysis presented in section 5.4 of this chapter.

Calculation of non-fundamental active power is based on the definitions of IEEE Std. 1459 [164]. The active power developed by a sinusoidal source is calculated by Equation A.1 considering the average value of the instantaneous power during a selected measurement time interval:

$$P = \frac{1}{kT}\int_0^{kT} p(t)\mathrm{d}t = \frac{1}{kT}\int_0^{kT} v(t)i(t)\mathrm{d}t \tag{A.1}$$

where $p(t)$ is the instantaneous power; $v(t)$ and $i(t)$ are the instantaneous values of pantograph voltage and current, respectively; T is the fundamental time period (20 ms) corresponding to a 50 Hz fundamental frequency; and k is a positive integer number.

In non-sinusoidal conditions, the instantaneous voltage and the corresponding instantaneous current are expressed by Equations A.2 and A.3, where v_0 and i_0 are the DC voltage current terms, v_1 and i_1 are the fundamental voltage and current terms, etc.

$$v(t) = v_0 + v_1(t) + v_2(t) + v_3(t) + ... \tag{A.2}$$

$$i(t) = i_0 + i_1(t) + i_2(t) + i_3(t) + ... \tag{A.3}$$

By considering that a non-sinusoidal source may contain also interharmonics, subsynchronous harmonics and direct voltage and current, Equations A.2 and A.3 can be written as:

$$v(t) = v_1(t) + v_{\mathrm{H}}(t) \tag{A.4}$$

$$i(t) = i_1(t) + i_{\mathrm{H}}(t) \tag{A.5}$$

where the terms $v_{\mathrm{H}}(t)$ and $i_{\mathrm{H}}(t)$ include all the frequency components contained in the signal except the fundamental. Applying Equations A.4 and A.5 to A.1, the expression for active power takes the form:

$$P = \frac{1}{kT}\int_0^{kT} [v_0 + v_1(t)..][i_0 + i_1(t) + ..]\mathrm{d}t = \sum_{s=0}^{\infty} \frac{1}{kT}\int_0^{kT} v_s i_s \mathrm{d}t = \sum_{s=0}^{\infty} P_s \tag{A.6}$$

where v_s and i_s comprise direct terms, fundamental terms and harmonic terms respectively for the voltage and current waveforms; and P_s is the active power developed in the circuit by the sth harmonic order. Considering the presence of frequency components other than harmonics, Equation A.6 can be rewritten as:

$$P = P_1 + P_{\mathrm{H}} \tag{A.7}$$

where P is the active power; P_1 is the fundamental active power; and P_{H} is the non-fundamental active power. The fundamental active power is calculated by Equation A.8:

$$P_1 = V_1 I_1 \cos\theta_1 \tag{A.8}$$

where V_1 and I_1 are fundamental components of voltage and current extracted by applying the DFT algorithm to the voltage and current waveforms, and θ_1 is the angle difference between fundamental voltages and currents. The remaining non-fundamental active power P_{H}, which contains frequency components with and without an integer

relationship to the fundamental, as well as any DC component, is calculated by Equation A.9:

$$P_{\mathrm{H}} = V_0 I_0 + \sum_{h=2}^{\infty} V_h I_h \cos\theta_h = P - P_1 \tag{A.9}$$

Equations A.1, A.8 and A.9 are used to extract active power, fundamental active power and non-fundamental active power considering voltage and current waveforms.

Appendix B

Code of Analysis in Matlab for Chapter 6

load('TI_T_1') % Load waveform recording. It contains quantities Ip – pantograph current, Vp – pantograph voltage, x – time.
t=x; %Define the time t variable.

% Design of the FIR filter to filter the waveform.
fs=50000; % Define sampling frequency.
cutoff=100; % Set the desired cutoff frequency in Hz.
wn=cutoff/(fs/2); % Calculate the frequency constraint or cutoff frequency of the filter.
h = fir1(200,wn,'low'); % Filter calculation. Where (x,y,z) are: x is the filter order, wn cutoff frequency, and 'low' is the filter type.
freqz(h,1,1024) % Plot the frequency response of the filter.
y=filter(h,1,Ip); % Filters the input pantograph current data.

% Plot the distorted and filtered waveform.
figure;
plot(t,Ip,t,y)
grid on
title ('Distorted and Filtered Waveform')

```
xlabel ('Time (s)')
ylabel ('Voltage (V)')
legend ('Distorted','Filtered')

% Hilbert calculation
Signal=hilbert(y); % Performs the Hilbert transform on signal y.
Amplitude=abs(Signal); % Calculates the instantaneous amplitude of the signal.
Phase=atan2(imag(xa),real(Signal)); % Calculates the instantaneous phase.
Phase=unwrap(Phase); % Apply phase wraping to correct for the phase jumps.
Rate_of_change_of_phase=(diff(Phase)/20); % Calculates the rate of change of phase,
where 20 is the 20us sampling interval.
Rate_of_change_of_phase=Rate_of_change_of_phase.*1000; % Convert the value to mili-
radian.

% Plot the instantaneous current, the instantaneous phase and the instantaneous rate
of change of phase (ROCOP).
delete = 500; % Delete the first 500 samples to eliminate signal spikes appearing at the
beginning of the analysed window as a result of derivative starting point.
ROCOP = Rate_of_change_of_phase;
figure;
subplot(3,1,1)
plot(t(100:length(t)-100,1),Ip(100:length(Ip)-100,1),'r');
xlabel('Time (s)')
ylabel('Current Ip (A)')
subplot(3,1,2)
plot(t(delete:length(t)-delete,1),Phase(delete:length(Phase)-delete,1),'b');
xlabel('Time (s)')
ylabel('Phase (rad)')
subplot(3,1,3)
plot(t(delete:length(t)-(delete+1),1),ROCOP(delete:length(ROCOP)-delete,1),'m')
```

```
xlabel('Time (s)')
ylabel('ROCOP (mrad/us)')

% Filter the rate of change of phase (ROCOP) using a moving average filter.
movingAve = movmean(abs(Rate_of_change_of_phase),50);
% Plot the rate of change of phase
figure;
plot(t(delete:length(t)-(delete+1),1),movingAve(delete:length(movingAve)-delete,1),'b')
xlabel('Time (s)')
ylabel('ROCOP (mrad/us)')
```

Bibliography

[1] "EUR-Lex European Commission. (2011) Roadmap to a Single European Transport Area – Towards a competitive and resource efficient transport system. [White paper]," https://eur-lex.europa.eu/legal-content/EN/TXT/?uri=celex%3A52011DC0144, accessed: 14-07-2021.

[2] "Eurostat. Energy, transport and environment statistics – 2020 edition," https://ec.europa.eu/eurostat/web/products-statistical-books/-/ks-dk-20-001, accessed: 14-07-2021.

[3] "Eurostat. Railway passenger transport statistics - quarterly and annual data," https://ec.europa.eu/eurostat/statistics-explained/index.php?title=Railway_passenger_transport_statistics_-_quarterly_and_annual_data#In_2019.2C_national_transport_represented_more_than_two_thirds_of_the_total_transport_in_all_countries, accessed: 14-07-2021.

[4] M. Brenna, F. Foiadelli, and D. Zaninelli, *Electrical Railway Transportation Systems*. John Wiley & Sons, 2018.

[5] "Eurostat. Electricity production, consumption and market overview ," https://ec.europa.eu/eurostat/statistics-explained/index.php?title=Electricity_production,_consumption_and_market_overview#Electricity_generation, accessed: 15-07-2021.

[6] Euramet, "Final Publishable Report - Metrology for smart energy management in electric railway systems," https://www.euramet.org/research-innovation/search-research-projects/details/?tx_eurametctcp_project[project]=1484&

tx_eurametctcp_project[controller]=Project&tx_eurametctcp_project[action]
=show, 2021, accessed: 15-07-2021.

[7] S. M. Mousavi Gazafrudi, A. Tabakhpour Langerudy, E. F. Fuchs, and K. Al-Haddad, "Power Quality Issues in Railway Electrification: A Comprehensive Perspective," *IEEE Transactions on Industrial Electronics*, vol. 62, no. 5, pp. 3081–3090, 2015.

[8] Z. He, Z. Zheng, and H. Hu, "Power quality in high-speed railway systems," *International Journal of Rail Transportation*, vol. 4, no. 2, pp. 71–97, 2016.

[9] A. Mariscotti, "Measuring and Analyzing Power Quality in Electric Traction Systems," *International Journal of Measurement Technologies and Instrumentation Engineering (IJMTIE)*, vol. 2, no. 4, pp. 21–42, 2012.

[10] H. Hu, Y. Shao, L. Tang, J. Ma, Z. He, and S. Gao, "Overview of Harmonic and Resonance in Railway Electrification Systems," *IEEE Transactions on Industry Applications*, vol. 54, no. 5, pp. 5227–5245, 2018.

[11] A. Mariscotti, "Results on the Power Quality of French and Italian 2×25 kV 50 Hz railways," in *2012 IEEE International Instrumentation and Measurement Technology Conference Proceedings*, 2012, pp. 1400–1405.

[12] Y. Seferi, S. M. Blair, C. Mester, and B. G. Stewart, "Power Quality Measurement and Active Harmonic Power in 25 kV 50 Hz AC Railway Systems," *Energies*, vol. 13, no. 21, p. 5698, 2020.

[13] Y. Seferi, P. Clarkson, S. M. Blair, A. Mariscotti, and B. G. Stewart, "Power Quality Event Analysis in 25 kV 50 Hz AC Railway System Networks," in *2019 IEEE 10th International Workshop on Applied Measurements for Power Systems (AMPS)*, 2019, pp. 1–6.

[14] "IEC 61000-4-30:2015, Electromagnetic compatibility (EMC) – Part 4-30: Testing and measurement techniques – Power quality measurement methods."

[15] "IEC 61000-4-7, Electromagnetic compatibility (EMC) – Part 4-7: Testing and Measurement Techniques—General Guide on Harmonics and Interharmonics Measurements and Instrumentation, for Power Supply Systems and Equipment Connected Thereto," 2008.

[16] A. D. Femine, D. Gallo, D. Giordano, C. Landi, M. Luiso, and D. Signorino, "Power Quality Assessment in Railway Traction Supply Systems," *IEEE Transactions on Instrumentation and Measurement*, vol. 69, no. 5, pp. 2355–2366, 2020.

[17] A. D. Femine, D. Gallo, C. Landi, and M. Luiso, "Discussion on DC and AC Power Quality Assessment in Railway Traction Supply Systems," in *2019 IEEE International Instrumentation and Measurement Technology Conference (I2MTC)*, 2019, pp. 1–6.

[18] G. Crotti, D. Giordano, P. Roccato, A. Delle Femine, D. Gallo, C. Landi, M. Luiso, and A. Mariscotti, "Pantograph-to-ohl arc: Conducted effects in dc railway supply system," in *2018 IEEE 9th International Workshop on Applied Measurements for Power Systems (AMPS)*, 2018, pp. 1–6.

[19] G. Crotti, A. Delle Femine, D. Gallo, D. Giordano, C. Landi, M. Luiso, A. Mariscotti, and P. E. Roccato, "Pantograph-to-ohl arc: Conducted effects in dc railway supply system," *IEEE Transactions on Instrumentation and Measurement*, vol. 68, no. 10, pp. 3861–3870, 2019.

[20] B. Tellini, M. Macucci, R. Giannetti, and G. A. Antonacci, "Conducted and Radiated Interference Measurements in the Line-Pantograph System," *IEEE Transactions on Instrumentation and Measurement*, vol. 50, no. 6, pp. 1661–1664, 2001.

[21] S. Midya, D. Bormann, T. Schutte, and R. Thottappillil, "Pantograph Arcing in Electrified Railways—Mechanism and Influence of Various Parameters—Part I: With DC Traction Power Supply," *IEEE Transactions on Power Delivery*, vol. 24, no. 4, pp. 1931–1939, 2009.

[22] D. Bormann, S. Midya, and R. Thottappillil, "DC Components in Pantograph Arcing: Mechanisms and Influence of Various Parameters," in *2007 18th Inter-*

national Zurich Symposium on Electromagnetic Compatibility. IEEE, 2007, pp. 369–372.

[23] F. Fan, A. Wank, Y. Seferi, and B. G. Stewart, "Pantograph Arc Location Estimation using Resonant Frequencies in DC Railway Power Systems," *IEEE Transactions on Transportation Electrification*, pp. 1–1, 2021.

[24] C. Muscas, "Power Quality Monitoring in Modern Electric Distribution Systems," *IEEE Instrumentation Measurement Magazine*, vol. 13, no. 5, pp. 19–27, 2010.

[25] "EN 50470-3:2006 Electricity metering equipment (a . c .) — Part 3: Particular requirements — Static meters for active energy (class indexes A, B and C)," 2006.

[26] "IEC 62053-22:2020 Electricity metering equipment - Particular requirements - Part 22: Static meters for AC active energy (classes 0,1S, 0,2S and 0,5S)," 2020.

[27] "CENELEC EN 50463-2:2017 Railway applications – Energy measurement on board trains – Part 2: Energy measuring," 2017.

[28] "CENELEC EN 50160 Voltage Characteristics of Electricity Supplied by Public Electricity Networks," 2010.

[29] "IEEE Recommended Practice for Monitoring Electric Power Quality," *IEEE Std 1159-2019 (Revision of IEEE Std 1159-2009)*, pp. 1–98, 2019.

[30] A. Mariscotti, "Direct Measurement of Power Quality Over Railway Networks With Results of a 16.7-Hz Network," *IEEE Transactions on Instrumentation and Measurement*, vol. 60, no. 5, pp. 1604–1612, 2010.

[31] D. Giordano, P. Clarkson, F. Gamacho, H. E. van den Brom, L. Donadio, A. Fernandez-Cardador, C. Spalvieri, D. Gallo, D. Istrate, A. De Santiago Laporte, A. Mariscotti, C. Mester, N. Navarro, M. Porzio, A. Roscoe, and M. Šíra, "Accurate Measurements of Energy, Efficiency and Power Quality in the Electric Railway System," in *2018 Conference on Precision Electromagnetic Measurements (CPEM 2018)*, 2018, pp. 1–2.

[32] G. Rietveld, "Analysis Of The Propagation Of Power Quality Phenomena Using Wide-Area Measurements."

[33] P. S. Wright, J. P. Braun, G. Rietveld, H. E. van den Brom, and G. Crotti, "Smart Grid Power Quality and Stability Measurements in Europe," in *29th Conference on Precision Electromagnetic Measurements (CPEM 2014)*, 2014, pp. 70–71.

[34] "IEEE/IEC International Standard - Measuring relays and protection equipment - Part 118-1: Synchrophasor for power systems - Measurements," *IEC/IEEE 60255-118-1:2018*, pp. 1–78, 2018.

[35] A. G. Phadke, H. Volskis, R. M. de Moraes, T. Bi, R. N. Nayak, Y. K. Sehgal, S. Sen, W. Sattinger, E. Martinez, O. Samuelsson, D. Novosel, V. Madani, and Y. A. Kulikov, "The Wide World of Wide-area Measurement," *IEEE Power and Energy Magazine*, vol. 6, no. 5, pp. 52–65, 2008.

[36] S. M. Blair, M. H. Syed, E. Guillo-Sansano, Q. Hong, C. D. Booth, G. M. Burt, A. Hinojos, and I. Avila, "Review of Approaches for Using Synchrophasor Data for Real-Time Wide-Area Control," in *2019 International Conference on Smart Grid Synchronized Measurements and Analytics (SGSMA)*, 2019, pp. 1–7.

[37] A. G. Phadke, J. S. Thorp, and K. J. Karimi, "State Estimlatjon with Phasor Measurements," *IEEE Transactions on Power Systems*, vol. 1, no. 1, pp. 233–238, 1986.

[38] R. O. Burnett, M. M. Butts, T. W. Cease, V. Centeno, G. Michel, R. J. Murphy, and A. G. Phadke, "Synchronized phasor measurements of a power system event," *IEEE Transactions on Power Systems*, vol. 9, no. 3, pp. 1643–1650, 1994.

[39] N. Save, M. Popov, A. Jongepier, and G. Rietveld, "PMU-based power system analysis of a medium-voltage distribution grid," *CIRED - Open Access Proceedings Journal*, vol. 2017, no. 1, pp. 1927–1930, 2017.

[40] R. Puddu, K. Brady, C. Muscas, P. A. Pegoraro, and A. Von Meier, "PMU-Based Technique for the Estimation of Line Parameters in Three-Phase Electric

Distribution Grids," in *2018 IEEE 9th International Workshop on Applied Measurements for Power Systems (AMPS)*, 2018, pp. 1–5.

[41] Euramet, "Final Publishable Report - Standard Tests and Requirements for Rate-of-Change of Frequency (ROCOF) Measurements in Smart Grids," 2019.

[42] M. Bollen, "What is power quality?" *Electric Power Systems Research*, vol. 66, no. 1, pp. 5–14, 2003, power Quality. [Online]. Available: https://www.sciencedirect.com/science/article/pii/S0378779603000671

[43] A. Ferrero, "Measuring electric power quality: Problems and perspectives," *Measurement*, vol. 41, no. 2, pp. 121–129, 2008, advances in Measurements of Electrical Quantities. [Online]. Available: https://www.sciencedirect.com/science/article/pii/S0263224106000480

[44] M. H. Bollen and I. Y. Gu, *Signal processing of power quality disturbances*. John Wiley & Sons, 2006, vol. 30.

[45] D. Saxena, K. Verma, and S. Singh, "Power quality event classification: an overview and key issues," *International journal of engineering, science and technology*, vol. 2, no. 3, pp. 186–199, 2010.

[46] K. Kawahara, S.-I. Hase, Y. Mochinaga, Y. Hisamizu, and T. Inoue, "Compensation of voltage drop using static VAr compensator at sectioning post in AC electric railway system," in *Proceedings of Power Conversion Conference - PCC '97*, vol. 2, 1997, pp. 955–960 vol.2.

[47] "CENELEC EN 50163, Railway applications – Supply voltages of traction systems," 2004.

[48] A. F. Zobaa and S. H. E. A. Aleem, *Power quality in future electrical power systems*. Institution of Engineering & Technology, 2017.

[49] S. Chattopadhyay, M. Mitra, and S. Sengupta, "Electric power quality," in *Electric power quality*. Springer, 2011, pp. 5–12.

[50] S. Watari, M. Kunitake, K. Kitamura, T. Hori, T. Kikuchi, K. Shiokawa, N. Nishitani, R. Kataoka, Y. Kamide, T. Aso *et al.*, "Measurements of geomagnetically induced current in a power grid in Hokkaido, Japan," *Space Weather*, vol. 7, no. 3, 2009.

[51] R. Marshall, H. Gorniak, T. Van Der Walt, C. Waters, M. Sciffer, M. Miller, M. Dalzell, T. Daly, G. Pouferis, G. Hesse *et al.*, "Observations of geomagnetically induced currents in the Australian power network," *Space Weather*, vol. 11, no. 1, pp. 6–16, 2013.

[52] C. T. Gaunt and G. Coetzee, "Transformer failures in regions incorrectly considered to have low GIC-risk," in *2007 IEEE Lausanne Power Tech*, 2007, pp. 807–812.

[53] S. Watari, S. Nakamura, and Y. Ebihara, "Measurement of geomagnetically induced current (gic) around tokyo, japan," *Earth, Planets and Space*, vol. 73, no. 1, pp. 1–19, 2021.

[54] R. Marshall, M. Dalzell, C. Waters, P. Goldthorpe, and E. Smith, "Geomagnetically induced currents in the New Zealand power network," *Space Weather*, vol. 10, no. 8, 2012.

[55] C.-M. Liu, L.-G. Liu, and Y. Yang, "Monitoring and Modeling Geomagnetically Induced Currents in Power Grids of China," in *2009 Asia-Pacific Power and Energy Engineering Conference*, 2009, pp. 1–4.

[56] M. Karimi-Ghartemani, B. Ooi, and A. Bakhshai, "Application of Enhanced Phase-Locked Loop System to the Computation of Synchrophasors," *IEEE Transactions on Power Delivery*, vol. 26, no. 1, pp. 22–32, 2011.

[57] A. Derviškadić, P. Romano, and M. Paolone, "Iterative-Interpolated DFT for Synchrophasor Estimation: A Single Algorithm for P- and M-Class Compliant PMUs," *IEEE Transactions on Instrumentation and Measurement*, vol. 67, no. 3, pp. 547–558, 2018.

[58] D. Belega and D. Petri, "Accuracy of synchrophasor measurements provided by the sine-fit algorithms," in *2012 IEEE International Energy Conference and Exhibition (ENERGYCON)*, 2012, pp. 921–926.

[59] A. J. Roscoe, I. F. Abdulhadi, and G. M. Burt, "P and M Class Phasor Measurement Unit Algorithms Using Adaptive Cascaded Filters," *IEEE Transactions on Power Delivery*, vol. 28, no. 3, pp. 1447–1459, 2013.

[60] W. A. Wilkinson and M. D. Cox, "Discrete wavelet analysis of power system transients," *IEEE Transactions on Power Systems*, vol. 11, no. 4, pp. 2038–2044, 1996.

[61] B. Bhargava, "Railway Electrification Systems and Configurations," in *1999 IEEE Power Engineering Society Summer Meeting. Conference Proceedings (Cat. No.99CH36364)*, vol. 1, 1999, pp. 445–450 vol.1.

[62] A. Steimel, "Power-Electronic Grid Supply of AC Railway Systems," in *2012 13th International Conference on Optimization of Electrical and Electronic Equipment (OPTIM)*, 2012, pp. 16–25.

[63] A. Mariscotti, "Data sets of measured pantograph voltage and current of European AC railways," *Data in Brief*, vol. 30, p. 105477, 2020. [Online]. Available: https://www.sciencedirect.com/science/article/pii/S2352340920303711

[64] G. Crotti, A. D. Femine, D. Gallo, D. Giordano, C. Landi, M. Luiso, A. Mariscotti, and P. E. Roccato, "Pantograph-to-OHL Arc: Conducted Effects in DC Railway Supply System," *IEEE Transactions on Instrumentation and Measurement*, vol. 68, no. 10, pp. 3861–3870, 2019.

[65] A. M. L. Tortia, "Turin-Milan high-speed railway-line, 2x25 kV 50 Hz AC electrified. EMC problems in earthing of exposed conductive parts," in *International Symposium on Power Electronics, Electrical Drives, Automation and Motion, 2006. SPEEDAM 2006.*, 2006, pp. 1127–1132.

[66] L. Battistelli, M. Pagano, D. Proto, A. Amendola, L. Candurro, and A. Pignotti, "Short Circuit Modelling and Simulation of 2×25 kV High Speed Railways," in *2008 Second Asia International Conference on Modelling Simulation (AMS)*, 2008, pp. 702–707.

[67] C. Courtois, "Why the 2 x 25 kv alternative?" in *IEE Colloquium on 50kV Autotransformer Traction Supply Systems-the French Experience.* IET, 1993, pp. 1–1.

[68] G. D'Antona, M. Brenna, and N. Manta, "Modeling and Measurement of the Voltage Transients at the Phase to Phase Changeover Section of the Italian High Speed Railway System," in *2012 IEEE International Workshop on Applied Measurements for Power Systems (AMPS) Proceedings*, 2012, pp. 1–5.

[69] A. Pfeiffer, W. Scheidl, M. Eitzmann, and E. Larsen, "Modern rotary converters for railway applications," in *Proceedings of the 1997 IEEE/ASME Joint Railroad Conference*, 1997.

[70] D. Serrano-Jiménez, L. Abrahamsson, S. Castaño-Solís, and J. Sanz-Feito, "Electrical railway power supply systems: Current situation and future trends," *International Journal of Electrical Power & Energy Systems*, vol. 92, pp. 181–192, 2017.

[71] "Eurostat," https://ec.europa.eu/eurostat/data/database, accessed: 09-01-2021.

[72] "Wikipedia," https://en.wikipedia.org/wiki/List_of_countries_by_rail_transport_network_size#cite_note-unece-4, accessed: 11-01-2021.

[73] "CENELEC EN 50388 Railway Applications — Power supply and rolling stock — Technical criteria for the coordination between power supply (substation) and rolling stock to achieve interoperability," 2012.

[74] C. R. Bayliss, C. Bayliss, and B. Hardy, *Transmission and distribution electrical engineering.* Elsevier, 2012.

[75] S. Gao, X. Li, X. Ma, H. Hu, Z. He, and J. Yang, "Measurement-Based Compartmental Modeling of Harmonic Sources in Traction Power-Supply System," *IEEE Transactions on Power Delivery*, vol. 32, no. 2, pp. 900–909, 2016.

[76] N. Mohan, T. M. Undeland, and W. P. Robbins, *Power electronics: converters, applications, and design*. John wiley & sons, 2003.

[77] C. Xie, S. Tennakoon, R. Langella, D. Gallo, A. Testa, and A. Wixon, "Harmonic Impedance Measurement of 25 kV Single Phase AC Supply Systems," in *Ninth International Conference on Harmonics and Quality of Power. Proceedings (Cat. No. 00EX441)*, vol. 1. IEEE, 2000, pp. 214–219.

[78] G. Crotti, D. Giordano, D. Signorino, A. D. Femine, D. Gallo, C. Landi, M. Luiso, A. Biancucci, and L. Donadio, "Monitoring Energy and Power Quality On Board Train," in *2019 IEEE 10th International Workshop on Applied Measurements for Power Systems (AMPS)*, 2019, pp. 1–6.

[79] Y. Seferi, S. M. Blair, C. Mester, and B. G. Stewart, "A Novel Arc Detection Method for DC Railway Systems," *Energies*, vol. 14, no. 2, p. 444, 2021.

[80] R. J. Hill, M. Fracchia, P. Pozzobon, and G. Sciutto, "A Frequency Domain Model for 3 kV DC Traction DC-side Resonance Identification," *IEEE Transactions on Power Systems*, vol. 10, no. 3, pp. 1369–1375, 1995.

[81] A. Mariscotti and P. Pozzobon, "Synthesis of Line Impedance Expressions for Railway Traction Systems," *IEEE Transactions on Vehicular Technology*, vol. 52, no. 2, pp. 420–430, 2003.

[82] A. Betts, J. Hall, and P. Keen, "Condition monitoring of pantographs," in *International Conference on Main Line Railway Electrification 1989*. IET, 1989, pp. 129–133.

[83] M. Brenna, A. Capasso, M. Falvo, F. Foiadelli, R. Lamedica, and D. Zaninelli, "Investigation of resonance phenomena in high speed railway supply systems: Theoretical and experimental analysis," *Electric Power*

Systems Research, vol. 81, no. 10, pp. 1915–1923, 2011. [Online]. Available: https://www.sciencedirect.com/science/article/pii/S0378779611001295

[84] A. Kusko and S. M. Peeran, "Tuned Filters for Traction Rectifier Sets," *IEEE Transactions on Industry Applications*, vol. IA-21, no. 6, pp. 1571–1579, 1985.

[85] M. Popescu, A. Bitoleanu, and M. Dobriceanu, "Harmonic Current Reduction in Railway Systems," *WSEAS transactions on systems*, vol. 7, no. 7, pp. 689–698, 2008.

[86] V. Vasanthi and S. Ashok, "Harmonic Issues in Electric Traction System," in *2011 International Conference on Energy, Automation and Signal.* IEEE, 2011, pp. 1–5.

[87] L. Hu, R. E. Morrison, and D. J. Young, "Reduction Of Harmonic Distortion And Improvement Of Voltage Form Factor In Compensated Railway Systems by Means of a Single Arm Filter," in *ICHPS V International Conference on Harmonics in Power Systems.*, 1992, pp. 83–88.

[88] L. Zanotto, R. Piovan, V. Toigo, E. Gaio, P. Bordignon, T. Consani, and M. Fracchia, "Filter Design for Harmonic Reduction in High-Voltage Booster for Railway Applications," *IEEE Transactions on Power Delivery*, vol. 20, no. 1, pp. 258–263, 2005.

[89] P.-C. Tan, P. C. Loh, and D. G. Holmes, "A Robust Multilevel Hybrid Compensation System for 25-kV Electrified Railway Applications," *IEEE Transactions on Power Electronics*, vol. 19, no. 4, pp. 1043–1052, 2004.

[90] W. Song, S. Jiao, Y. W. Li, J. Wang, and J. Huang, "High-Frequency Harmonic Resonance Suppression in High-Speed Railway Through Single-Phase Traction Converter With LCL Filter," *IEEE Transactions on Transportation Electrification*, vol. 2, no. 3, pp. 347–356, 2016.

[91] Zhiwen Zhang, Bin Wu, Longfu Luo, Lawu Zhou, and Fusheng Liu, "Multi-Purpose Balanced Transformer with Harmonic Eliminating Capability for Rail-

way Traction Applications," in *2008 IEEE Power and Energy Society General Meeting - Conversion and Delivery of Electrical Energy in the 21st Century*, 2008, pp. 1–8.

[92] H. E. Mazin and W. Xu, "Harmonic cancellation characteristics of specially connected transformers," *Electric Power Systems Research*, vol. 79, no. 12, pp. 1689–1697, 2009. [Online]. Available: https://www.sciencedirect.com/science/article/pii/S0378779609001679

[93] A. Luo, C. Wu, J. Shen, Z. Shuai, and F. Ma, "Railway Static Power Conditioners for High-speed Train Traction Power Supply Systems Using Three-phase V/V Transformers," *IEEE Transactions on Power Electronics*, vol. 26, no. 10, pp. 2844–2856, 2011.

[94] Qunzhan Li, Wei Liu, Zeliang Shu, Shaofeng Xie, and Fulin Zhou, "Co-phase power supply system for HSR," in *2014 International Power Electronics Conference (IPEC-Hiroshima 2014 - ECCE ASIA)*, 2014, pp. 1050–1053.

[95] J. K. Phipps, J. P. Nelson, and P. K. Sen, "Power Quality and Harmonic Distortion on Distribution Systems," *IEEE Transactions on Industry Applications*, vol. 30, no. 2, pp. 476–484, 1994.

[96] M. H. Bollen, "Understanding power quality problems," in *Voltage sags and Interruptions*. IEEE press, 2000.

[97] M. H. Bollen, R. Das, S. Djokic, P. Ciufo, J. Meyer, S. K. Rönnberg, and F. Zavodam, "Power Quality Concerns in Implementing Smart Distribution-Grid Applications," *IEEE Transactions on Smart Grid*, vol. 8, no. 1, pp. 391–399, 2016.

[98] M. Tanta, V. Monteiro, T. J. C. Sousa, A. P. Martins, A. S. Carvalho, and J. L. Afonso, "Power quality phenomena in electrified railways: Conventional and new trends in power quality improvement toward public power systems," in *2018 International Young Engineers Forum (YEF-ECE)*, 2018, pp. 25–30.

[99] R. Morrison, "Power Quality Issues on AC Traction Systems," in *Ninth International Conference on Harmonics and Quality of Power. Proceedings (Cat. No.00EX441)*, vol. 2, 2000, pp. 709–714 vol.2.

[100] A. D. Femine, D. Gallo, D. Giordano, C. Landi, M. Luiso, and D. Signorino, "Synchronized Measurement System for Railway Application," *Journal of Physics: Conference Series*, vol. 1065, p. 052040, aug 2018. [Online]. Available: https://doi.org/10.1088/1742-6596/1065/5/052040

[101] A. T. Langerudy, A. Mariscotti, and M. A. Abolhassani, "Power Quality Conditioning in Railway Electrification: A Comparative Study," *IEEE Transactions on Vehicular Technology*, vol. 66, no. 8, pp. 6653–6662, 2017.

[102] A. Gargoom, "Digital signal processing techniques for improving the automatic classification of power quality events," Ph.D. dissertation, University of Adelaide, School of Electrical and Electronic Engineering, 2007, accessed: 26-01-2022.

[103] A. Moschitta, P. Carbone, and C. Muscas, "Performance Comparison of Advanced Techniques for Voltage Dip Detection," *IEEE Transactions on Instrumentation and Measurement*, vol. 61, no. 5, pp. 1494–1502, 2012.

[104] E. Perez and J. Barros, "Voltage Event Detection and Characterization Methods: A Comparative Study," in *2006 IEEE/PES Transmission Distribution Conference and Exposition: Latin America*, 2006, pp. 1–6.

[105] E. Feilat, "Voltage Dip Estimation Techniques, an Overview," in *Proceedings of the 7th Regional Conference of CIGRE National Committees in Arab Countries, Amman, Jordan*, 2007, pp. 3–5.

[106] G. Heydt, P. Fjeld, C. Liu, D. Pierce, L. Tu, and G. Hensley, "Applications of the Windowed FFT to Electric Power Quality Assessment," *IEEE Transactions on Power Delivery*, vol. 14, no. 4, pp. 1411–1416, 1999.

[107] J. Bruna, J. Melero, J. D. de Aguilar, and M. Romero, "A Novel Method for Voltage Event Characterization," in *15th International Congress of Metrology, Paris, France*, 2011.

[108] H. Amaris, C. Alvarez, M. Alonso, D. Florez, T. Lobos, P. Janik, J. Rezmer, and Z. Waclawek, "Computation of Voltage Sag Initiation with Fourier based Algorithm, Kalman Filter and Wavelets," in *2009 IEEE Bucharest PowerTech*, 2009, pp. 1–6.

[109] Y. Wang, X.-Y. Xiao, and M. Bollen, "Challenges in the Calculation methods of Point-on-Wave Characteristics for Voltage Dips," in *2016 17th International Conference on Harmonics and Quality of Power (ICHQP)*, 2016, pp. 513–517.

[110] J. Barros and E. Perez, "Limitations in the Use of R.M.S. Value in Power Quality Analysis," in *2006 IEEE Instrumentation and Measurement Technology Conference Proceedings*, 2006, pp. 2261–2264.

[111] M. Albu and G. Heydt, "On the Use of RMS Values in Power Quality Assessment," *IEEE Transactions on Power Delivery*, vol. 18, no. 4, pp. 1586–1587, 2003.

[112] N. Kagan, E. Ferrari, N. Matsuo, S. Duarte, A. Sanommiya, J. Cavaretti, U. Castellano, and A. Tenorio, "Influence of RMS variation measurement protocols on electrical system performance indices for voltage sags and swells," in *Ninth International Conference on Harmonics and Quality of Power. Proceedings (Cat. No.00EX441)*, vol. 3, 2000, pp. 790–795 vol.3.

[113] H. van den Brom, D. Giordano, D. Gallo, A. Wank, and Y. Seferi, "Accurate Measurement of Energy Dissipated in Braking Rheostats in DC Railway Systems," in *2020 Conference on Precision Electromagnetic Measurements (CPEM)*, 2020, pp. 1–2.

[114] G. Crotti, D. Giordano, D. Signorino, A. Delle Femine, D. Gallo, C. Landi, M. Luiso, A. Biancucci, and L. Donadio, "Monitoring Energy and Power Qual-

ity On Board Train," in *2019 IEEE 10th International Workshop on Applied Measurements for Power Systems (AMPS)*. IEEE, 2019, pp. 1–6.

[115] J. Arrillaga, B. C. Smith, N. R. Watson, and A. R. Wood, *Power system harmonic analysis*. John Wiley & Sons, 1997.

[116] W. CIGRE, "36-05,"Harmonics, characteristic parameters, methods of study, estimates of existing values in the network,"," *Electra*, vol. 77, pp. 35–54, 1981.

[117] B. Milešević, I. Uglešić, and B. Filipović-Grčić, "Power quality analysis in electric traction system with three-phase induction motors," *Electric power systems research*, vol. 138, pp. 172–179, 2016.

[118] A. Župan, A. T. Teklić, and B. Filipović-Grčić, "Modeling of 25 kV Electric Railway System for Power Quality Studies," in *Eurocon 2013*. IEEE, 2013, pp. 844–849.

[119] M. Brenna, F. Foiadelli, and D. Zaninelli, "Electromagnetic Model of High Speed Railway Lines for Power Quality Studies," *IEEE Transactions on Power Systems*, vol. 25, no. 3, pp. 1301–1308, 2010.

[120] C. Stackler, F. Morel, P. Ladoux, and P. Dworakowski, "Modelling of a 25 kV-50 Hz Railway Infrastructure for Harmonic Analysis," *European Journal of Electrical Engineering*, vol. 22, no. 2, pp. 87–96, 2020.

[121] S. Sane, S. Sharma, and S. K. Prasad, "Harmonic Analysis for AC and DC Supply in Traction Substation of Mumbai," in *2015 IEEE International Conference on Electrical, Computer and Communication Technologies (ICECCT)*, 2015, pp. 1–5.

[122] "IEEE Recommended Practice and Requirements for Harmonic Control in Electric Power Systems," *IEEE Std 519-2014 (Revision of IEEE Std 519-1992)*, pp. 1–29, 2014.

[123] P. Swart, J. D. Van Wyk, and M. Case, "On techniques for localization of sources producing distortion in three-phase networks," *European transactions on electrical power*, vol. 6, no. 6, pp. 391–396, 1996.

[124] A. Ferrero, "Measuring electric power quality: Problems and perspectives," *Measurement*, vol. 41, no. 2, pp. 121–129, 2008.

[125] "Commission regulation (EU) No 1302/2014 of 18 November 2014 concerning a technical specification for interoperability relating to the 'rolling stock — locomotives and passenger rolling stock' subsystem of the rail system in the European Union."

[126] R. F. Ammerman and P. Sen, "Modeling High-Current Electrical Arcs: A Volt-Ampere Characteristic Perspective for AC and DC Systems," in *2007 39th North American Power Symposium*. IEEE, 2007, pp. 58–62.

[127] O. Bruno, A. Landi, M. Papi, and L. Sani, "Phototube sensor for monitoring the quality of current collection on overhead electrified railways," *Proceedings of the institution of mechanical engineers, part f: Journal of rail and rapid transit*, vol. 215, no. 3, pp. 231–241, 2001.

[128] S. Midya, D. Bormann, A. Larsson, T. Schutte, and R. Thottappillil, "Understanding Pantograph Arcing in Electrified Railways-Influence of Various Parameters," in *2008 IEEE International Symposium on Electromagnetic Compatibility*. IEEE, 2008, pp. 1–6.

[129] T. Usuda, M. Ikeda, and Y. Yamashita, "Prediction of contact wire wear in high speed railways," in *Proc. of 9th World Congress on Railway Research*, 2011, pp. 1–10.

[130] A. Balestrino, O. Bruno, P. GIORGI, A. Landi, M. PAPI, L. Sani, A. Giuseppe, and S.-P. Elettriche, "Electric welding effect: detection via phototube sensor and maintenance activities," in *CDROM of the World Congress on Railway Research, Koln*, 2001, pp. 19–23.

[131] "CENELEC EN 50367:2012 Railway applications – Current collection systems — Technical criteria for the interaction between pantograph and overhead line (to achieve free access)," 2012.

[132] A. Mariscotti and D. Giordano, "Experimental characterization of pantograph arcs and transient conducted phenomena in dc railways," *Acta Imeko*, vol. 9, pp. 10–17, 2020.

[133] H.-H. Huang and T.-H. Chen, "Development of method for assessing the current collection performance of the overhead conductor rail systems used in electric railways," *Proceedings of the Institution of Mechanical Engineers, Part F: Journal of Rail and Rapid Transit*, vol. 222, no. 2, pp. 159–168, 2008.

[134] T. Li, G. Wu, L. Zhou, G. Gao, W. Wang, B. Wang, D. Liu, and D. Li, "Pantograph Arcing's Impact on Locomotive Equipments," in *2011 IEEE 57th Holm Conference on Electrical Contacts (Holm)*. IEEE, 2011, pp. 1–5.

[135] G. Gao, X. Yan, Z. Yang, W. Wei, Y. Hu, and G. Wu, "Pantograph–Catenary Arcing Detection Based on Electromagnetic Radiation," *IEEE Transactions on Electromagnetic Compatibility*, vol. 61, no. 4, pp. 983–989, 2018.

[136] A. Mariscotti, A. Marrese, N. Pasquino, and R. S. L. Moriello, "Time and frequency characterization of radiated disturbance in telecommunication bands due to pantograph arcing," *Measurement*, vol. 46, no. 10, pp. 4342–4352, 2013.

[137] "CENELEC EN 50317:2012 Railway applications – Current collection systems — Requirements for and validation of measurements of the dynamic interaction between pantograph and overhead contact line," 2012.

[138] "CENELEC EN 50119:2020 Railway applications – Fixed installations — Electric traction overhead contact lines," 2020.

[139] S. Barmada, A. Landi, M. Papi, and L. Sani, "Wavelet multiresolution analysis for monitoring the occurrence of arcing on overhead electrified railways," *Proceedings of the Institution of Mechanical Engineers, Part F: Journal of Rail and Rapid Transit*, vol. 217, no. 3, pp. 177–187, 2003.

[140] A. Landi, L. Menconi, and L. Sani, "Hough transform and thermo-vision for monitoring pantograph-catenary system," *Proceedings of the Institution of Me-*

chanical Engineers, Part F: Journal of Rail and Rapid Transit, vol. 220, no. 4, pp. 435–447, 2006.

[141] I. Aydin, "A new approach based on firefly algorithm for vision-based railway overhead inspection system," *Measurement*, vol. 74, pp. 43–55, 2015.

[142] S. Barmada, M. Raugi, M. Tucci, and F. Romano, "Arc detection in pantograph-catenary systems by the use of support vector machines-based classification," *IET Electrical Systems in Transportation*, vol. 4, no. 2, pp. 45–52, 2013.

[143] İ. Aydın, O. Yaman, M. Karaköse, and S. B. Çelebi, "Particle swarm based arc detection on time series in pantograph-catenary system," in *2014 IEEE International Symposium on Innovations in Intelligent Systems and Applications (INISTA) Proceedings*. IEEE, 2014, pp. 344–349.

[144] S. Barmada, M. Tucci, M. Menci, and F. Romano, "Clustering techniques applied to a high-speed train pantograph–catenary subsystem for electric arc detection and classification," *Proceedings of the Institution of Mechanical Engineers, Part F: Journal of Rail and Rapid Transit*, vol. 230, no. 1, pp. 85–96, 2016.

[145] "MyRailS website. Available online: https://myrails.it/ (accessed on 14 January 2021)."

[146] P. Thakur and A. Singh, "A novel way to quantify the magnitude of voltage sag," *Electrical Engineering*, vol. 95, no. 4, pp. 331–340, 2013.

[147] D. Gallo, C. Landi, and M. Luiso, "Accuracy Analysis of Algorithms Adopted in Voltage Dip Measurements," *IEEE Transactions on Instrumentation and Measurement*, vol. 59, no. 10, pp. 2652–2659, 2010.

[148] A. Mariscotti and D. Slepicka, "Analysis of frequency stability of 16.7 Hz railways," in *2011 IEEE International Instrumentation and Measurement Technology Conference*, 2011, pp. 1–5.

[149] A. Mariscotti and D. Slepicka, "The Frequency Stability of the 50 Hz French Railway," in *2012 IEEE International Instrumentation and Measurement Technology Conference Proceedings*, 2012, pp. 1406–1410.

[150] "IEC TR 61000-2-8, Electromagnetic compatibility (EMC) — Part 2-8: Environment — Voltage dips and short interruptions on public electric power supply systems with statistical measurement results," 2002.

[151] D. Signorino, D. Giordano, A. Mariscotti, D. Gallo, A. D. Femine, F. Balic, J. Quintana, L. Donadio, and A. Biancucci, "Dataset of measured and commented pantograph electric arcs in dc railways," *Data in Brief*, vol. 31, p. 105978, 2020. [Online]. Available: https://www.sciencedirect.com/science/article/pii/S2352340920308726

[152] L. Marple, "Computing the Discrete-Time "Analytic" Signal via FFT," *IEEE Transactions on signal processing*, vol. 47, no. 9, pp. 2600–2603, 1999.

[153] Z. M. Hussain, A. Z. Sadik, and P. O'Shea, *Digital signal processing: an introduction with MATLAB and applications.* Springer Science & Business Media, 2011.

[154] W. Van Drongelen, *Signal processing for neuroscientists.* Academic press, 2018.

[155] D. T. Romero and G. Jovanovic, "Digital FIR Hilbert transformers: fundamentals and efficient design methods," *MATLAB-A Fundam. Tool Sci. Comput. Eng. Appl*, vol. 1, pp. 445–482, 2012.

[156] M. Feldman, "Hilbert transform in vibration analysis," *Mechanical systems and signal processing*, vol. 25, no. 3, pp. 735–802, 2011.

[157] T. Jayasree, D. Devaraj, and R. Sukanesh, "Power quality disturbance classification using Hilbert transform and RBF networks," *Neurocomputing*, vol. 73, no. 7-9, pp. 1451–1456, 2010.

[158] J. A. Santos-Hernandez, M. Valtierra-Rodriguez, J. P. Amezquita-Sanchez, R. D. J. Romero-Troncoso, and D. Camarena-Martinez, "Hilbert filter based

FPGA architecture for power quality monitoring," *Measurement*, vol. 147, p. 106819, 2019.

[159] J. R. Razo-Hernandez, M. Valtierra-Rodriguez, D. Granados-Lieberman, G. Tapia-Tinoco, and J. R. Rodriguez-Rodriguez, "A Phasor Estimation Algorithm Based on Hilbert Transform for P-class PMUs," *Advances in Electrical and Computer Engineering*, vol. 18, no. 3, pp. 97–105, 2018.

[160] N. E. Huang, Z. Shen, S. R. Long, M. C. Wu, H. H. Shih, Q. Zheng, N.-C. Yen, C. C. Tung, and H. H. Liu, "The empirical mode decomposition and the hilbert spectrum for nonlinear and non-stationary time series analysis," *Proceedings of the Royal Society of London. Series A: mathematical, physical and engineering sciences*, vol. 454, no. 1971, pp. 903–995, 1998.

[161] O. P. Mahela, A. G. Shaik, and N. Gupta, "A critical review of detection and classification of power quality events," *Renewable and Sustainable Energy Reviews*, vol. 41, pp. 495–505, 2015.

[162] O. Ozgonenel, T. Yalcin, I. Guney, and U. Kurt, "A new classification for power quality events in distribution systems," *Electric Power Systems Research*, vol. 95, pp. 192–199, 2013.

[163] S. W. Smith, "CHAPTER 15 - Moving Average Filters," in *Digital Signal Processing*, S. W. Smith, Ed. Boston: Newnes, 2003, pp. 277–284. [Online]. Available: https://www.sciencedirect.com/science/article/pii/B9780750674447500522

[164] "IEEE Standard Definitions for the Measurement of Electric Power Quantities Under Sinusoidal, Nonsinusoidal, Balanced, or Unbalanced Conditions - Redline," *IEEE Std 1459-2010 (Revision of IEEE Std 1459-2000) - Redline*, pp. 1–52, 2010.